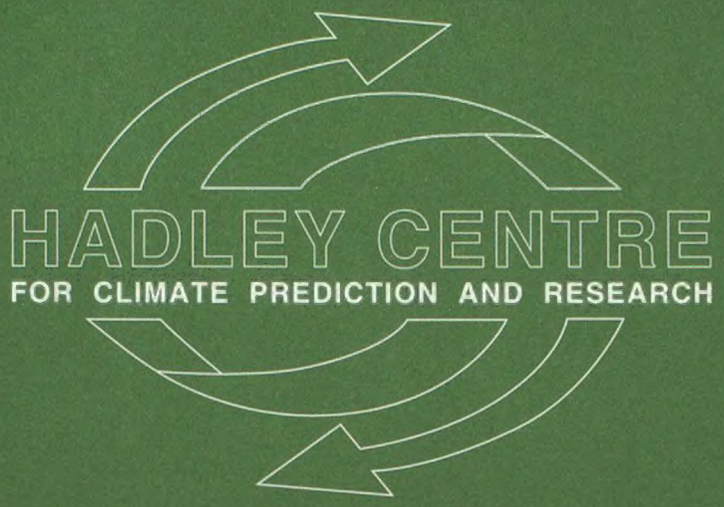

Simulation of the Indian Monsoon and Tropical Intraseasonal Variability by a General Circulation Model

by

P M Inness and D Gregory

CRTN 52

November 1994

CLIMATE
RESEARCH
TECHNICAL
NOTE

Hadley Centre
Meteorological Office
London Road
Bracknell
Berkshire RG12 2SY

CLIMATE RESEARCH TECHNICAL NOTE NO. 52

SIMULATION OF THE INDIAN MONSOON AND TROPICAL INTRASEASONAL VARIABILITY BY A GENERAL CIRCULATION MODEL

by

P M Inness and D Gregory

November 1994

Hadley Centre for Climate Prediction and Research
Meteorological Office
London Road
Bracknell
Berkshire RG12 2SY

NOTE: This paper has not been published. Permission to quote from it should be obtained from the Director of the Hadley Centre.

Abstract

The ability of a version of the Hadley Centre Model at climate resolution to simulate the Indian Monsoon flow is considered. The sensitivity of the simulation to changes in the physical parametrizations used is discussed together with the impact of model resolution. The Indian region is known to be strongly affected by the Intraseasonal Oscillation which in the past has been poorly represented in GCMs. The structure and period of the oscillation in the Unified Model is analysed and its impact upon tropical rainfall diagnosed.

CONTENTS

1. Introduction

2. Model Description and Experiments

3. Simulation of the Indian Monsoon

3.1 Standard Simulation
3.2 The Role of Convective Downdraughts
3.3 Sensitivity to Changes in Entrainment Formulation
3.4 Sensitivity of Monsoon to SST variations
3.5 Sensitivity to Resolution

4. Analysis of the Intraseasonal Oscillation

4.1 Wave Period and Propagation
4.2 Interannual Variability due to SSTs
4.3 Sensitivity to Convective Downdraughts
4.4 Sensitivity to Changes in Entrainment Formulation
4.5 Spatial Influence of the Oscillation upon Tropical Convection
4.6 Factors Important for the Simulation of the Intraseasonal Oscillation

5. Summary

6. References

7. Acknowledgements

8. List of Figures

1. Introduction.

The tropical circulation is important for the maintenance of the general circulation of the atmosphere, the latent heat released in tropical convective systems driving large-scale motions which have impacts not only in the tropics but also in mid-latitudes. In the northern hemisphere summer, the south Asian Monsoon dominates the circulation in the tropics, with intense convective systems releasing large amounts of latent heat. Although the monsoon is often conceptualized as being a giant sea-breeze circulation, it is in fact a complex system resulting from interactions of the diabatic heating field, orography and land/sea surface with large scale dynamical processes. The monsoon flow and resulting rainfall over the Indian sub-continent exhibit a large degree of variability both from year to year and within an individual season.

Since the Indian monsoon involves large transports of heat, moisture and momentum it is essential that general circulation models (GCMs) should be able to accurately represent the monsoon circulation and these associated transports. Because of the dependence of local agriculture on the monsoon rains it is important that changes in monsoon flow due to increased greenhouse gases be assessed and some effort has been directed to this using the results of coupled ocean - atmosphere models. However, many GCMs show large systematic errors in their monsoon simulations and so such assessments must be treated as provisional.

The report of a WCRP TOGA/MONEG workshop on monsoon variability (1992) examines the monsoon simulations from GCMs of 17 modelling centres and notes that the systematic errors fall into 2 broad groups. In the first group the low level jet over the Arabian Sea is too weak and the flow is too landward over south-east China. In the second group the low level jet is too strong and the jet tends to extend too far east, over the Philippines and into the west Pacific often with troughing and heavy precipitation in the same region. The same report also notes that the flow simulated by one model (an early version of the UK Met. Office Unified Model) was very sensitive to changes in physical processes. Given the importance of the flow in this region to both the global circulation and the large population of the Indian sub-continent it is vital that improved simulation of the monsoon by GCMs be achieved.

It is well known that tropical convective activity is very variable on a wide range of time and space scales. Since the advent of satellite observations, it has become clear that the time mean ITCZ is in fact made up of many individual convective cells which exhibit a large degree of transient behaviour. Although in the time mean it appears that there are preferred locations for stationary convective activity to develop, analysis of the time evolution of the circulation shows that these apparently stationary features are modulated by various propagating phenomena. These range in scale from small cloud clusters embedded in easterly waves, which may have a lifetime of several days, up to planetary scale waves and, on timescales of several years, the ENSO cycle also modulates tropical convective activity.

It is becoming increasingly clear that transient tropical convective activity has an important role in determining the state of the time mean circulation both in the tropics and at extra-tropical latitudes through teleconnection mechanisms discussed by Wallace and Gutzler (1981) and many others. Thus it is important that an atmospheric GCM should be able to accurately simulate the various timescales of transient tropical convective activity. One major mode of variability is the

intraseasonal (30 to 60 day) mode, with an eastward propagating disturbance on this timescale first being observed by Madden and Julian (1972).This mode appears to propagate around the equator in a similar way to a Kelvin wave although the phase speed is slower than would be expected for a pure Kelvin wave. It also appears that the convection in certain regions of the tropics is more sensitive to the passage of the oscillation than in others, for although the oscillation in the zonal wind field is observed at all longitudes, its effect on convective activity is only clearly observable in the west Pacific and Indian Oceans, and to a lesser extent the West Atlantic and Caribbean. Studies of the ability of GCMs to simulate this oscillation in the past (e.g. Slingo and Madden, 1991) have suggested that the period of the intraseasonal signal is too short (20-30 days) although the reasons for this have not been clearly identified. There is also a large degree of variation in the period of the oscillation at different times of the year, both in models and observations. In addition, there appears to be a geographical dependence on the phase speed of the oscillation. An observational study by Weickmann and Khalsa (1990) suggests that the phase speed of the oscillation is slowed as it passes through the warm pool region of the West Pacific and Indian Oceans. It may be that the failure of GCMs to represent this retardation in the warm pool region results in a phase speed, which when averaged around the length of the equator, is too fast.

Although it is important that GCMs be able to represent the mean circulation of the tropics, the ability of a GCM to represent the various scales of transient tropical convection must be considered to be an essential part of model validation. If the GCM is to be used for long term climate prediction experiments, the model should reproduce the correct mean climate, composed of the correct ensemble of regimes that contribute to that mean. As an example, the mean circulation in the Atlantic sector of the northern hemisphere mid-latitudes is determined by the relative dominance of blocking anticyclones and mobile westerly cyclonic systems. In a climate prediction experiment with increased greenhouse gases, it is possible that the climate of this region may change due to a change in the relative dominance of these two regimes. Similar arguments can be applied to the tropical atmosphere, i.e. the mean climate simulated by the model must be composed of the correct balance of stationary and transient features for us to have confidence in results produced from experiments conducted with changes in atmospheric carbon dioxide.

This report will examine the ability of the UKMO Unified Model GCM at climate resolution (the Hadley Centre Model) to simulate the flow of the Indian monsoon. The sensitivity of the simulation to changes in the convection scheme will be discussed (the inclusion of a convective downdraught and reformulation of entrainment rates/importance of shallow convection). The ability of the model to simulate intraseasonal tropical variability will be assessed with comparison being made to other models and observational data, and the importance of this mode of atmospheric variability to the forcing of tropical rainfall will be discussed.

2. Model Description and Experiments.

The model used to perform the integrations discussed in this report is the UKMO Unified GCM at climate resolution (the Hadley Centre Model). An overview of the Unified Model is given in Cullen (1993), but the salient points are described briefly here. It is of grid point type with a horizontal resolution of 2.5° x 3.75° and 19 layers in the vertical, using a hybrid sigma/pressure vertical co-ordinate. A conservative split-explicit integration scheme is used, and cloud water and

ice are included as prognostic variables. The annual cycle of radiation is imposed on the model which employs an interactive radiation scheme (Ingram, 1994) together with a prognostic cloud scheme (Smith (1990), Smith (1994)). The boundary layer scheme is formulated in terms of conserved variables and so can represent both dry and cloudy boundary layers (Smith, 1994). Mixing coefficients are stability dependent, using a moist Richardson number. Surface hydrology and soil temperature models are also included (Warrilow et al (1986), Dolman and Gregory (1992)). Mean orography is used together with the gravity wave drag scheme described by Palmer et al (1986), but rather than limiting the gravity wave stress by a cut-off of orographic variance, a dependence upon the Froude number of the boundary layer flow is used (Wilson and Swinbank, 1991). A mass-flux convection scheme with stability closure (Gregory and Rowntree, 1990) is used which has recently been modified to include convective downdraughts associated with deep convection (Gregory and Bett 1994). Climatologically varying sea surface temperatures (SSTs) are imposed on the model as a lower boundary condition.

The data examined from the standard version of the model are taken from the first 5 years of a 20-year control integration, initiated from a UKMO analysis for the 1st of June 1991. A parallel 5-year integration from the same initial conditions was then performed with the downdraught scheme switched off.

The impact of interannual variability of SST is also examined using results from the UKMO Atmospheric Model Intercomparison Project (AMIP) integration. This is a 10-year simulation using an observed SST and sea ice dataset for the decade 1979 -1988. A description of AMIP is supplied by Gates (1992). This period includes the extreme ENSO warm event of 1982-83 as well as another ENSO warm phase in 1986-87, so some assessment of the effects of ENSO on tropical intraseasonal variability can be made.

Comparisons are made between the Indian monsoon as simulated by the Unified Model and UKMO analysis archive climatology data, which is derived from model analyses from the Unified Model and previous versions of the UKMO operational forecast model averaged over 10 years from 1983 to 1992. Assessments of the model's precipitation simulation are based on comparisons with the climatology of Jaeger (1976). The nature of intraseasonal variability in the model is also compared to UKMO model analysis archive data. This dataset is on a high resolution (1.875° x 1.5°) grid, and has been interpolated onto the climate model grid prior to analysis. There are a small number of individual days of missing data in this dataset due to operational problems. For the purposes of spectral analysis, these missing days have been filled in by forming a mean field of the 2 days on either side of the missing record.

3 . Simulation of the Indian Monsoon.

This section will describe the Unified Model's simulation of the Indian Monsoon, with particular reference to the mean sea level pressure field, the low level wind field and the precipitation distribution and intensity. Systematic errors will be discussed and the effect of including the downdraught scheme on these errors will be assessed. Some comments on the effects of changes to the entrainment rate formulation will be made, with reference to the sensitivity of the model to the amount of mixing being performed by shallow convection. The impact of model resolution

upon the simulation will also be addressed.

3.1 Standard Simulation.

3.1.1. Mean Sea Level Pressure.

Inherent in the development of the monsoon circulation is the formation of a low pressure area over the continental landmass. This development is complicated by the presence of the Himalayas, resulting in a complex low pressure area across the mountains and the Tibetan Plateau. Figure 1 shows the 5 year mean p_{msl} field for June, July and August (JJA) from the model standard simulation and the 10 year mean JJA p_{msl} field from the analysis archive climatology. The archive climatology shows a structure with a low centre at 30°N, 90°E and a secondary centre at 30°N, 68°E. The model reproduces the position of these centres well but the central pressures are too low, particularly the western centre which is 7hPa too deep. However, it must be borne in mind that the presence of the Himalayas makes the verification and even the definition of p_{msl} in this region very difficult. Observations are sparse and station observations at very high elevations have to be interpolated to mean sea level.

The position of the monsoon trough, which extends from the more westerly of the two low pressure centres mentioned above, into the Bay of Bengal, is crucial to a correct simulation of rainfall over India during the monsoon season. This trough marks the tracks of the individual depression systems which bring precipitation across central and northern India. The model does not simulate this trough particularly well. The pressure gradient in the trough is too strong and too zonal. The axis of the trough is located in the centre of the Bay of Bengal rather than lying down the east coast of India. This will have an effect on both the low level wind over India and also on the precipitation field, which will be discussed in detail below.

The major error in the model simulation of the p_{msl} field in the Indian Ocean and West Pacific region is the development of a trough in the West Pacific, with its major axis along 22°N and a central pressure of about 1001hPa The development of this trough results in major systematic errors in the precipitation and wind fields, associated with over vigorous convective activity in the region.

3.1.2. 850hPa Winds.

The shape of the low level flow through the Indian Ocean and across the sub-continent is one of the characteristic signatures of the Indian summer monsoon. Figure 2 shows a plot of the mean JJA 850hPa winds from model and analysis. A first comparison of the model flow with climatology shows that the basic shape of this flow is captured reasonably well. There are easterly winds to the south of the equator which turn northwards and form a cross-equatorial jet along the African coast. This then turns to westerly flow with the jet maximum positioned over the Arabian Sea off the Horn of Africa. The westerly jet extends across central and southern India into the Bay of Bengal with some turning of the flow into Bangladesh. However, closer inspection shows that there are significant errors in the model simulation.

Firstly, the monsoon jet is too vigorous throughout its extent. South of the equator, the easterly flow is 5ms^{-1} too strong. The low level jet maximum in the model is correctly positioned, at 10°N, 55°W but maximum speeds in the model are in excess of 25 ms^{-1} compared with 20ms^{-1} in the climatology. The flow over the Bay of Bengal is about 10ms^{-1} too strong and too zonal, without the correct degree of cyclonic curvature over the Bay of Bengal and into Bangladesh. This is associated with the strong pressure gradient in the model simulation in this region referred to above. The main error however is the extension of the westerly jet over the Philippines and out into the West Pacific in association with the erroneous troughing in this region. The analysis data shows no penetration of westerly winds in excess of 5ms^{-1} east of the Philippines, whereas the model jet extends out to 140°E before the flow reduces below 5ms^{-1} and curves cyclonically towards Japan. Studying daily model output shows that this extended jet is not a fixed feature, but exhibits a lot of variability in both strength and position on the intraseasonal timescale. At times the flow is very zonal with westerly flow extending out into the Pacific beyond 150°E. At other times the flow east of the Philippines exhibits cyclonic curvature around the trough, becoming south-easterly or easterly to the south of Japan. There is some evidence that westerly wind bursts in the West Pacific in the model are related to the passage of the intraseasonal oscillation through the region. Figure 3 shows that 850hPa westerly wind anomalies in the west Pacific for year 2 of the standard integration tend to be preceded by positive 250hPa velocity potential anomalies, with a lag of between 5 and 10 days. During the northern hemisphere winter, spring and early summer, the velocity potential anomalies are associated with the passage of the intraseasonal oscillation as will be discussed more fully in section 4.1. Hence the westerly wind bursts appear to be triggered by the passage of the intraseasonal oscillation through the west Pacific region. However, the oscillation appears to break down in the model from late July through to September, and the relationship between low level wind and upper level velocity potential also appears to break down during this period.

3.1.3. Precipitation.

The rainfall produced by the Indian summer monsoon is vital to the agriculture and economy of the entire sub-continent. In terms of modelling the atmospheric circulation, the distribution of monsoon rainfall is also extremely important since the convection processes involved in its formation represent large redistributions of atmospheric heat and moisture. These processes become more important still when using coupled atmosphere-ocean GCMs (AOGCMs) since large exchanges of heat and moisture between ocean and atmosphere occur in this region. Hence in long period AOGCM integrations for climate change assessment, a correct distribution of tropical convection, particularly in the Indian Ocean and west Pacific, is vitally important for an accurate simulation. If the distribution of convective activity is wrong then corrections have to be applied to the ocean-atmosphere heat fluxes to maintain a realistic heat balance.

Looking at the mean model precipitation field in fig4(a), there are three major maxima all centred on 15°N. One maximum occurs just off the Indian west coast, one in the middle of the Bay of Bengal and the third to the west of the Philippines at about 135°E. This field can be compared with that of the Jaeger precipitation climatology (fig4(b)), bearing in mind the difficulties of compiling an accurate climatology, particularly over sparsely populated regions and the oceans. The maximum off the Indian west coast is correct in terms of both magnitude and position. However, the maximum over the Bay of Bengal is both too intense and wrongly located . The climatology

shows an elongated maximum of between 10 and 20mm per day, extending along the coast of Burma and into Bangladesh, whereas the model has a maximum of 28mm per day over the ocean. Studying the model's upper level divergence field (fig 5) shows a strong area of divergence over the Bay of Bengal. This indicates that the model is developing very strong deep convection with vigorous ascent throughout the depth of the troposphere in this region, resulting in heavy precipitation. The model maximum to the east of the Philippines is also in error. This indicates that the troughing and jet extension are due to the model developing over-intense convection in this region. Gill (1980) shows, using a very simple model, that a region of strong diabatic heating situated to the north of the equator will produce a strong westerly jet along its southern flank. In the GCM, this low level jet feature becomes linked to the monsoon jet resulting in the apparent extension of the monsoon flow into the Pacific.

Although the model has large precipitation errors over the oceans, its development of precipitation over land areas is reasonable, although eastern China is too dry and the precipitation minimum on the Indian east coast is not apparent.

3.2 The role of convective downdraughts.

Downdraughts are an important component of convective systems, being driven by cooling provided by the evaporation of falling precipitation and water loading. They have a substantial impact on the structure and moisture budget of the sub-cloud layer, transporting cold dry air down from the mid-troposphere. The convection scheme used in the standard simulation discussed above contains a representation of such processes. A second experiment was carried out in order to study the importance of downdraught processes in the Indian monsoon. The downdraught part of the convection scheme was removed, although evaporation of falling rain was allowed below cloud base.

The mean diagnostics from the parallel integration with no downdraught (figs 6(a), (b) and (c)) show several differences from the integration with the downdraught scheme included. Firstly the trough in the west Pacific is not as deep as in the downdraught run, although it still has the same characteristic form. The precipitation maximum associated with this trough is also smaller, suggesting that the convection in this region is less vigorous when the scheme is not applied. The strength of the low level jet is also weaker throughout its length in the run with no downdraught, although here it is now too weak with windspeeds being generally about $5ms^{-1}$ below climatological values except east of the Philippines where the jet still extends along the southern flank of the erroneous trough.

Although the downdraught scheme worsens the troughing error in the west Pacific, it clearly improves the distribution of rainfall over India. With no downdraught, the whole of India is too dry by around 3mm per day on average. The p_{msl} pattern over India and the Bay of Bengal is different in the two integrations. With no downdraught,the gradient is weaker and the monsoon trough has its axis along the Indian east coast rather than extending from the head of the Bay southwards to the east of Sri Lanka. This resembles the pressure pattern observed during monsoon breaks, and so the lack of rainfall over India with no convective downdraughts may be attributed to the model simulating a break monsoon throughout the monsoon season. The evolution of precipitation over the monsoon season is shown for one year of both the integrations in figure 7. This diagram also

includes a timeseries of the monsoon precipitation from an integration with modified entrainment rate, which will be discussed in section 3.3. In the standard experiment, the monsoon sets in very abruptly in June. The precipitation through the monsoon season is then characterized by quasi-regular variability on a timescale of around 10 days. With no downdraught included, the monsoon never becomes properly established over land areas of the sub-continent. There is a weak onset around June 15th, but the rainfall then dies away rapidly, becoming re-established again from the middle of July through to the middle of August, but total precipitation is very low throughout this period. This is consistent with the theory that the model simulates a break monsoon throughout the JJA period in the integration with no downdraught. South of the equator between 60°E and 90°E the integration with no downdraught produces a larger area of excessive precipitation (values greater than 10mm per day) than the standard integration. However, the climatology in this region should be treated with caution due to a lack of observational data.

Looking at the difference in potential temperature between the 2 lowest model layers gives a measure of the stability of this layer thus indicating how readily convection will be initiated in the 2 integrations. (fig 8) The smaller the difference in potential temperature between the 2 layers, the greater the initial buoyancy of an ascending parcel. Including the downdraught scheme decreases the stability almost everywhere over the oceans, particularly in the west Pacific. Looking at the specific humidity in the lowest layer gives another indication of the likelihood of convective activity (fig 9). The lowest model layer is much drier over central India when the downdraught scheme is not included, and therefore less convective activity is likely to be triggered over land compared with the standard integration. This lack of moisture in the lowest model layer can be attributed to the mean position of the monsoon trough which resembles that observed during monsoon breaks. The low level flow which normally carries moist air from the Bay of Bengal into central India is thus disrupted throughout the monsoon season, resulting in much reduced precipitation over land areas of the sub-continent.

3.3 Sensitivity to changes in entrainment formulation.

In the standard version of the UM, the rate of entrainment of environment air into convective clouds decreases linearly with pressure as,

$$E = e \, . \, A_e \, . \, p/p_*^2 \qquad (1)$$

where E is the entrainment rate (s^{-1}),

p is pressure (Pa),

p_* surface pressure (Pa),

and e and A_e are empirical coefficients, chosen to be 3 and 1.5 in the standard scheme.

The formulation is described in detail in Gregory and Rowntree (1990) and is used because of the bulk cloud formulation used in the convection scheme, i.e. one cloud model is used to represent the impact of an ensemble of differing cloud elements. Observations suggest that shallow convection has higher entrainment rates than deep convection. Hence in the boundary layer where deep and shallow convection coexist, a higher "net" entrainment of mass might be expected to exist over an ensemble of convective elements, while near the tropopause only deep convection is present and

so entrainment rates should be lower. The above form gives approximately the correct variation across the troposphere with an entrainment rate of $4x10^{-5}$ s^{-1} in the boundary layer and $1x10^{-5}$ s^{-1} in the upper troposphere.

The boundary layer scheme of the Unified Model has recently been modified to improve the representation of turbulent mixing (Smith, 1994) resulting in more vigorous mixing in cases when convection is present. Thus the amount of mixing provided by the convection scheme in the boundary layer may need to be reduced. Also recent comparison of the performance of the convection scheme against simulations of deep convection by an explicit cloud model (Gregory et al, 1994) have shown that the height of the cloud top is underestimated by the convection scheme due to ascents being too dilute. Improved results were obtained when entrainment rates near cloud base were reduced.

In light of these developments a modified entrainment formulation was included into the convection scheme making the entrainment rate constant with height but allowing variation between different types of convection (similar to the formulation used in the mass flux scheme of Tiedtke (1987)).

For deep convection and mid-level convection,

$$E = e \, . \, A_e / p_* \qquad (2)$$

while for shallow convection

$$E = S \, . \, e \, . \, A_e / p_* \qquad (3)$$

where S is a scaling factor.

The specification of the initial convective mass flux is also modified;

$$M_I = C \, . \, B/(p_1 - p_2) \qquad (4)$$

where M_I is the initial convective mass flux,

B is the parcel buoyancy on lifting a parcel of air from the initial convecting layer (at pressure p_1) to the next model layer (at pressure p_2)

and C is an empirical constant.

In the standard scheme C is chosen to be $5.17x10^{-4}$ and is a measure of how efficiently the convection scheme stabilises the atmosphere. In the revised scheme different values can be defined for differing types of convection although for the simulations presented below the standard value has been used for all types of convection.

Essentially the modification to entrainment in the convective clouds reduced the mixing by convection in the boundary layer. The change to the boundary layer mixing scheme should

compensate for this.

A set of sensitivity studies were performed, varying the values of e and S in order to determine the best values for use in the climate model. It is found that reducing the entrainment rate in deep convection can have a significant effect in reducing the error in the west Pacific (as illustrated by the below results). Figure 10 shows the mean JJA p_{msl}, 850hPa wind and precipitation over the monsoon/west Pacific region from one 3 year integration with the modified entrainment formulation with e and S set to 0.3 and 4 respectively. There is still a trough in the west Pacific but the central pressure is now 1008hPa as opposed to 1001hPa in the standard simulation. The central pressure in the monsoon low near 30°N 75°E is closer to observations, with the shape and gradient of the monsoon trough which extends from this centre into the Bay of Bengal also being much more realistic. In the 850hPa wind field, the strength of the flow in the jet core is more realistic. However, to the south of the equator the easterly flow is still too strong. There is more landward turning of the jet as it crosses the Bay of Bengal, and the jet extension to the east of the Philippines has been removed, although the flow is now slightly too landward over south-east Asia and into eastern China.

The distribution of precipitation over the Bay of Bengal and land areas of the Indian sub-continent and south-east Asia is much improved in this simulation. The excessive maxima over the Bay of Bengal and the equatorial west Pacific have been removed, with the maximum extending from Bangladesh down the Burmese coast being of the correct magnitude and position. There is a drier region through the centre of India, but the error in this region is only of the order of 1mm per day. South-east China is no longer too dry. However, the model does now develop too much precipitation to the south of the equator along the axis of the low level easterly jet. This "split ITCZ" feature is common to several GCMs, for instance, the ECMWF model at spectral resolutions of T42 and above produces an almost identical feature (Sperber et al. 1993).

Figure 7 shows the evolution of precipitation averaged over land-points of the Indian sub-continent south of 25°N during the monsoon season from one year of the standard experiment, the integration with no downdraught in the convection scheme and the integration with modified entrainment formulation. The standard convection scheme produces a very sudden onset to the monsoon in the second half of June. Although this is an improvement on the scheme with no downdraught which fails to produce a monsoon onset, this is still rather unrealistic since the precipitation is averaged over the entire sub-continent south of 25°N and so a gradual increase might be expected as the monsoon rains move north and west across the region. Thereafter, the precipitation in the standard experiment is characterized by strong quasi-regular variability on synoptic timescales. The integration with modified entrainment rate shows a monsoon evolution with a gradual increase in precipitation through the second half of May and into June. The precipitation is not dominated by sharp regular peaks but shows somewhat less variability on a wider range of temporal scales, with a monsoon break observed around the 1st of July. This change in the character of the variability when the entrainment formulation is changed will be discussed further in section 4.4.

3.4 Sensitivity of Monsoon to SST variations.

The simulations so far considered have used a fixed sea surface temperature climatology, the evolution through the annual cycle being constant for each year. In reality, tropical sea surface temperatures (SSTs) show large variations, especially associated with the ENSO cycle in the Pacific basin. Observational studies have shown that monsoon rainfall over India is affected by these variations (see review by Kiladis and Sinha, 1991). Previous modelling studies have attempted to assess the ability of general circulation models to represent such correlations. The TOGA MONEG model intercomparison (WMO/TD - No.470) considered the large differences in rainfall over India between 1987 and 1988 between which a switch from the warm to the cold phase of ENSO rapidly occurred. While most of the 20 models involved could simulate the large-scale, global mean response to the change in Pacific SSTs, as characterized by changes in the pattern of divergent flow in the upper troposphere, none showed any realistic signature over India where in 1988 above average rainfall fell, the converse being so in 1987.

As part of the AMIP study (Gates, 1992) a 10 year integration of the Unified Model has been carried out with observed SSTs, starting from the 1st of December 1978. In effect this simulation can be regarded as a coupled model with a perfect ocean and so provides a powerful tool to assess the ability of the current generation of atmospheric GCMs to respond to changes in boundary forcing.

Although the SSTs vary from year to year, the 10 year mean climatology of p_{msl}, precipitation and low level wind over the AMIP decade are similar to those obtained from simulations of similar length with a fixed SST climatology, although more year to year variability is seen. Previous sections of the report have considered the ability of the Unified Model to represent the mean Indian monsoon flow and so the mean over the AMIP period will not be further considered. Rather the ability of the model to simulate interannual variations in monsoon rainfall will be discussed.

Figure 11 shows the evolution of the difference in p_{msl} between Tahiti and Darwin (the Southern Oscillation Index, SOI), rainfall over Northern India, 850hPa wind to the east of the Philippines and equatorial central and east Pacific SST meaned over June, July and August (JJA) for each year of the AMIP decade. Observed timeseries are also shown for SOI and rainfall over India.

The model is able to simulate the variation in SOI through the decade, with a correlation of 0.83 being found with observations, although a systematic bias of around 2.5hPa is seen. Lower values of the SOI are associated with warm SSTs in the equatorial Pacific (fig 11(d)). Hence the model appears to be able to represent the changes in large-scale flow associated with the ENSO cycle.

Rainfall over northern India (20-30°N, 70-90°E) (fig 11(b)) is underestimated by the model (by around 2mm per day). During the latter half of the decade the amplitude of the year to year variability is captured, although very poor correlations are seen in the first half of the AMIP period. It is tempting to suggest that the tropical atmosphere was more predictable during the late 1980s, but such a view must be expressed with caution. It is known that the response of tropical rainfall to changes in SST is dependent upon the state of the atmosphere. An ensemble of four 40 year integrations (from 1949 to 1990) using observed SSTs but started from differing initial conditions has been carried out under the Hadley Centre's Climate of the 20th Century project using the same

version of the model as used for the AMIP simulation. Over the AMIP period the sequence of ensemble mean rainfall shows less correlation with observations than that shown in figure 11(b). However, over the whole 40 year period, 26% of the variance in rainfall over northern India is explained by changes in SST, significant at the 99% level. However, over northern India, the correlation between the timeseries of CRU rainfall data and that from the model over the 40 year period is low. (Rowell, Hadley Centre, personal communication)

It has already been noted that the low level monsoon jet extends too far out over the west Pacific. Figure 11(c) shows the variation of mean JJA 850hPa wind to the east of the Philippines. In years with a low SOI (1979,82,86 and 87), the low level jet extends further eastwards. Figure 12 shows average 850hPa wind for the tropics over these years and also the average of years 1980,81,83,84, and 85 (1988 is excluded here and will be discussed later). Figure 12(c) shows the difference in 850hPa winds between these 2 sets of years, clearly showing the increased westerly winds east of the Philippines in the years with a low SOI.

In years with a low SOI, winds in excess of $20ms^{-1}$ extend across both the Arabian Sea and Bay of Bengal. The response of wind over the west Pacific appears due to a weakening of the trade winds in the central Pacific due to warmer SSTs, allowing a deepening of the spurious trough over the west Pacific. The precipitation difference between these two sets of years (fig. 13) shows increased rainfall in the central and eastern Pacific and South Pacific Convergence Zone (SPCZ). Increases are also seen along the axis of the stronger jet in the Bay of Bengal and Arabian sea in the 79,82,86,87 mean with decreased rainfall over northern India. Regions of increased rainfall are associated with increased vertical motion. Rainfall is also reduced over the Sahel as noted in other studies of the impact of ENSO upon global rainfall patterns.

The year 1988 has been excluded in the above analysis because of its distinctive behaviour. Figure 14 compares the 850hPa flow for years 1987 and 1988 in the AMIP integration. During 1988, the cold phase of ENSO, the monsoon jet is well simulated with a maximum over the Arabian sea and north-eastward flow along the coast of China, as is observed (not shown). This contrasts with 1987, the warm phase of ENSO, where the low level jet extends to the east of the Philippines but, unlike 1979,82 and 86, is weaker over the Indian region. Trade winds are stronger in the central Pacific during 1988, associated with the cooler SSTs and this appears to provide an inhibiting influence on the formation of a low level jet over the west Pacific.

Figure 15 shows that modelled precipitation over the Indian sub-continent and over the equatorial Indian ocean is greater during 1988 than 1987. The magnitude of the increase is in good agreement with the observed variation (fig 11(b) for northern India) and observations over the Indian sub-continent and south east Asia shown in fig16. These data are taken from the Global Precipitation Climatology project of the Deutscher Wetterdienst (DWD report no. DWD/WZN-1993/07-1), and are a blend of gauge measurements, satellite estimates and , in regions not well covered by gauges and satellites, ECMWF forecast model predictions. Increases in rainfall are seen over India and the Arabian Sea in good agreement with observations. To the east of Japan around 135°E, modelled differences are opposite to those observed, with increased precipitation south of 15°N and decreased values between 15°N and 30°N. Rainfall increases over Indonesia and decreases in the SPCZ in both the model and the observations. Decreases are also seen in the central Pacific and along the ITCZ in both the Pacific and Atlantic during 1988.

Rainfall over northern South America is also increased during 1988 as well as over the Sahel (although the modelled variation is smaller than observed).

The model appears able to simulate not only the global mean response of the switch between the warm and cold phases of ENSO but also many local changes. This is confirmed by the mean over the ensemble of runs from the climate of the 20th century experiment discussed previously. The ensemble mean precipitation over northern India is greater in 1988 than 1987 (Rowell, Hadley Centre, personal communication). Although over the 40 year period of these integrations there is little correlation between the observed and modelled precipitation over northern India, the above results suggest that in some situations the model is able to reproduce the observed interannual variability well.

Although it has been noted that the model has several systematic errors in both its simulation of the monsoon flow and rainfall, it appears able to some degree to represent the interannual variability of the monsoon over India and surrounding regions. This gives some hope that it may be able to represent changes in monsoon characteristics due to the mechanisms of climate change such as increased greenhouse gases.

3.5 Sensitivity to Resolution.

Climate models are currently being run at many modelling centres using a variety of different resolutions, determined largely by available computing resources. The advantages of running models at higher resolutions have to be carefully balanced against the increased costs and use of computer facilities before a decision can be made about the ideal resolution to use in a particular situation. If a GCM is to be used to estimate regional climate change due to increased greenhouse forcing then it must be capable of producing regional variations with a reasonable degree of accuracy. This is particularly important in the Indian region where there are large variations in precipitation over short distances, which have a major effect on the agriculture and economy of the region. In this section, the monsoon simulation at both lower and higher resolution than the standard climate configuration (2.5° x 3.75°) will be examined to determine whether any significant improvements are brought about by increasing the resolution, or whether there is any significant deterioration in the simulation at lower resolutions.

The low resolution version of the model has a grid spacing of 5° x 7.5°, which is roughly equivalent to a spectral resolution of T21, and 19 levels in the vertical. No changes have been made to the model physics apart from some small changes to values of coefficients which are sensitive to resolution (e.g. the coefficients in the gravity wave drag scheme). Figure 17 shows the mean p_{msl} and precipitation patterns for JJA from 2 years of integration at low resolution. The p_{msl} pattern is very similar to that from the standard resolution experiment (fig. 1(a)). The pressure gradient in the monsoon trough is too strong and too zonal, with the trough axis being too far east through the Bay of Bengal. The trough in the west Pacific is slightly deeper than in the standard experiment. The precipitation field at low resolution is also very similar to the standard resolution experiment (fig. 4(a)). The two maxima in the Bay of Bengal and the west Pacific are in the same positions and of similar magnitudes to the standard experiment. The maximum along the Indian west coast is not apparent in the low resolution experiment due to reduced orographic precipitation caused by the

Western Ghats, which are not resolved at all since the Indian peninsula is only one grid-box wide.

The high resolution experiment has a grid spacing of 0.83° x 1.25° and 19 levels in the vertical. This is the resolution used in the operational forecast version of the Unified Model. The physics package is the same as in the standard climate resolution experiment, with the addition of vertical diffusion to eliminate numerical instabilities. Again, some values of coefficients have been changed to provide better results at the increased resolution and the horizontal diffusion scheme is of a different order. This integration also includes a correction to the rate of evaporation of falling precipitation. At standard climate resolution, this has the effect of reducing the precipitation maxima over the Bay of Bengal and West Pacific, although the pattern of errors is similar. The mean p_{msl} and precipitation fields for JJA from 2 years of integration are shown in figure 18. There are several significant improvements in p_{msl} on the simulation at standard resolution. The magnitude of the pressure gradient across India is more realistic, with the trough axis lying down the Indian east coast. However, the gradient is still rather too zonal when compared to the climatology in figure 1(b). The trough in the west Pacific is still present but its magnitude is reduced. The precipitation simulation at high resolution also shows several significant improvements over the standard experiment. The maximum over the Bay of Bengal is shifted into a more realistic position over land at the head of the bay. However, it is still too intense. The east-west gradient of precipitation across the Indian peninsula is well captured, with a narrow maximum down the west coast and a minimum on the eastern side. Precipitation in the west Pacific is reduced to more realistic values and more rain falls over the islands of the maritime continent, which are too dry in both the standard and low resolution experiments.

Sperber et al (1993) provide a detailed account of the sensitivity to resolution changes of the monsoon simulation in the ECMWF GCM. They show that the largest changes in the mean state and variability on timescales greater than 1 month occur between resolutions of T21 and T42. At resolutions of T42 (roughly equivalent to the resolution of the standard UKMO climate model) and above, the ECMWF model produces a split ITCZ over the Indian Ocean and a realistic maximum in precipitation across Bangladesh. However, northern India is too dry at these higher resolutions whereas precipitation amounts in this region are more realistic at T21. This contrasts with the results from the Unified Model which show that apart from some loss of detail largely due to orography, there are no major differences between the standard and low resolution versions of the model. Sperber et al also study the variability of the monsoon on different timescales. They show that a spectral resolution of T42 does not represent the synoptic scale variability in the monsoon as well as higher resolution models (T106), and may therefore be inadequate for regional studies of the Indian summer monsoon.

4. Analysis of the Intraseasonal Oscillation.

Extensive studies of the nature of the intraseasonal oscillation in both the real atmosphere and in GCMs have been undertaken in recent years. (Hayashi and Golder, 1986, 1992, Lau and Chan,

1987, Slingo and Madden, 1991 etc.) In this section, the period, propagation and structure of the oscillation in the Unified Model are examined and compared with the results of other studies.

4.1 Wave period and propagation.

Initial studies of the intraseasonal oscillation (Madden and Julian, 1972 etc.) indicated that it consists of an eastward propagating wavenumber 1 disturbance with a period of between 30 and 60 days, although many studies refer to the "40 day wave", this being an apparent mean period for the oscillation. More recently (Hayashi and Golder 1992) it has been shown that there are probably 2 distinct eastward propagating wavenumber 1 disturbances in the tropical atmosphere, with periods of 25-30 and 40-50 days.

Analysis of wave period and propagation in the Unified Model is concentrated on the upper tropospheric velocity potential (VP) field. This is inherently a large scale field, removing the need to apply spatial filtering to isolate planetary scale phenomena. The gradient of velocity potential at a given level in the atmosphere is related to the strength of the divergent flow at that level. Thus VP gives a good indication of changes in deep tropospheric heating associated with convective activity.

In the time-longitude cross-sections (Hovmöller diagrams) of velocity potential discussed below, the annual mean has been subtracted from the data and a 20 to 70 day bandpass filter has been applied to isolate variability on the intraseasonal timescale. However, the spectral analyses have been performed on unfiltered data, but the coefficients corresponding to periods of 90 days and longer have been set to zero in the wavenumber one spectral density plots in order to highlight the intraseasonal variability.

Figure 19(a) shows time-longitude sections of 250hPa VP averaged between 5°N and 5°S from the standard integration. There are clearly visible eastward propagating disturbances which take between 20 and 60 days to circle the equator, although there is also a lot of variability which does not correspond to these disturbances. Several very clear eastward propagating disturbances are visible, e.g. between March and June of year 1 with a period of about 30 days, and between April and May of year 2 with a period of about 40 days. If these time/longitude sections are compared with those from the UKMO analysis dataset, (fig19(b)) the model oscillation signal is more noisy and less coherent than in the analysis data. The analysis data shows a signal that appears to propagate continuously with few breaks, whereas in the model, there are several periods when the wave appears to break down and no propagation is visible.

An analysis of the period and wavenumber of propagating disturbances has been performed using spectral analysis of the time-longitude cross-sections. The results of this analysis on the 5 years of model velocity potential are shown in figure 20. In this analysis, the raw velocity potential fields have been used i.e. no band-pass filter has been applied to remove high and low frequency variability. The annual and seasonal cycles show up as strong signals with periods greater than 90 days. The dominant intraseasonal signals are eastward moving wavenumber 1 disturbances with a broad range of periods between 18 and 60 days. Major peaks occur at 45 and 28 days in year 1, 28 days in year 2, 40 and 32 days in year 3, 40 days in year 4 and 51 days in year 5. The 5 year mean shows peaks at 45 and 28 days. There is quite a large degree of interannual variability in both the

strength and period of the oscillation in the model despite the fact that the SSTs do not vary from year to year.

We can compare these spectra with the spectra obtained from the UKMO analysis data at 250hPa. Since we are mainly interested in wavenumber 1 disturbances, the spectrum of this component has been plotted for both model and analysis data so that the magnitudes can be more easily compared. (figs 21(a) and (b)). The amplitudes of the oscillation are in good agreement with the analysis data, and the model produces signals with a similar range of periods to the analysis data. The model appears to produce a rather broader spectrum than the analysis data which is also reflected in the comparison of the 5 year means. The two main peaks in the analysis data (at 45 and 30 days) are stronger than the model spectrum peaks at 45 and 28 days. This is a consequence of the fact that in individual years, the model produces a broad range of spectral peaks with periods ranging from 18 to 72 days, whereas the analysis data tends to show only one or two sharply defined peaks in the range 30 to 60 days. Although climatologically fixed SSTs have been used to force the model integration, there is some degree of interannual variability in the amplitude and periods of the oscillation. This variability must be internal within the atmosphere. The degree of interannual variability of the oscillation period and strength in the model appears to be on a scale similar to that in the analysis data, although, as discussed in the following section, the latter may be influenced by variations in the sea surface temperature.

4.2 Interannual Variability of SSTs - AMIP run.

In this section, the effect of allowing the SSTs to vary realistically from year to year will be assessed, using results from the UKMO AMIP integration. This run uses a dataset of observed SSTs from 1979 to 1988 to study how the atmospheric GCM responds to changes in SST from year to year, with particular interest in how the model atmosphere responds to El Niño events.

The time-longitude plots and spectra from the UKMO AMIP integration can be compared with the analysis data (fig22(a) and (b)) and, since the AMIP run has been forced with observed SSTs, comparisons can also be made between individual years. In this case data at 200hPa is used since the 250hPa level winds were not archived on a daily basis in the AMIP integration. At this level, the power in the VP spectra is about twice that at 250hPa, and the model reproduces this change with height well.

Once again, the overall impression from the time-longitude cross-sections is that the model VP field is noisier than the analyses, with periods in which the eastwards propagation breaks down completely. Figure 23 shows the wavenumber 1 spectra for the AMIP integration (fig23(a)) and the analysis climatology (23(b)). It is seen that the spectra for the AMIP years tend to have a broader range of spectral peaks than the analysis spectra.

We can observe the effect of variation of SSTs in the AMIP spectra over the 10 year period. The power in the 1983 spectrum is much lower than in the other years. This year saw a major El Niño event, with warm water spread right across the equatorial Pacific rather than being concentrated on the western side. This reduction in the amplitude of the intraseasonal oscillation corresponds well with observational studies (Lau and Chan 1988) which show that the oscillation signal was suppressed during the mature and decay phase of the 1982-83 ENSO event.

There is a remarkable degree of correspondence in the strength and period of the oscillation between the model integration and the analysis data for the 3 years for which the 2 datasets overlap; 1986, 1987 and 1988. If we compare the wavenumber 1 spectra , we can see that the overall variability in the power between the 3 years is well reproduced by the model. In 1986 the analysis data shows very strong peaks at 45 and 30 days which are closely matched by peaks in the model spectrum at the same periods. In 1987, both the model and analysis spectra show much less power than 1986. Once again, this could be related to the ENSO cycle, with the intraseasonal signal being enhanced during the onset phase in 1986, and suppressed during the mature and decay phase through 1987. The model shows a rather flat noisy spectrum in 1987. This is also the case for the analysis data, although there is one distinct spectral peak at a period of 72 days. In 1988, the intraseasonal oscillation signal once again appears to be fairly strong in both model and analysis data. The analysis shows a double peak at longer periods (45 and 60 days) with a secondary, short period peak at 19 days. In the model, the major peak is the short period peak (this time at 24 days) but there is also a fairly strong peak at 72 days with a weaker signal at 45 days.

It seems to be a common feature of the intraseasonal oscillation in GCMs that the shorter period signals tend to be amplified. Hayashi and Golder (1992) have performed a similar analysis of the GFDL R30 GCM. They show that the model produces spectral peaks at 25-30 and 40-50 days, but the 25-30 day peak is of a similar magnitude to the 40-50 day peak instead of being rather smaller. As has already been shown, this is also the case in the climatologically fixed SST integration of the UKMO model.

If the time-longitude cross-section plots of the model and the analysis data (fig22) are compared, individual oscillation events in the corresponding years can be matched up. Between March and July of 1986, there is a strong disturbance that propagates 3 times around the equator in both the model and analysis data, with almost identical period. In the model, this signal breaks down altogether in July, whereas in the analysis data it is still apparent but somewhat weaker through July and August. In 1987, the oscillation appears rather noisy in both sets of data. In the model plot, there are no episodes of propagation which go around the full length of the equator after the beginning of April until October/November whereas the analysis plot shows several rather weak eastwards propagating disturbances throughout this period. In 1988, both the model and analysis data show a strong disturbance that propagates once around the equator between the beginning of March and the beginning of May. In the model, this disturbance then breaks down completely whereas the analysis shows that rather weak disturbances continue to propagate throughout the northern hemisphere summer. The model actually shows a westward propagating signal between June and July which has no counterpart in the analysis data.

Overall, the model seems to reproduce the intraseasonal oscillation well in the northern hemisphere winter and spring, even to the extent of reproducing individual propagating events. However, in the northern hemisphere summer, the model oscillation becomes very weak or breaks down altogether, whereas although the intraseasonal signal in the analysis data does weaken to some extent through this period, eastward propagating disturbances are observed throughout. The amplitude of the oscillation signal is well reproduced in the model and the periods of variability are also well reproduced although the model signal tends to be rather noisy. The model reproduces interannual variability in amplitude due to changes in SST from year to year (largely caused by El Niño) well, with the oscillation being enhanced during the onset phase of El Niño and suppressed

during the mature and decay phases.

4.3 Sensitivity to convective downdraughts.

Various studies have shown that the skill of GCMs in simulating intraseasonal variability in the tropics is very sensitive to the choice of convection scheme used in the model (e.g. Slingo et al. (1992)). In this section, the impact of the inclusion of a convective downdraught into the Unified Model mass-flux convection scheme on the representation of the intraseasonal oscillation will be assessed.

The parallel experiment with no downdraught scheme has been analysed in the same way as the standard experiment described above. The intraseasonal oscillation appears less coherent and regular. The wavenumber 1 spectra are shown in fig24. There are strong wavenumber 1 peaks at 36 days in year 2 and 51 and 20 days in year 4, but in year 3 the signal is very weak, and this is reflected in the 4 year mean.

Switching off the downdraught scheme appears to increase the intraseasonal variability of convection in the West Pacific, Indian Ocean and in the ITCZ across the Pacific (not shown). It is thought that, although the intraseasonal oscillation is weaker with no downdraught scheme, the strength of the convection in the Indian Ocean and West Pacific is more sensitive to its passage, resulting in more variability on this timescale. With the downdraught included, the convection in the West Pacific is already too vigorous and so the passage of the oscillation cannot enhance it further

4.4. Sensitivity to changes in entrainment formulation.

As has already been shown in section 3.3, one aspect of the tropical simulation of the Unified Model (i.e. the Indian monsoon), is sensitive to the formulation of entrainment rates in shallow and deep convection. This section will examine the effect of the same parametrization change on the model's simulation of the intraseasonal oscillation.

Figure 25(a) shows the time-longitude diagrams for 3 years of model integration with the revised entrainment formulation detailed in section 3.3. The eastwards propagating disturbance is clearly visible as are some westward propagating events (e.g. June/July of year 2), and there appears to be less noise in the signal than in the AMIP integration. However, the spectral analysis of the velocity potential shown in figure 25(b) shows that the amplitude of the signal is much weaker than in the standard experiment and is therefore also much weaker than the signal in the analysis data.

Slingo and Sperber (1994), in an analysis of models participating in the Atmospheric Model Intercomparison Project, show that GCMs which produce realistic intraseasonal variability also tend to produce a strong annual cycle in tropical upper tropospheric zonal wind, whereas models

with little or no intraseasonal oscillation also tend to have a weak annual cycle. This is the case in the Unified Model. Figure 26 shows 3 years of zonal wind at 200hPa averaged between 10°N and 10°S from the UKMO AMIP integration and the modified entrainment experiment (11 day running means plotted). In the AMIP integration, the magnitude of the intraseasonal variability has been shown to be of the correct order (section 4.2) and fig.26 shows that the amplitude of the annual cycle of 200hPa zonal wind is slightly too strong . However, when the intraseasonal variability in the tropics is reduced due to the change in convective parametrization, it is noted that the magnitude of the seasonal cycle in the 200hPa zonal wind in the tropics is also reduced, and an easterly bias is introduced relative to the AMIP data. The reduction in intraseasonal variability in the zonal wind when the entrainment change is made is also clear from this figure. This confirms the inference made by Slingo and Sperber that models with a convection scheme which produces strong intraseasonal variability are those whose diabatic heating processes respond strongly to the annual cycle of radiative forcing. They also point to evidence (Slingo et al., 1994) that a model which produces more realistic convection on synoptic timescales (< 20 days) also produces more realistic intraseasonal variability. The suggestion is that the ability of a GCM to simulate variability on any given timescale is related to the simulation of variability on a wide range of frequencies. The introduction of an easterly bias in the upper tropospheric zonal winds may also affect the extratropical teleconnection patterns of the model.

4.5 Spatial Influence of Wave on Tropical Convection.

Outgoing longwave radiation (OLR) is a good indicator of the degree of convective activity in the tropics as deep convective clouds have very cold tops resulting in low values of OLR. In order to examine the spatial influence of the intraseasonal oscillation, a set of filters has been applied to the OLR field. The filters isolate variability of OLR for 3 periods; 2 to 10 days (synoptic), 10 to 25 days and 25 to 70 days (intraseasonal).

Figure 27 shows the filtered OLR variance from year 4 of the standard integration with climatologically fixed SSTs. Between 30°N and 30°S, the largest values of variance in the model OLR are on the synoptic scale in the South Pacific Convergence Zone (SPCZ). On the intraseasonal timescale however, the greatest variability is in the West Pacific. This is consistent with observations which show that the intraseasonal oscillation has its greatest influence west of the dateline (Lau and Chan, 1988). It is well known (e.g. Yasunari, 1981) that the Indian monsoon is strongly modulated on the intraseasonal timescale. However, the model shows little variability on this timescale over land areas of India and south east Asia, suggesting that the influence of the intraseasonal oscillation in the model is limited to convection over ocean areas.

A spectral analysis of the variability of VP from the AMIP integration at 4 different longitudes has been performed. (not shown). This shows that the intraseasonal oscillation is strongest as it passes through the west Pacific warm pool region at 135°E. Strong peaks are also observed in the Indian Ocean at 90°E and there is a minimum in variability in the east Pacific at 120°W. The oscillation then picks up more power as it passes through the Atlantic. There is a great deal of interannual variability in both the strength and period of the oscillation at all longitudes, and no indication that the propagation speed of the oscillation slows down as it passes through the Indian Ocean and west Pacific.

4.6 Factors important for the simulation of the Intraseasonal Oscillation.

No single theory is universally accepted as being the sole explanation for the existence of the oscillation, and it is likely that a number of different factors combine to maintain the propagation. Many of the theories which exist are backed up with studies using simplified and idealised models of wave propagation (e.g. Yamagata and Hayashi (1984)). When using a full GCM it is difficult to isolate mechanisms which might be driving the oscillation, but if the GCM produces a realistic oscillation signal, then it is reasonable to assume that the parametrization schemes are representing the necessary physical processes. Hayashi and Golder (1992) provide a review of the main theories which currently exist to explain the structure of the intraseasonal oscillation. It is generally excepted that the oscillation consists of a wavenumber 1 Kelvin wave which propagates around the equator, with its structure modified by forced Rossby waves of wavenumbers 1 and 2.

Factors which may be important to the correct simulation of the intraseasonal oscillation include the modification of the intrinsic vertical wavelength by viscosity due to cumulus momentum transport, instability due to the evaporation-wind feedback mechanism, convergence of moisture in the surface layer and geographical modulation of eastward-moving wavenumber 1 heating. Swinbank et al. (1987) have shown that tropical wave disturbances with an intraseasonal period can be excited in a GCM with an ocean covered globe on which SSTs are independent of longitude. Thus it can be concluded that orography, land-sea contrasts and zonal variations in SST are not essential to the generation of the intraseasonal oscillation. Hayashi and Golder (1992) also show that an ocean-surface model with zonally symmetric SSTs can produce an intraseasonal oscillation signal. However, it has been shown above that the interannual variation of the longitudinal distribution of SST does have a large effect on modulating the amplitude of the oscillation from year to year. Moisture effects such as the parametrization of latent heat release have an effect on the period of the wave propagation.

In a provisional analysis of twelve model representations of the AMIP period, Slingo and Sperber (1994) show that despite the improved nature of the simulation of mean climate by current climate models, there is a wide variation in their ability to represent the salient features of the intraseasonal oscillation. Some have no coherent signal at intraseasonal frequencies while others have representations of a similar quality to that described above. Further analysis of this ensemble of models may reveal factors which are important for the accurate simulation of the oscillation. One such factor initially identified by these workers is the ability of models to represent the planetary scale response to diabatic heating. Models whose diabatic heating processes respond strongly to the seasonal cycle appear to be those with a strong intraseasonal signal. This is the case in the Unified Model simulation and so indicates that the model's convection scheme responds realistically to forcing. However further analysis is necessary before such hypotheses can be confirmed.

5. Summary.

The ability of the UKMO Unified GCM to simulate the Indian monsoon has been examined and its

performance evaluated. The main features of the flow are captured although several systematic errors have been noted. The impact of including a convective downdraught within the convection scheme has been described and preliminary results from changing the way in which convective entrainment is calculated have shown that the monsoon simulation is very sensitive to the amount of mixing performed by deep and shallow convection. The simulation of precipitation over the Indian sub-continent and the west Pacific can be significantly improved by a careful choice of the entrainment coefficients in deep and shallow convection. It is clear that further investigation of the interaction of the convection and boundary layer schemes is necessary before the correct choice of coefficients can be made.

Results from the UKMO AMIP integration with annually varying SSTs have shown that the model is capable of reproducing some of the interannual variability in the monsoon that is actually observed. It is encouraging that the model can represent such climatic variability despite the systematic errors noted and gives more confidence to the use of the current model in studies of the change in Indian climate with increasing concentrations of greenhouse gases.

As well as the mean simulation of the tropical circulation, the model's representation of the intraseasonal oscillation has also been analysed and results discussed. Unlike many other climate models the Unified Model seems to reproduce the observed amplitudes and periods well, but the oscillation is somewhat more noisy and less coherent than observations, and generally breaks down during the northern hemisphere summer. The interannual variation in the model's intraseasonal oscillation has also been examined using results from the 10 year AMIP integration. The model produces good agreement with observations, with an enhanced oscillation signal during the onset phase of ENSO warm events and a suppressed signal during the mature and decay phase of ENSO.

6. Acknowledgements

This work was partially supported by the Commission of the European Communities under Contract EPOC-0003-C(MB).

7. References

Cullen, M.J.P., 1993: The Unified Forecast/Climate Model., *Meteorological Magazine*, **122.** 81-94

Cullen, M.J.P. and Davies, T., 1991: A Conservative Split-Explicit Integration Scheme with 4th Order Horizontal Advection., *Quart. J. Roy. Met. Soc.*, **117.** 993-1002

Dolman, A.J. and Gregory, D., 1992: The Parametrization of Rainfall Interception in GCMs., *Quart. J. Roy. Met. Soc.*, **118.** 455-467

Gates, W.L., 1992: The Atmospheric Model Intercomparison Project. *Bull. Amer. Meteor. Soc.*,**73**, 1962-1970.

GPCC, 1993: Global Area-mean Monthly Precipitation Totals for the Year 1988 (Preliminary Estimates derived from Rain-gauge Measurements, Satellite Observations and Numerical Weather Prediction Results). Deutscher Wetterdienst report no. DWD/WZN-1993/07-1.

Gill, A.E., 1980: Some Simple Solutions for Heat Induced Tropical Circulations. *Quart. J. Roy. Met. Soc.*, **106.** 447-462.

Gregory, D. and Rowntree, P.R., 1990: A Mass Flux Convection Scheme with Representation of Cloud Ensemble Characteristics and Stability Dependent Closure. *Mon. Wea. Rev.*, **118.** 1483-1506.

Gregory, D. and Bett, S., 1994: Representation of Downdraught Associated with Deep Convection using the Mass Flux Approach., In Preparation

Gregory, D., Kershaw, R. and Inness, P.M., 1994: Improved Convection Schemes Through Comparison with Explicit Simulations of Deep Convection., In Preparation.

Hayashi, Y. and Golder, D.G., 1986: Tropical Intraseasonal Oscillations Appearing in a GFDL General Circulation Model and FGGE Data. Part 1: Phase Propagation. *J. Atmos. Sci.*, **43.** 3058-3068.

Hayashi, Y. and Golder, D.G., 1992: Tropical 40-50 and 25-30 Day Oscillations Appearing in Realistic and Idealized GFDL Climate Models and the ECMWF Dataset. *J. Atmos. Sci.*, **50.** 464-494.

Jaeger, L., 1976: Monatskarten des Niederschlags fur die Ganze Erde. *Berichte des Deutschen Wetterdienstes*, **18.** No. 139.

Ingram, W.J., 1993: Radiation., Unified Model Documentation Paper No. 22, available from The Unified Model Librarian, FR-Div., Meteorological Office, London Rd, Bracknell, Berks. RG12 2SX

Kiladis, G.N. and Sinha, S.K., 1991: ENSO, Monsoon and Drought in India. In: ENSO Teleconnections Linking Worldwide Climate Anomalies: Scientific Basis and Societal Impact (M.H.Glantz, R.W. Katz, N.Nicholls, Eds, Cambridge University Press), 431-458

Lau, K-M. and Chan, P.H., 1988: Intraseasonal and Interannual Variations of Tropical Convection: A Possible Link Between the 40-50 Day Oscillation and ENSO? *J. Atmos. Sci.*, **45**. 506-521.

Madden, R.A. and Julian, P.R., 1971: Detection of a 40-50 day Oscillation in the Zonal Wind in the Tropical Pacific. *J. Atmos. Sci.*, **28**. 702-708.

Palmer, T.N., Shutts, G.J. and Swinbank, R., 1986: Alleviation of a Systematic Westerly Bias in General Circulation and Numerical Weather Prediction Models through an Orographic Gravity Wave Drag Parametrization. *Quart. J. Roy. Met. Soc.*, **112.** 1001-1039

Slingo, J.M. and Madden, R.A., 1991: Characteristics of the Tropical Intraseasonal Oscillation in the NCAR Community Climate Model., *Quart. J. Roy. Met. Soc.* **117**., 1129-1169.

Slingo, J.M. and Sperber, K.R., 1994: Variability in the Tropics: Synoptic to Intraseasonal Timescales, AMIP Diagnostic Subproject No. 1, Progress Report, PCMDI, University of California, Lawrence Livermore National Laboratory, Livermore, CA 94550, USA.

Slingo, J.M., Blackburn, M., Betts, A., Brugge, R., Hoskins, B.J., Miller, M.J., Steenman-Clark, L., and Thuburn, J., 1994: Mean Climate and Transience in the Tropics of the UGAMP GCM: Sensitivity to Convective Parametrization., *Quart. J. Roy. Met. Soc.* (to appear July Part A).

Smith, R.N.B., 1990: A Scheme for Predicting Layer Clouds and their Water Content in a General Circulation Model., *Quart. J. Roy. Met. Soc.*, **116**. 435-460

Smith, R.N.B., 1994: Experience and Developments with the Layer Cloud and Boundary Mixing Scheme in the UKMO Unified Model., Workshop on the Parametrization of the Cloud Top Boundary Layer, 8-11 June 1993, 319-340, ECMWF, Reading, Berks.

Sperber, K.R., Hameed, S., Potter, G.L. and Boyle, J.S., 1993: Simulation of the Indian and East-Asian Summer Monsoon in the ECMWF Model: Sensitivity to Horizontal Resolution. PCMDI Report no. 12., University of California, Lawrence Livermore National Laboratory, Livermore, CA 94550, USA.

Swinbank, R., Palmer, T.N. and Davey, M.K., 1987: Numerical Simulations of the Madden-Julian Oscillation. *J. Atmos. Sci.*, **45**. 774-788.

Tiedtke, M., 1989: A Comprehensive Mass flux Scheme for Cumulus Parametrization in Large-scale Models., *Mon.Wea. Rev.*, **117.** 1779-1800

Tiedtke, M., Heckley, W.A. and Slingo, J.M., 1988: Tropical Forecasting at ECMWF: The Influence of Physical Parametrization on the Mean Structure of Forecasts and Analyses., *Quart. J. Roy. Met. Soc.*, **114**. 639-664

WMO/TD - No. 470, 1992: Simulation of Interannual and Intraseasonal Monsoon Variability., Report of workshop, NCAR, Boulder, Colorado, USA. (21st-24th October 1991)

Wallace, J.M. and Gutzler, D.S., 1981: Teleconnections in the Geopotential Height Field During the Northern Hemisphere Winter. *Mon. Wea. Rev.*, **109.** 784-812.

Warrilow, D.A., Sangster, A.B. and Slingo, A., 1986: Modelling of Land Surface Processes and Their Influence on European Climate., Dynamical Climatology Technical Note No. 38, Available from Hadley Centre, Meteorological Office, London Rd, Bracknell, Berks. RG12 2SY

Weickmann, K.M. and Khalsa, J.S., 1990: The Shift of Convection from the Indian Ocean to the Western Pacific Ocean during a 30-60 day Oscillation. *Mon. Wea. Rev.*, **118**. 964-978.

Wilson, C.A. and Swinbank, R., 1991: Gravity Wave Drag., Unified Model Documentation Paper No. 22, available from The Unified Model Librarian, FR-Div., Meteorological Office, London Rd, Bracknell, Berks. RG12 2SZ

Yamagata, T. and Hayashi, Y., 1984: A Simple Diagnostic Model for the 30-50 day Oscillation in the Tropics. *J. Meteor. Soc. Japan*, **62**. 709-717.

Yasunari, T., 1981: Structure of Indian Summer Monsoon with around 40-day Period. *J. Meteor. Soc. Japan*, **59**. 336-354.

List of Figures.

1 p_{msl} averaged over June, July and August. (Pa)
(a). 5 year mean from standard model integration.
(b). 10 year mean from UKMO analysis archive data.

2 850hPa winds averaged over June, July and August. (ms^{-1})
(a). 5 year mean from standard model integration.
(b). 10 year mean from UKMO analysis archive data.

3. 20-70 day band-pass filtered 850hPa zonal wind and 250hPa velocity potential anomalies. Averaged over the west Pacific, 5-20°N ,120-150°E. From one year of standard integration. The velocity potential values have been multiplied by 10^{-6}.

4 Precipitation averaged over June, July and August. ($mm.day^{-1}$. Values above $5mm.day^{-1}$ shaded.)
(a). 5 year mean from standard model integration .
(b). Jaeger precipitation climatology.

5. Model divergence at 250hPa averaged over June, July and August. 5 year mean from standard integration. (Contour interval 10^6 s^{-1})

6 (a). Model p_{msl} averaged over June, July and August. 5 year mean from integration with no convective downdraught. (Pa)
(b). As (a) but for 850hPa wind. (ms^{-1})
(c). As (a) but for precipitation. ($mm.day^{-1}$. Values above $5mm.day^{-1}$ shaded.)

7. Evolution of precipitation averaged over land areas of India south of 25°N from May 1st to September 30th. For one year of integration for standard integration, integration with no convective downdraughts and integration with modified entrainment formulation. ($mm.day^{-1}$)

8 Potential temperature difference between lowest 2 model layers, (level 2 minus level 1) averaged over June, July and August. (K)
(a). 5 year mean from standard integration.
(b). 5 year mean from the integration with no convective downdraught.

9 Specific humidity in lowest model layer averaged over June, July and August. ($kg.kg^{-1}$)
(a). 5 year mean from standard integration
(b). 5 year mean from the integration with no convective downdraught.

10 (a). Model p_{msl} averaged over June,July and August. 5 year mean from integration with modified entrainment formulation. (Pa)

(b). As (a) but for 850hPa winds. (ms^{-1})

(c). As (a) but for precipitation. ($mm.day^{-1}$)

11. timeseries of; (a) modelled and observed p_{msl} difference between Tahiti and Darwin.

(b) modelled and observed precipitation averaged over northern India, 20-30°N, 70-90°E.

(c) 850hPa zonal wind averaged over west Pacific, 10-20°N, 130-150°E.

(d) sea surface temperature averaged over central and eastern Pacific, 2.5°S-2.5°N, 120-180°W.

All timeseries created from June, July, August averages over the AMIP decade (1979-88). (Observational data from University of East Anglia Climate Research Unit.)

12 (a). 850hPa wind averaged over June, July and August. 4 year mean created from years 1979, 82, 86 and 87 in the model AMIP integration. (ms^{-1})

(b). As (a) but for years 1980, 81,83, 84 and 85 in the AMIP integration.

(c). 850hPa wind difference from (a) - (b) above.

13. Difference in precipitation between years (1979, 82, 86 and 87) and (1980, 81, 83, 84 and 85) averaged over June, July and August from model AMIP integration. Contours at +/- 1.0, 2.0, 5.0 $mm.day^{-1}$.

14 850hPa wind averaged over June, July and August for model AMIP integration ($m.s^{-1}$);

(a) 1987

(b) 1988

(c) 1988 minus 1987.

15. Difference in precipitation between years 1988 and 1987 averaged over June, July and August from model AMIP integration. Contours at +/- 1.0, 2.0, 5.0 $mm.day^{-1}$.

16. Difference in precipitation between years 1988 and 1987 averaged over June, July and August from Global Precipitation Climatology Centre of the Deutscher Wetterdienst, which is a blend of surface and satellite observations and ECMWF forecast model predictions. Contours at 1.0, 2.0, 5.0 $mm.day^{-1}$.

17. (a) p_{msl} averaged over June, July and August. 2 year mean from low resolution (5° x 7.5°) integration. (Pa)

(b) Precipitation averaged over June, July and August. 2 year mean from low resolution integration. ($mm.day^{-1}$)

18. (a) p_{msl} averaged over June, July and August. 2 year mean from high resolution (0.83° x 1.25°) integration. (Pa)

(b) Precipitation averaged over June, July and August. 2 year mean from high resolution integration. ($mm.day^{-1}$)

19. Time-longitude cross-sections of 250hPa velocity potential averaged between 5°N and 5°S. Bandpass (20-70 day) filtered. (contour interval 3 x 10^6 m^2s^{-2}) from;

(a) Model standard integration

(b) UKMO analysis archive data.

20. Wavenumber/frequency spectra of 250hPa velocity potential averaged between 5°N and 5°S from 5 years of model standard integration. (contour intervals 0.2, 0.5,1.0,2.0,5.0,10.0 x 10^{12} m^4s^{-4}).

21. Wavenumber 1 spectra of 250hPa velocity potential averaged between 5°N and 5°S. Coefficients at periods of 90 days and greater have been set to zero to emphasise the intraseasonal variability.

(Power spectral density values have been divided by 10^{12} m^4s^{-4}.)

(a) 5 years of model standard integration.

(b) 5 years of UKMO analysis archive data.

22. Time-longitude cross-sections of 200hPa velocity potential averaged between 5°N and 5°S, Bandpass (20-70 day) filtered. (contour interval 3 x 10^6 m^2s^{-2}) from;

(a) 10 years of model AMIP integration

(b) 5 years of UKMO analysis archive data

23. Wavenumber 1 spectra of 200hPa velocity potential averaged between 5°N and 5°S, Coefficients at periods of 90 days and greater have been set to zero to emphasise the intraseasonal variability.

(Power spectral density values have been divided by 10^{12} m^4s^{-4}.) from

(a) 10 years of model AMIP integration

(b) 5 years of UKMO analysis archive data

24. As (19) but for 4 years of model integration with no convective downdraughts.

25. (a) Time-longitude cross-sections of 200hPa velocity potential averaged between 5°N and 5°S, bandpass (20-70 day) filtered. (contour interval 3 x 106 m^2s^{-2}) from integration with modified entrainment formulation.

(b) Wavenumber 1 spectra of 200hPa velocity potential averaged between 5°N and 5°S, from integration with modified entrainment formulation.

Coefficients at periods of 90 days and greater have been set to zero to emphasise the intraseasonal variability. (Power spectral density values have been divided by $10^{12}m^4s^{-4}$.)

26. Timeseries of zonal mean zonal wind (u) averaged between 10°N and 10°S from UKMO analyses, AMIP integration and modified entrainment integration. It should be noted that the years shown for the 3 series are not concurrent, so direct comparisons between individual years are not possible. The aim is to show the general differences in the amplitude and bias in the seasonal cycles.

27. Variance of outgoing longwave radiation (OLR) from year 4 of the standard model integration. $((W.m^{-2})^2)$ Bandpass filters have been applied to separate the variance into;
    (a) Periods between 2 and 10 days.
    (b) Periods between 10 and 25 days.
    (c) Periods between 25 and 70 days.

(a)

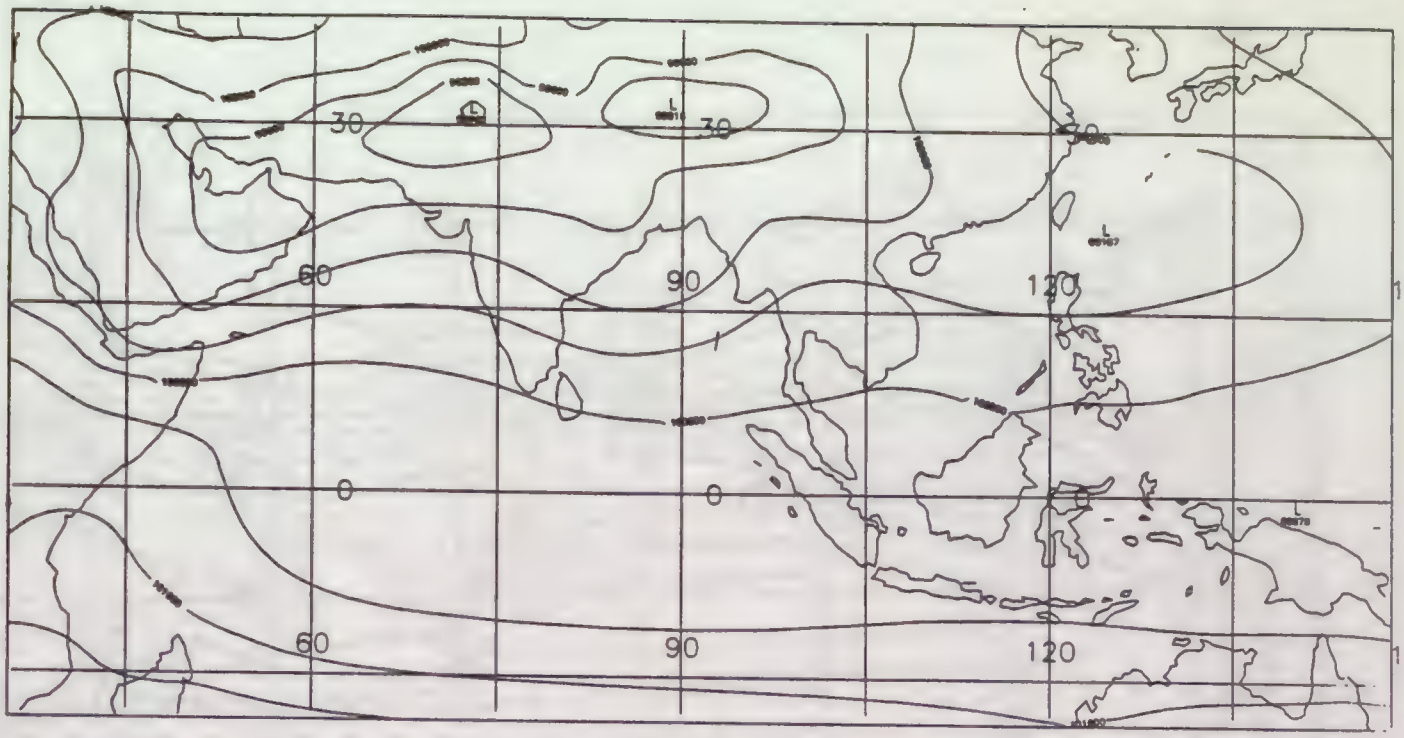

(b)

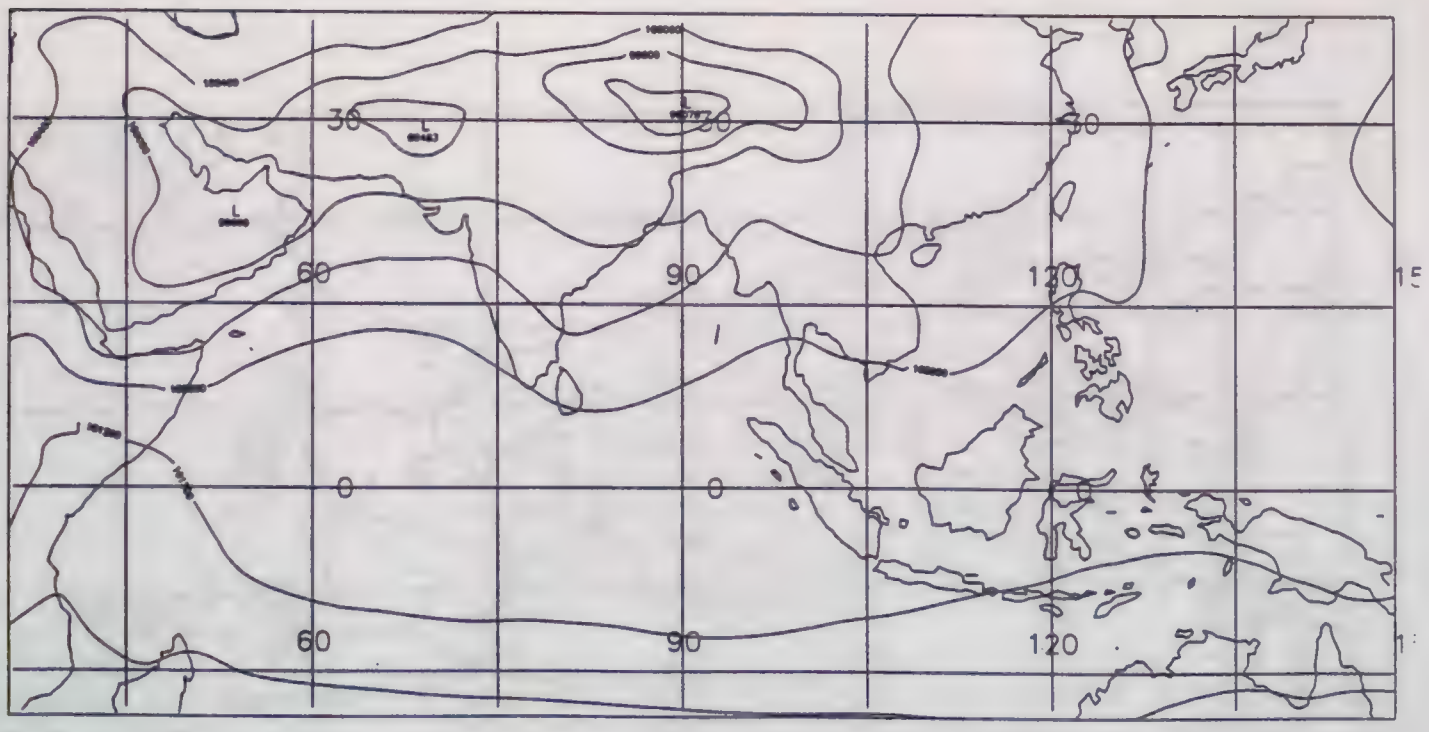

Figure 1.

(a)

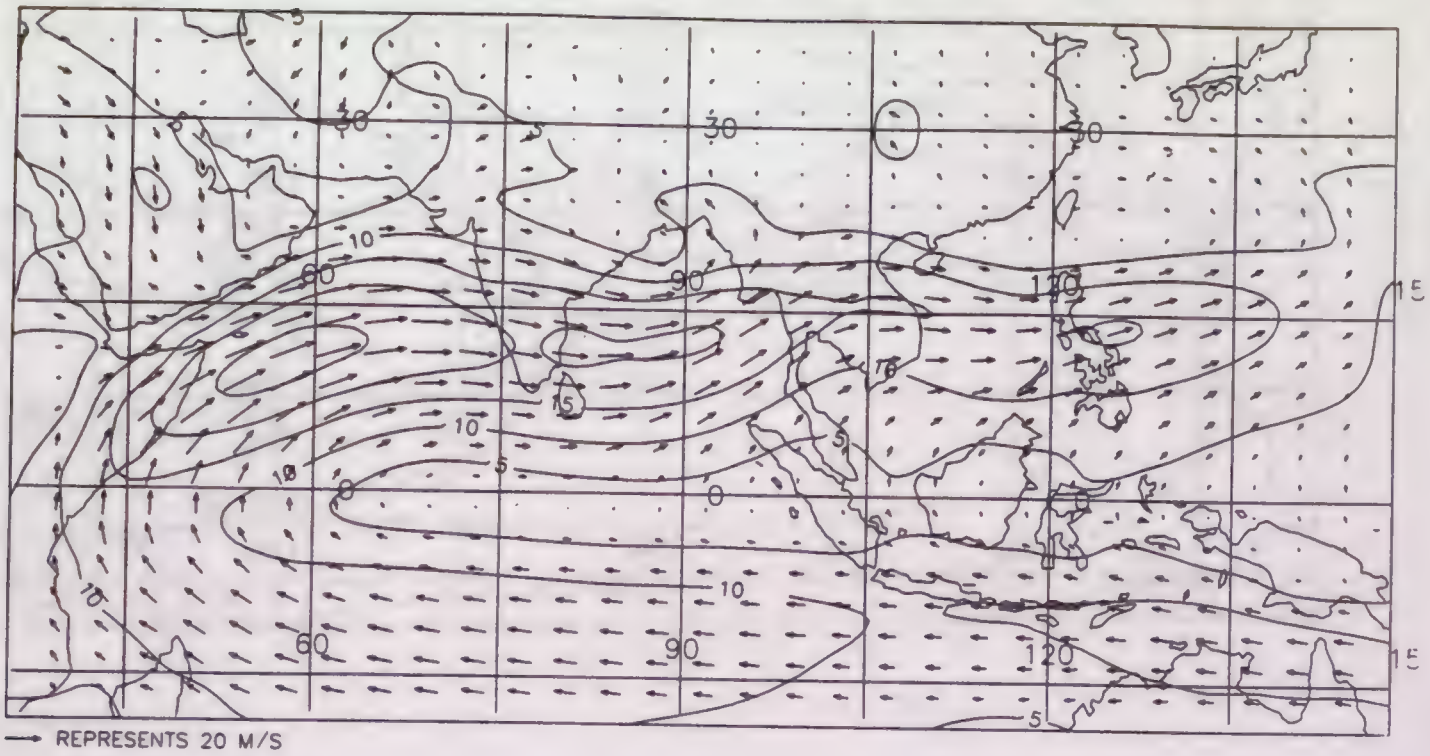
30
30
30
10
60
90
120
15
10
5
0
10
60
90
120
5
REPRESENTS 20 M/S

(b)

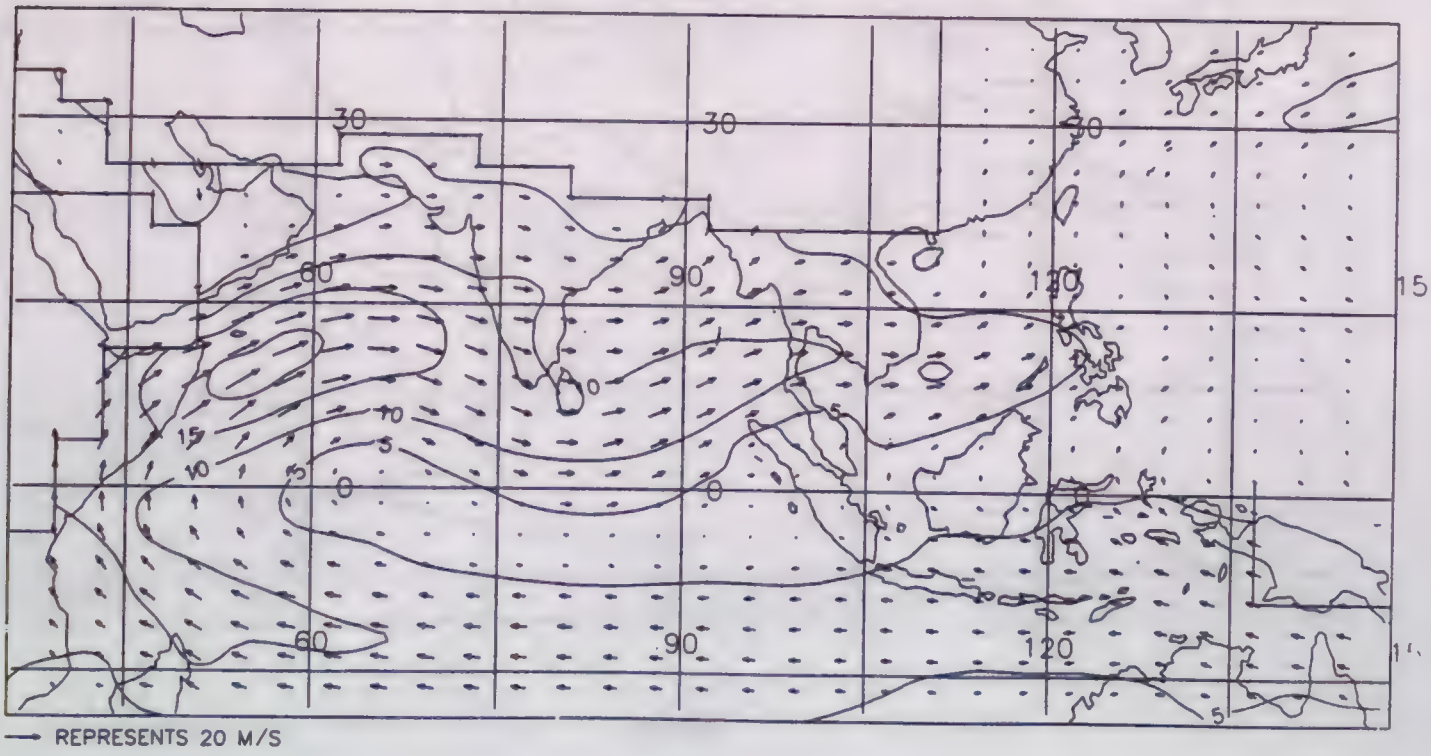
30
30
30
60
90
120
15
10
5
0
60
90
120
5
REPRESENTS 20 M/S

Figure 2.

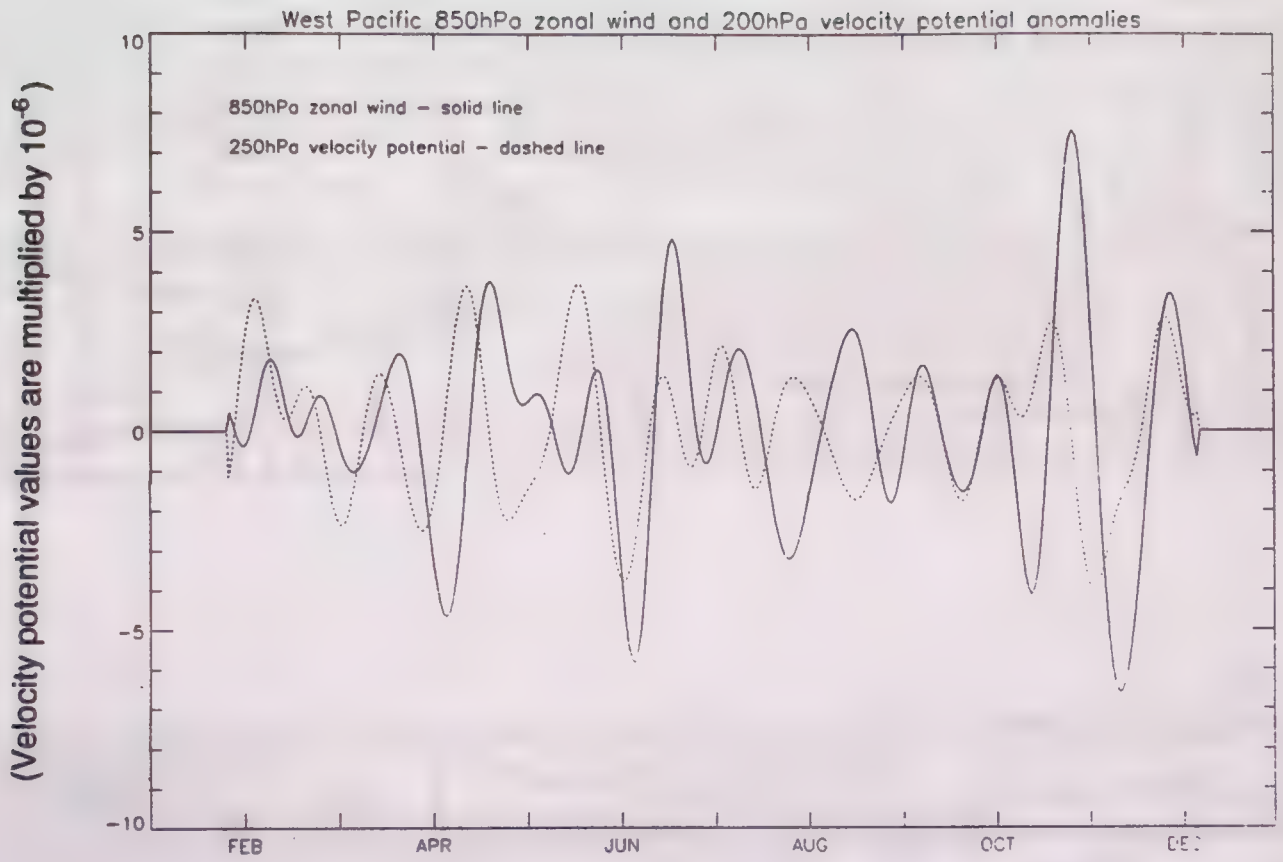
West Pacific 850hPa zonal wind and 200hPa velocity potential anomalies
850hPa zonal wind – solid line
250hPa velocity potential – dashed line
(Velocity potential values are multiplied by 10^{-6})
10
5
0
-5
-10
FEB
APR
JUN
AUG
OCT

Figure 3.

(a)

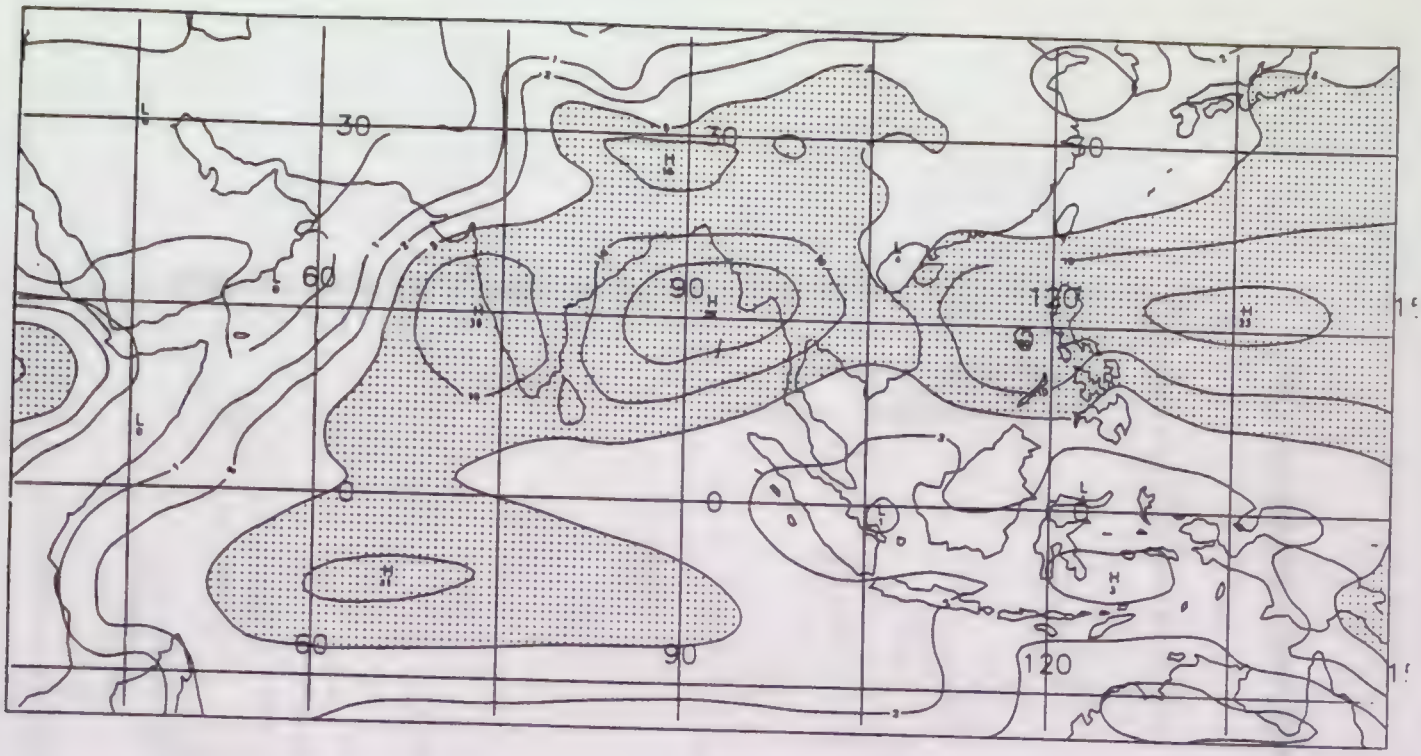

(b)

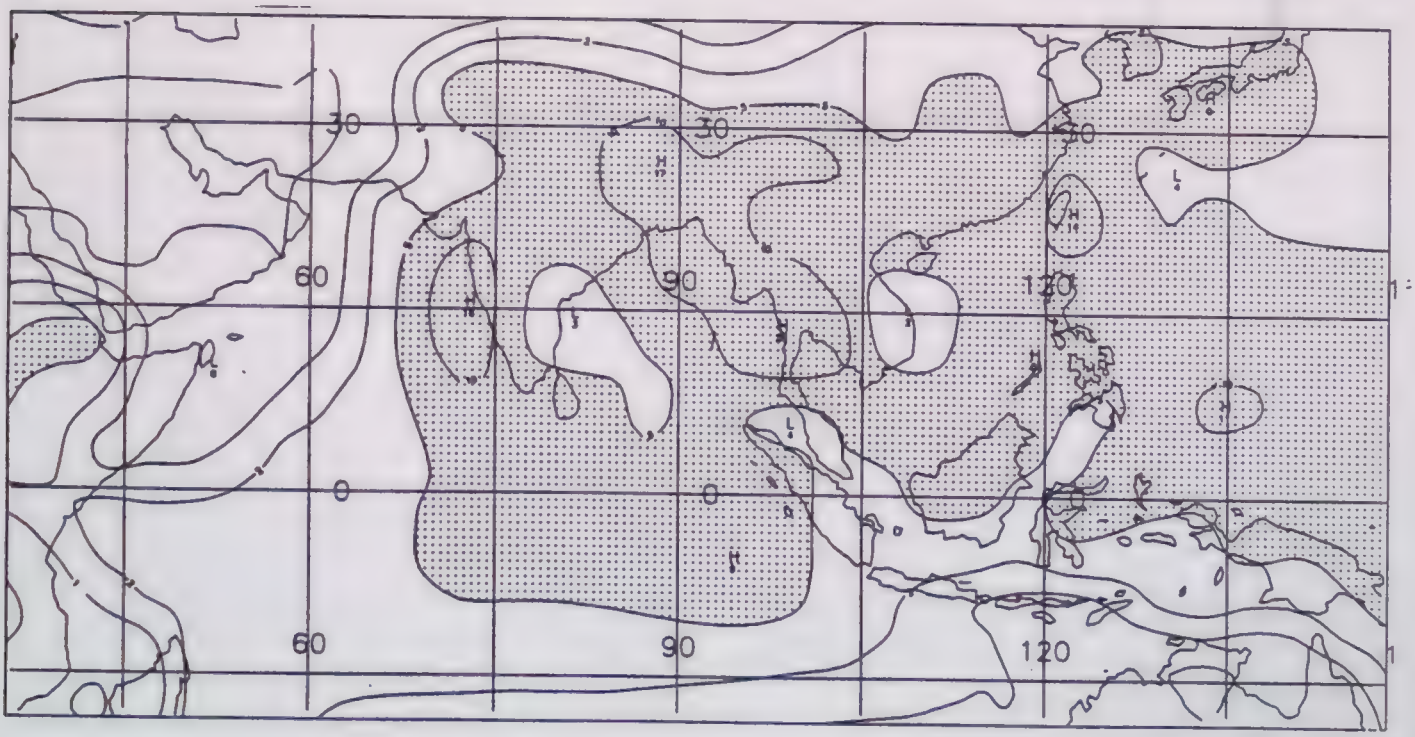

Figure 4.

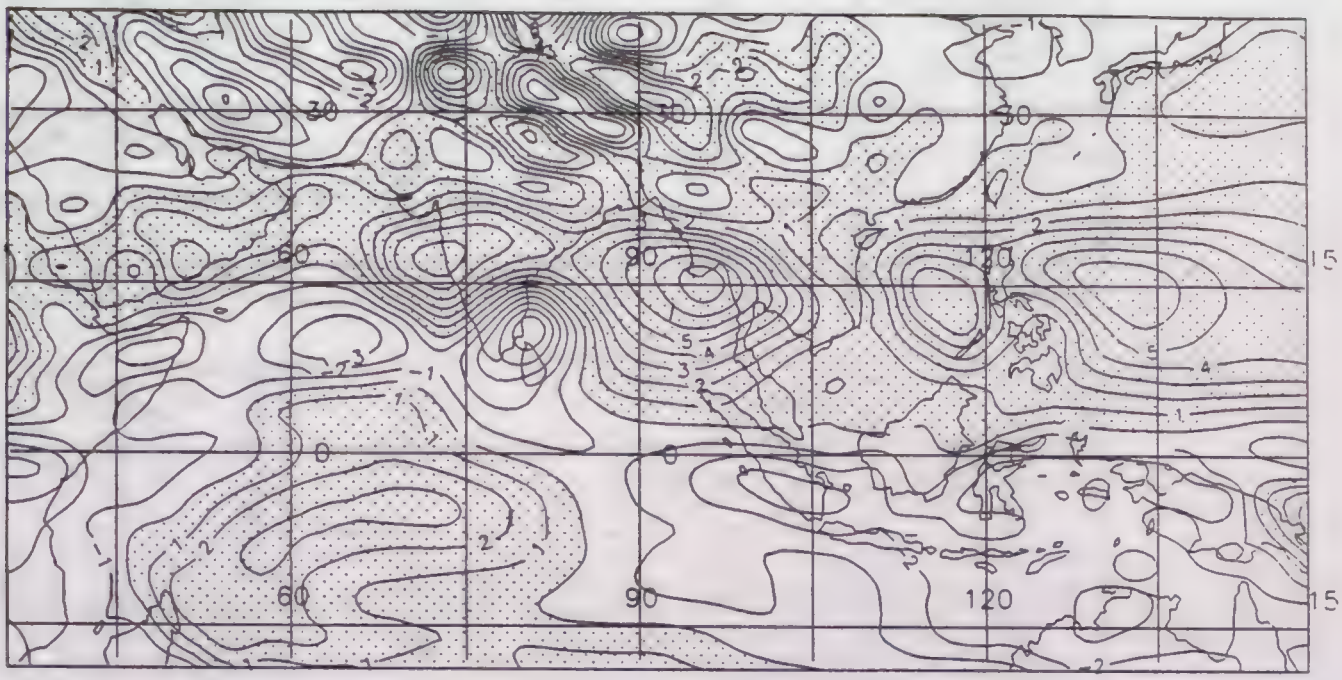

Figure 5.

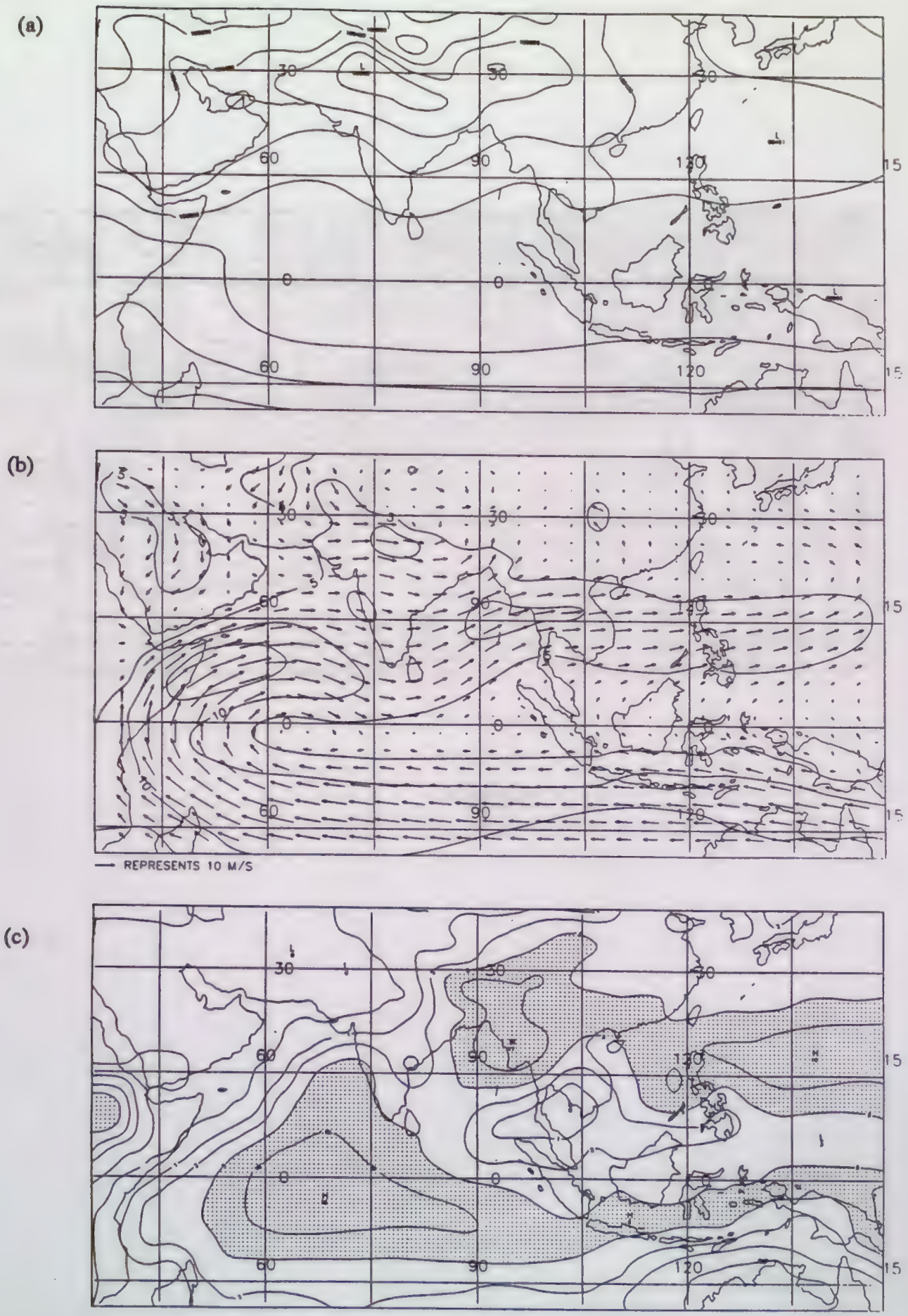

Figure 6.

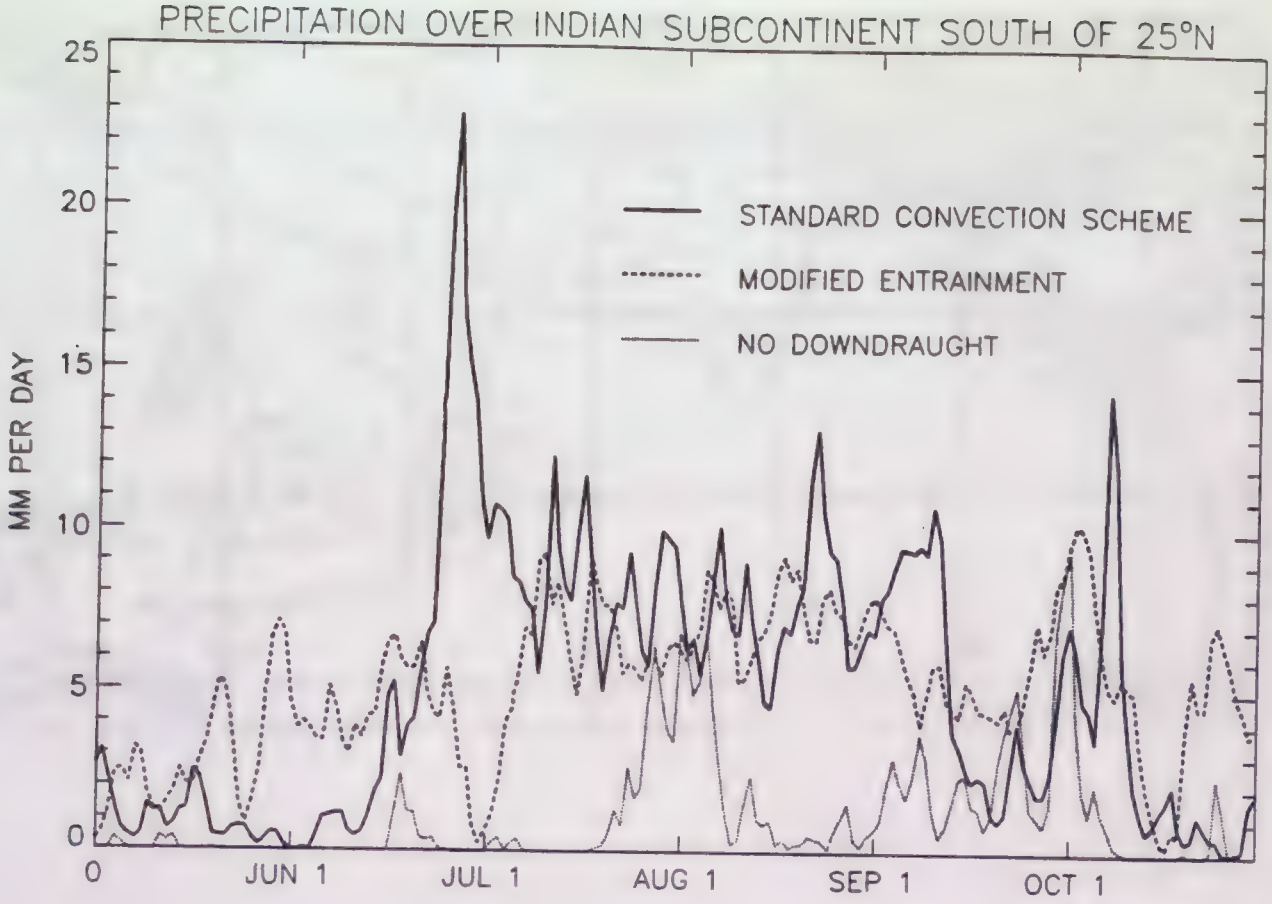
PRECIPITATION OVER INDIAN SUBCONTINENT SOUTH OF 25°N
MM PER DAY
25
20
15
10
5
0
0
JUN 1
JUL 1
AUG 1
SEP 1
OCT 1
STANDARD CONVECTION SCHEME
MODIFIED ENTRAINMENT
NO DOWNDRAUGHT

Figure 7

(a)

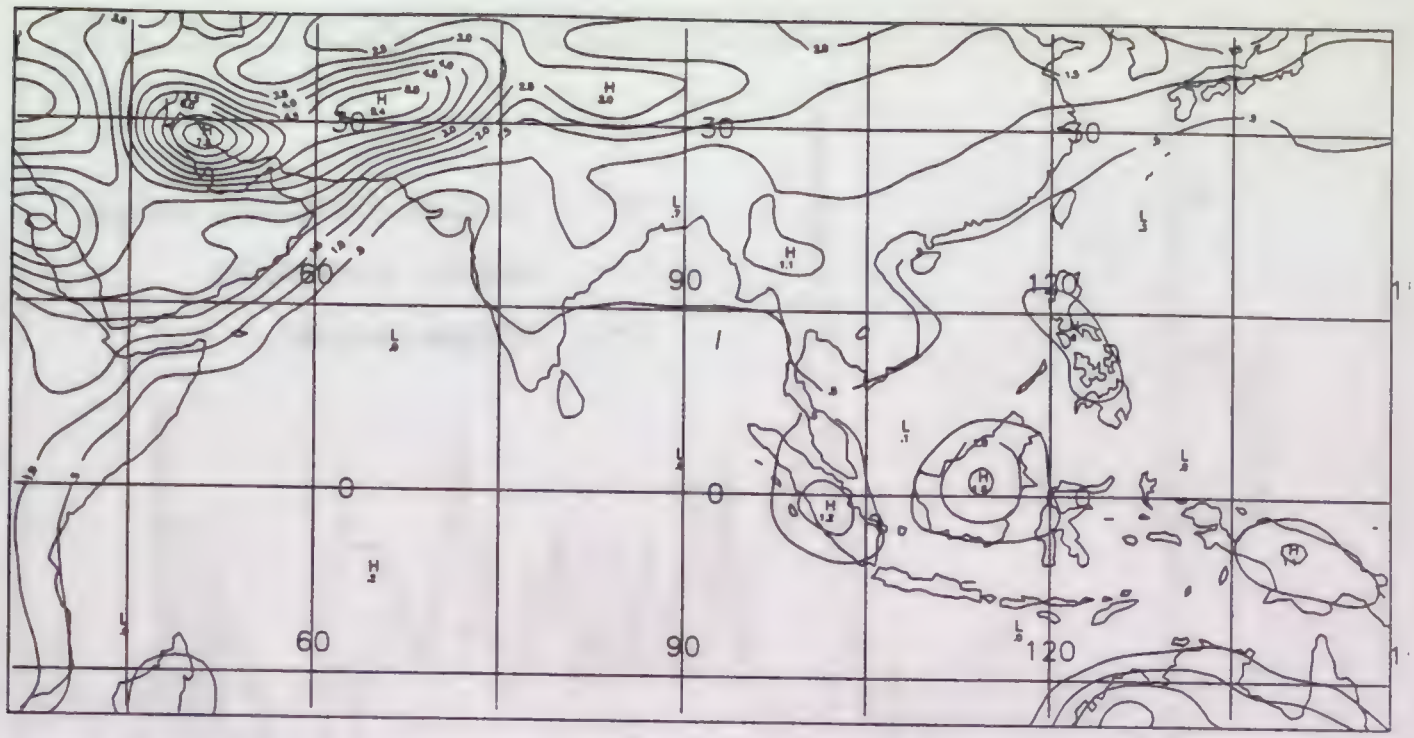

(b)

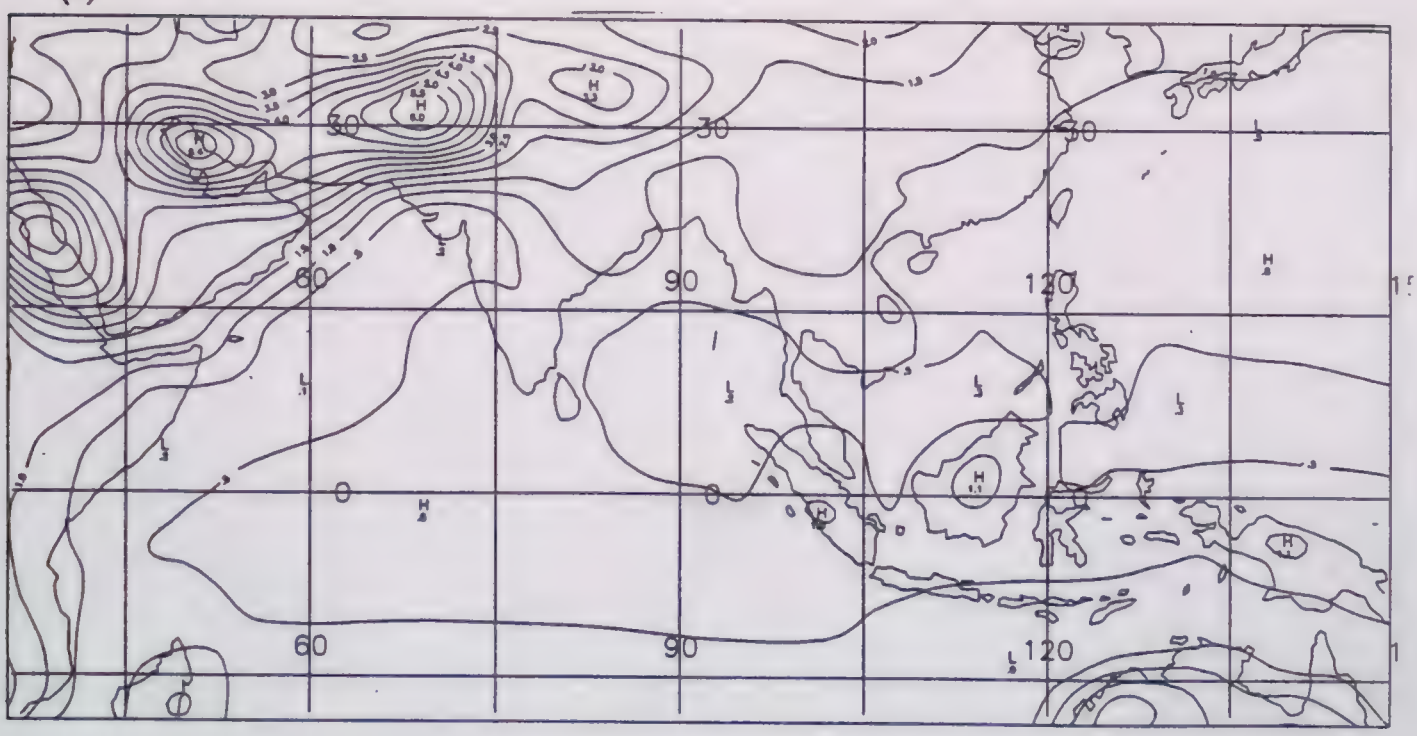

Figure 8.

(a)

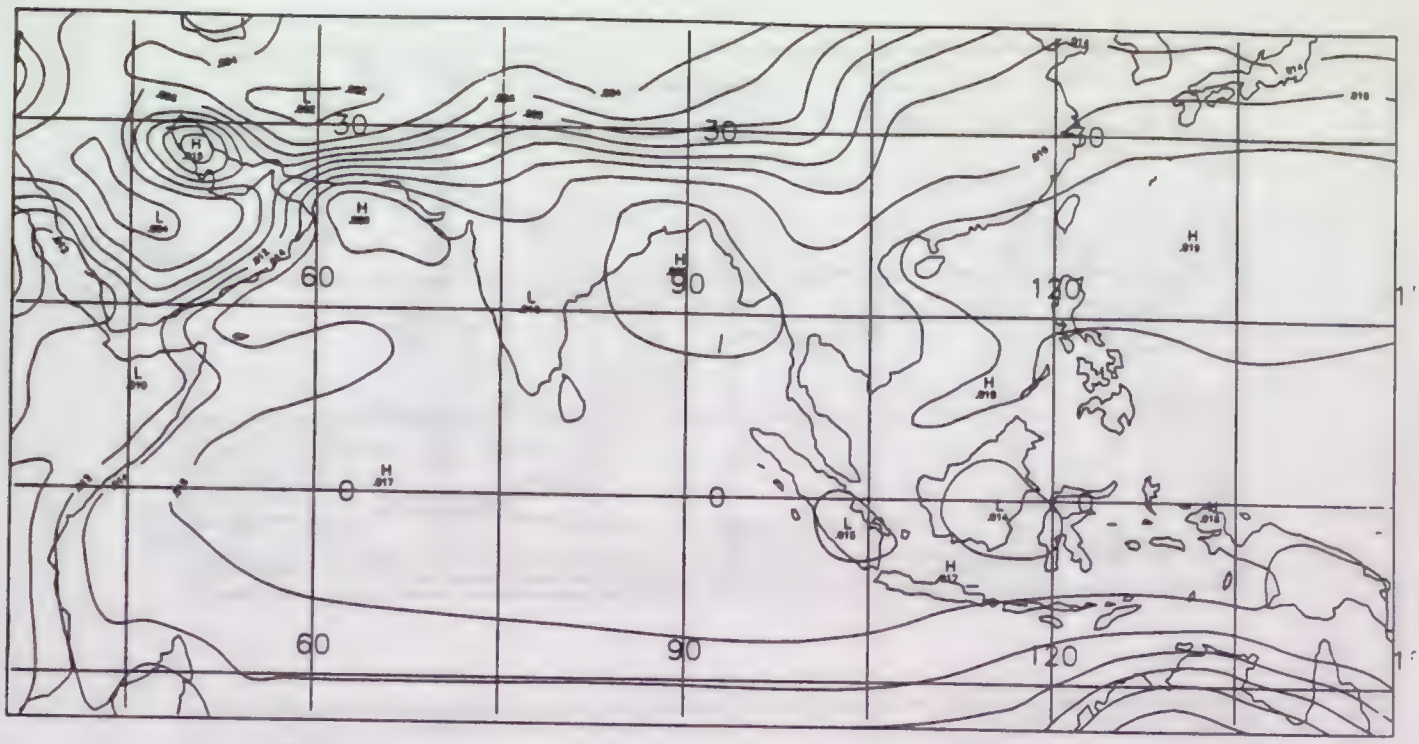

(b)

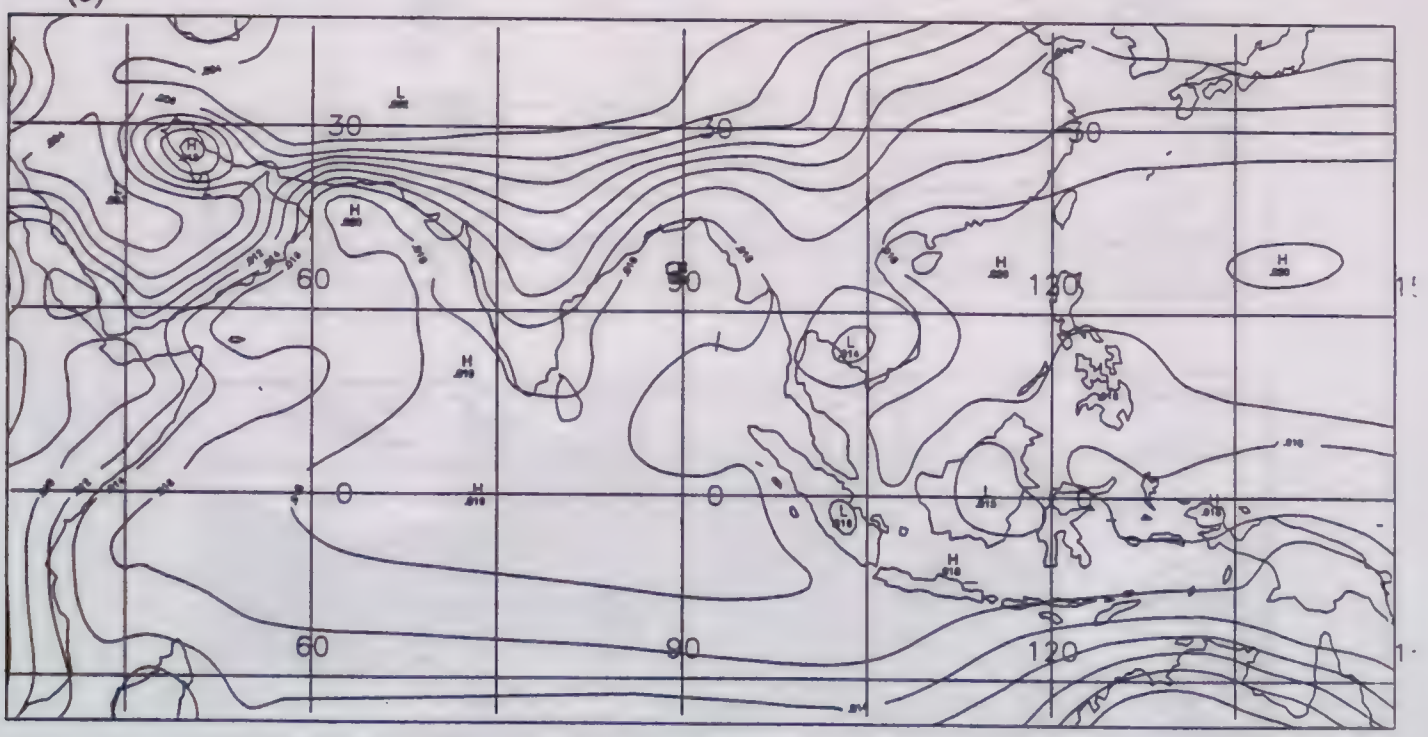

Figure 9.

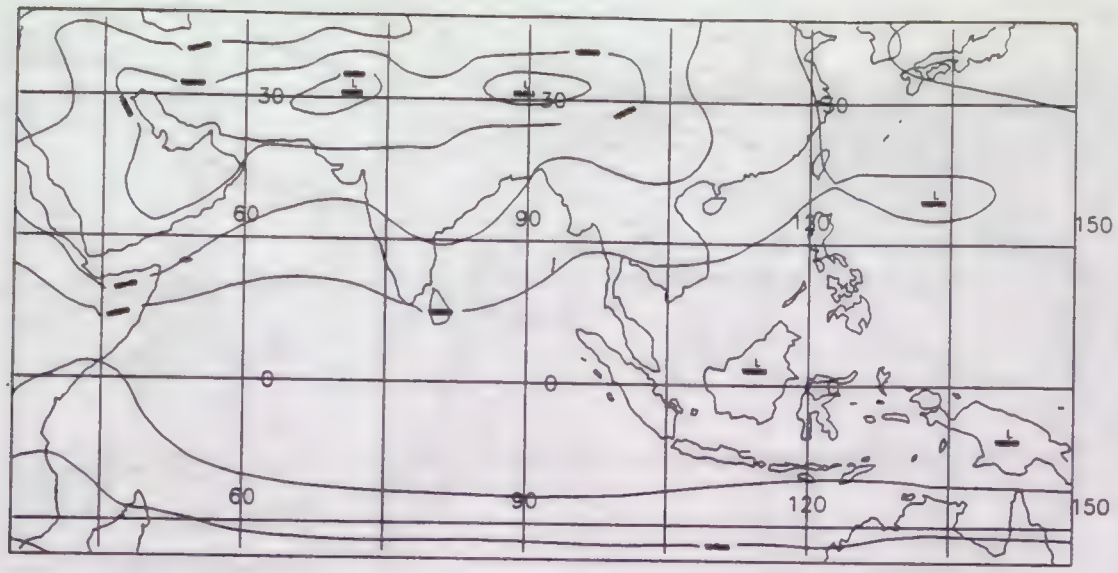
30
30
30
60
90
120
150
0
0
60
90
120
150

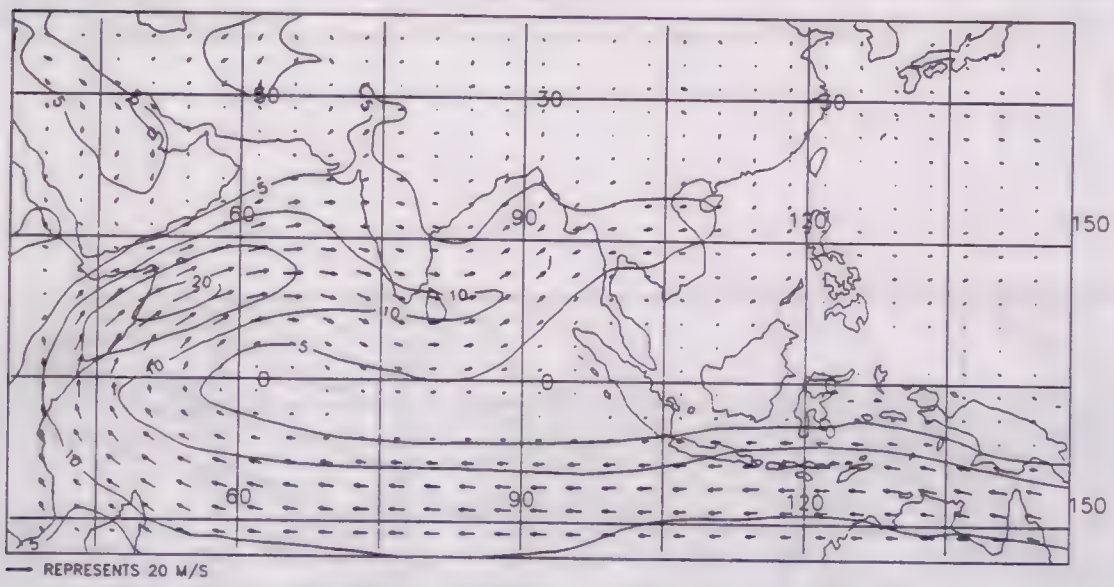
30
30
30
60
90
120
150
30
10
10
5
0
0
60
90
120
150
— REPRESENTS 20 M/S

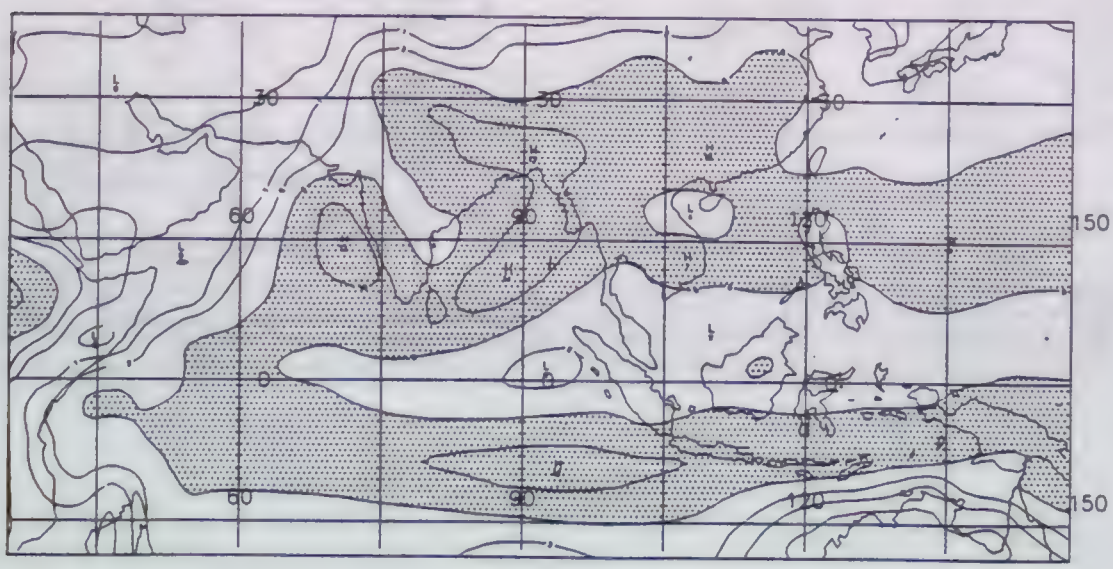
30
30
30
60
90
120
150
0
60
90
120
150

Figure 10

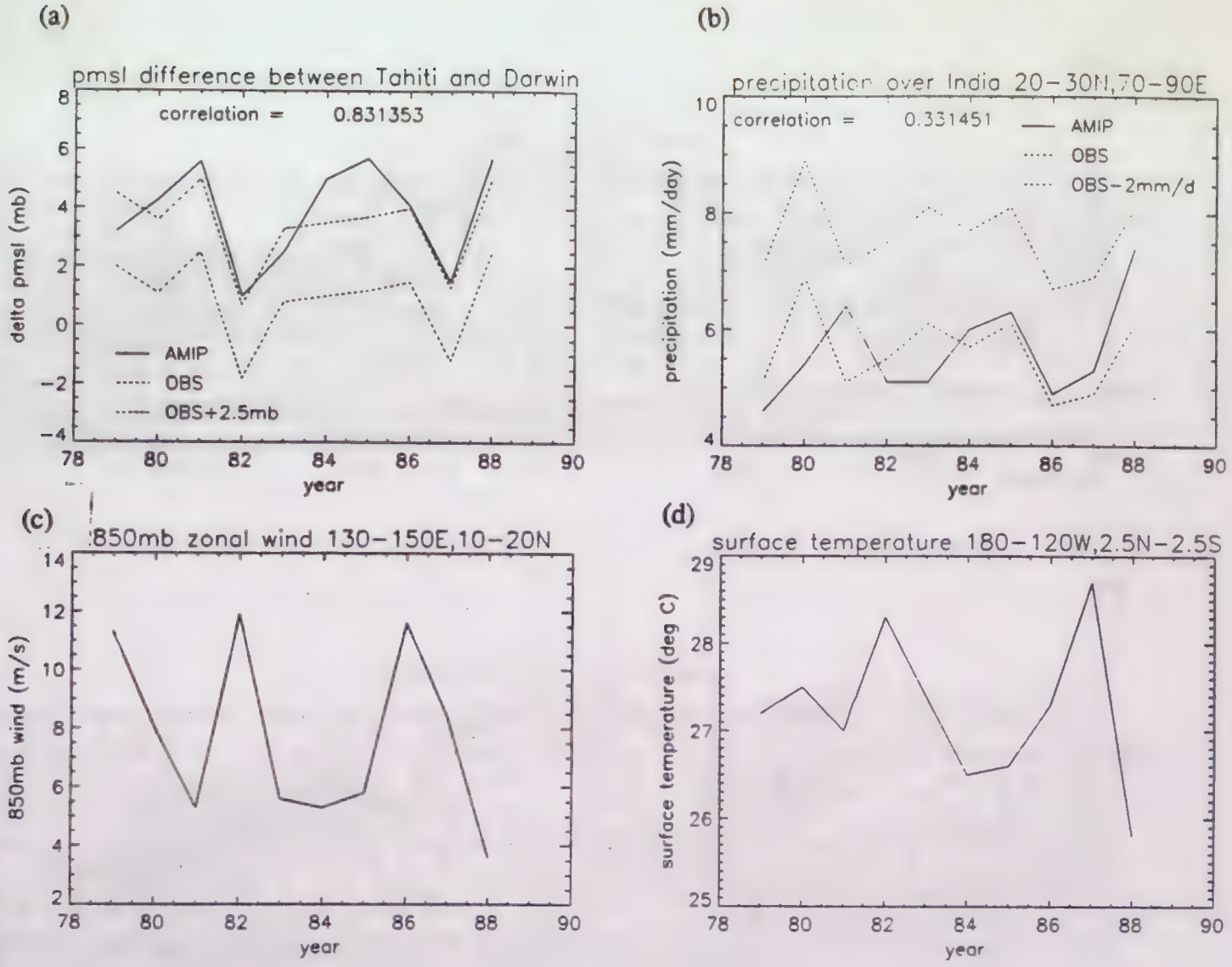
(a)
pmsl difference between Tahiti and Darwin
correlation = 0.831353
delta pmsl (mb)
AMIP
OBS
OBS+2.5mb
year
(b)
precipitation over India 20-30N,70-90E
correlation = 0.331451
precipitation (mm/day)
AMIP
OBS
OBS-2mm/d
year
(c)
850mb zonal wind 130-150E,10-20N
850mb wind (m/s)
year
(d)
surface temperature 180-120W,2.5N-2.5S
surface temperature (deg C)
year

Figure 11

(a)

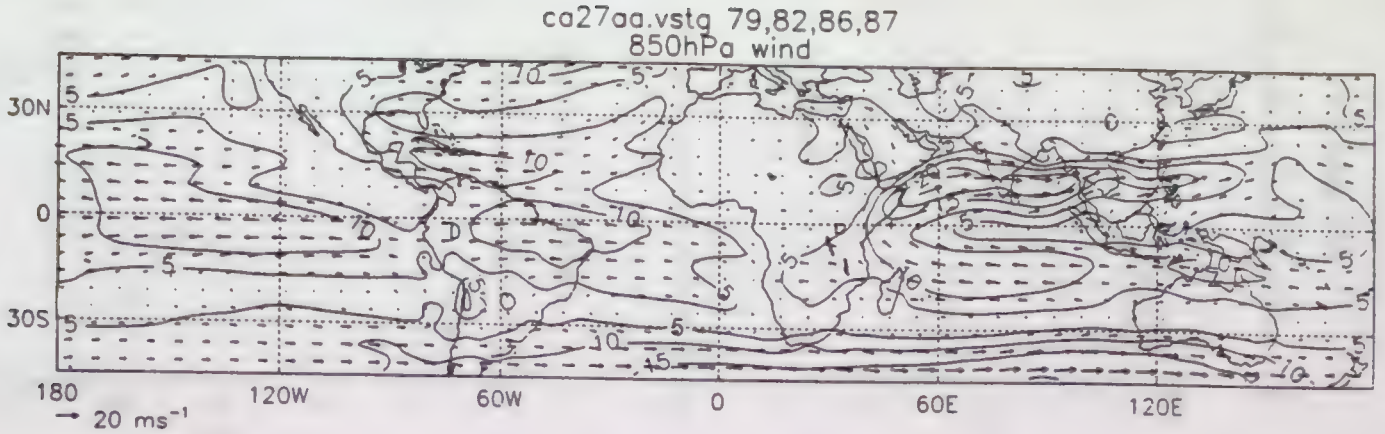

(b)

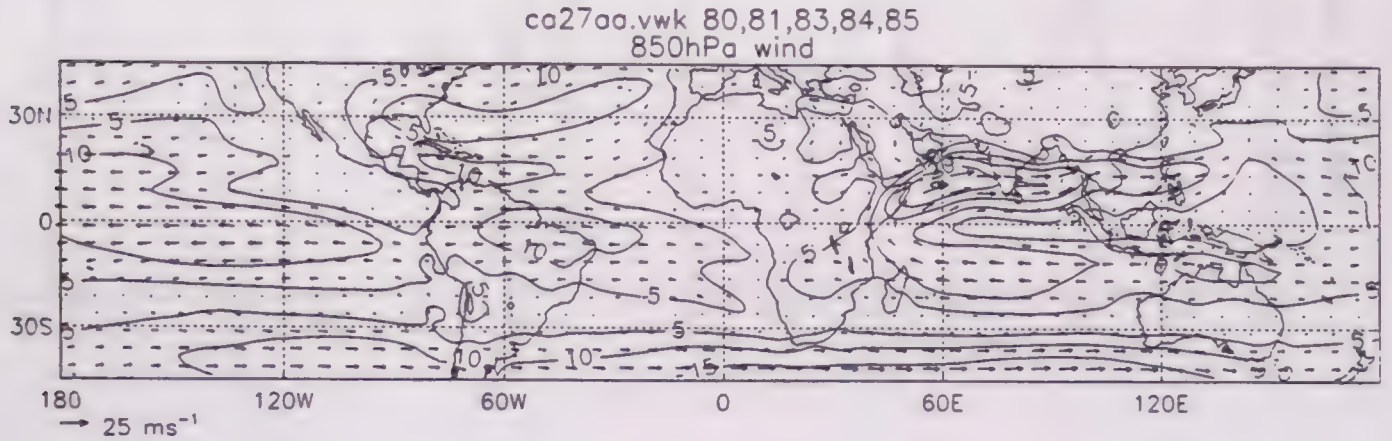

(c)

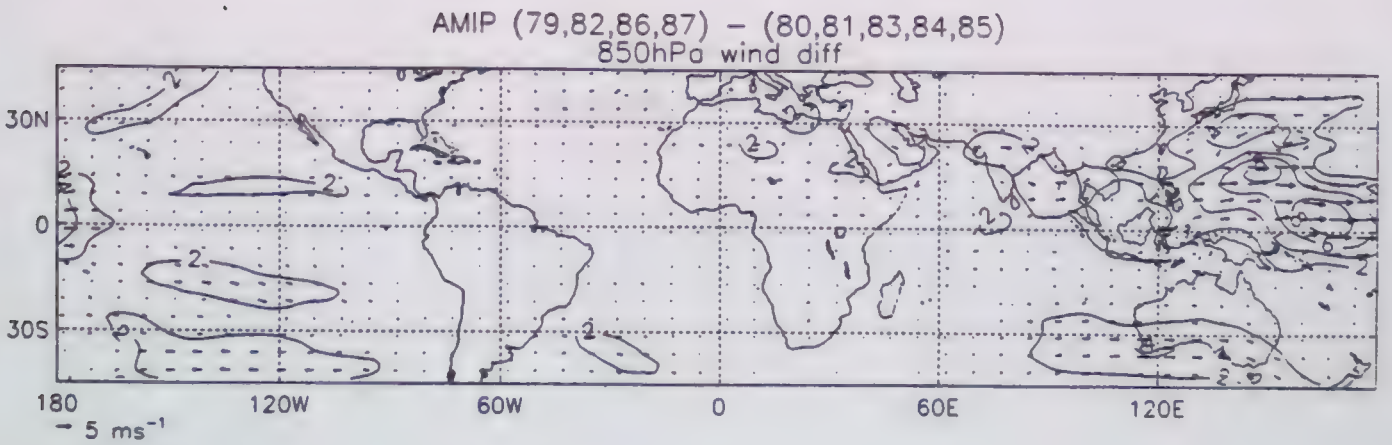

Figure 12.

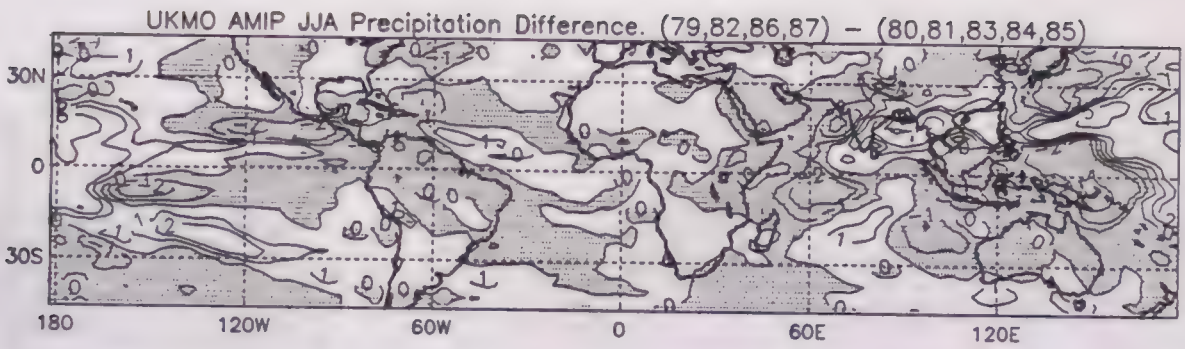
UKMO AMIP JJA Precipitation Difference. (79,82,86,87) – (80,81,83,84,85)
30N
0
30S
180
120W
60W
0
60E
120E

Figure 13

(a)

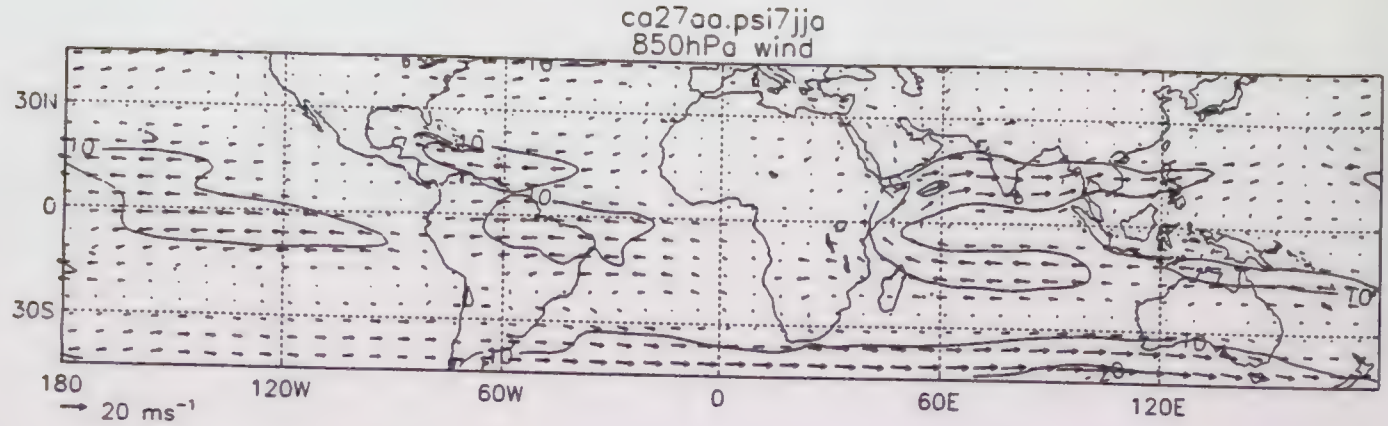

(b)

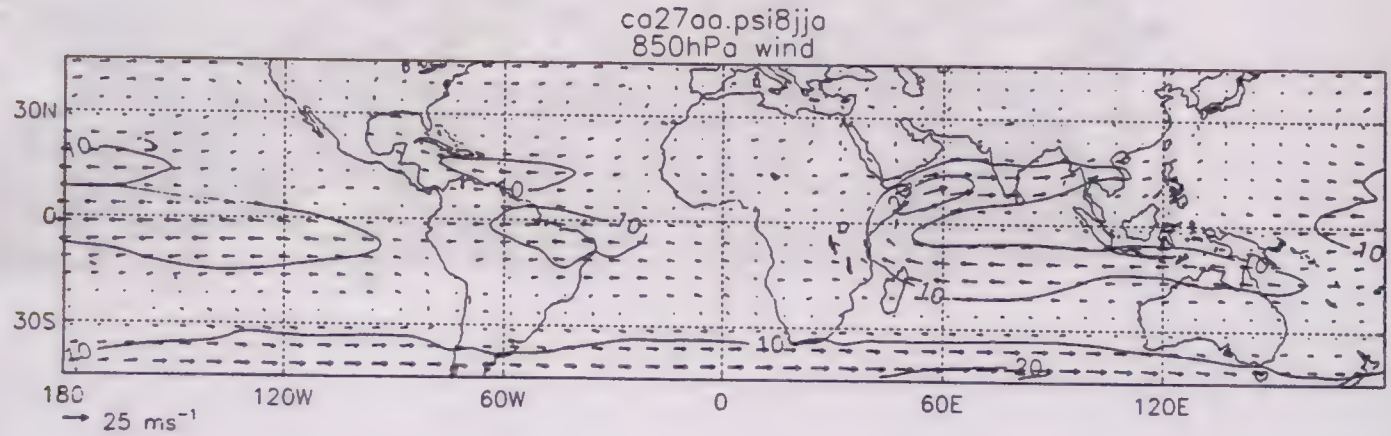

(c)

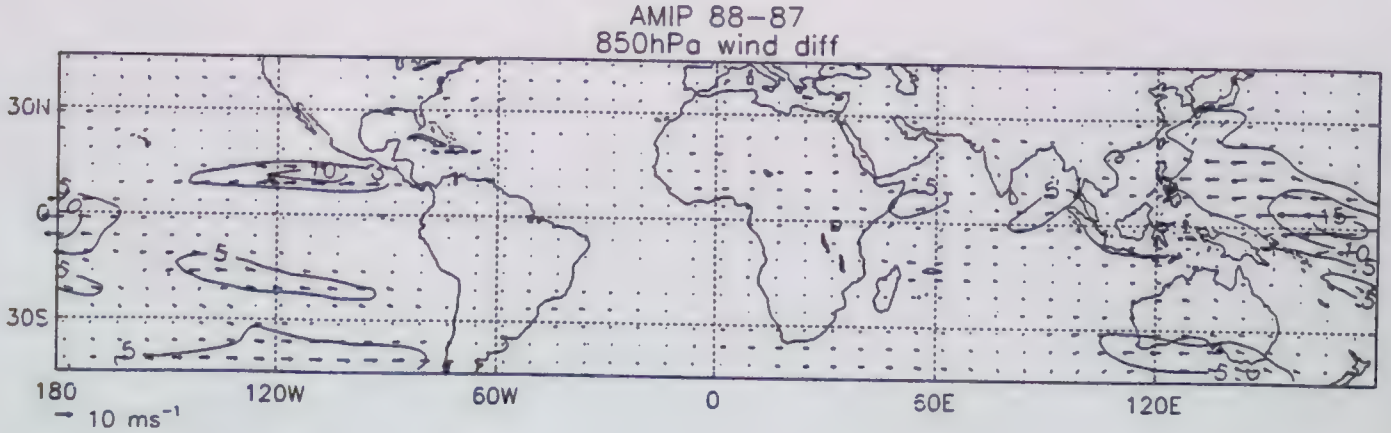

Figure 14.

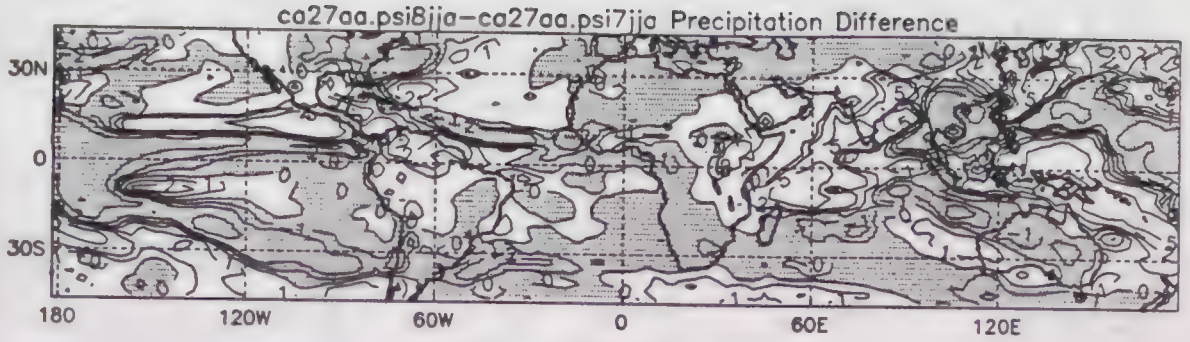

Figure 15

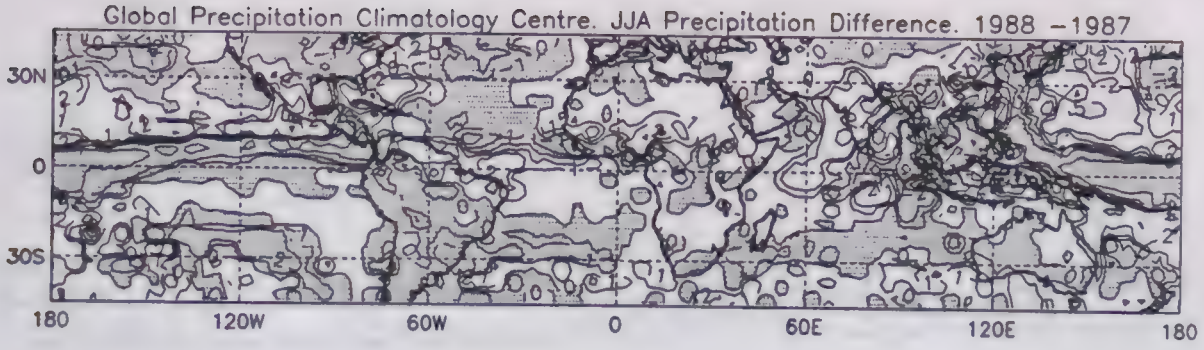

Figure 16

(a)

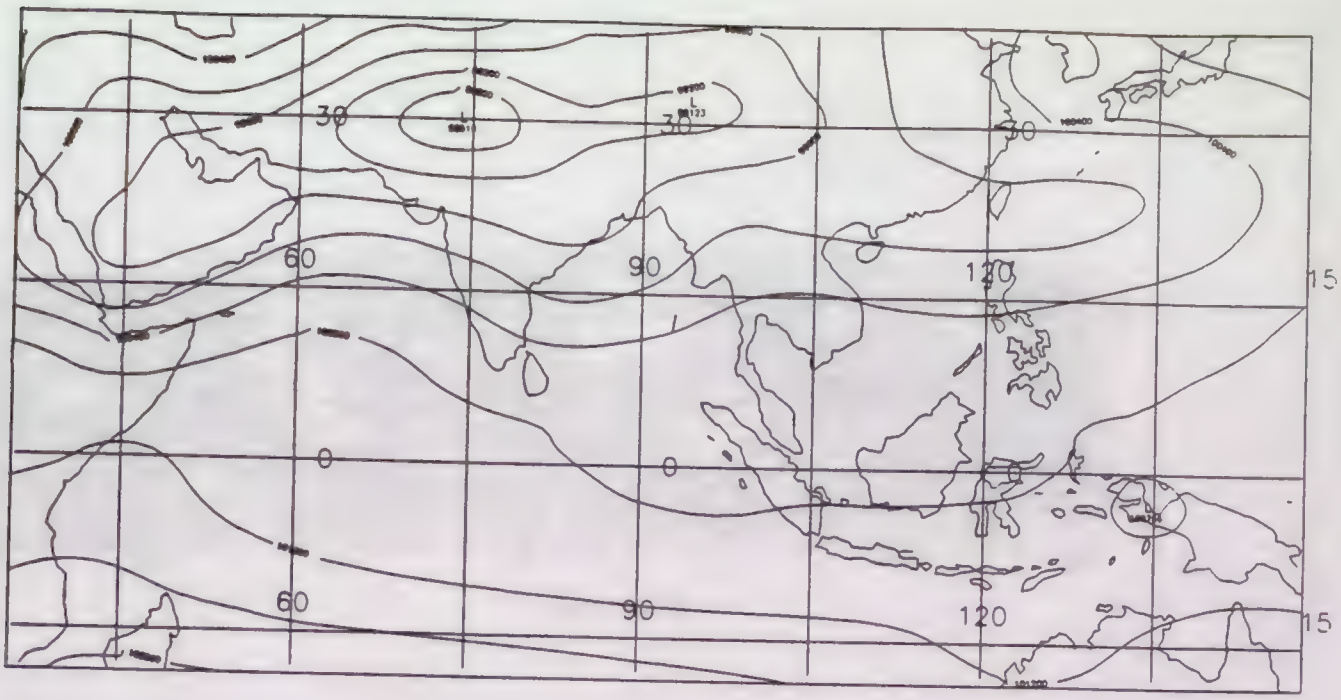
30
30
30
60
90
120
15
0
0
0
60
90
120
15

(b)

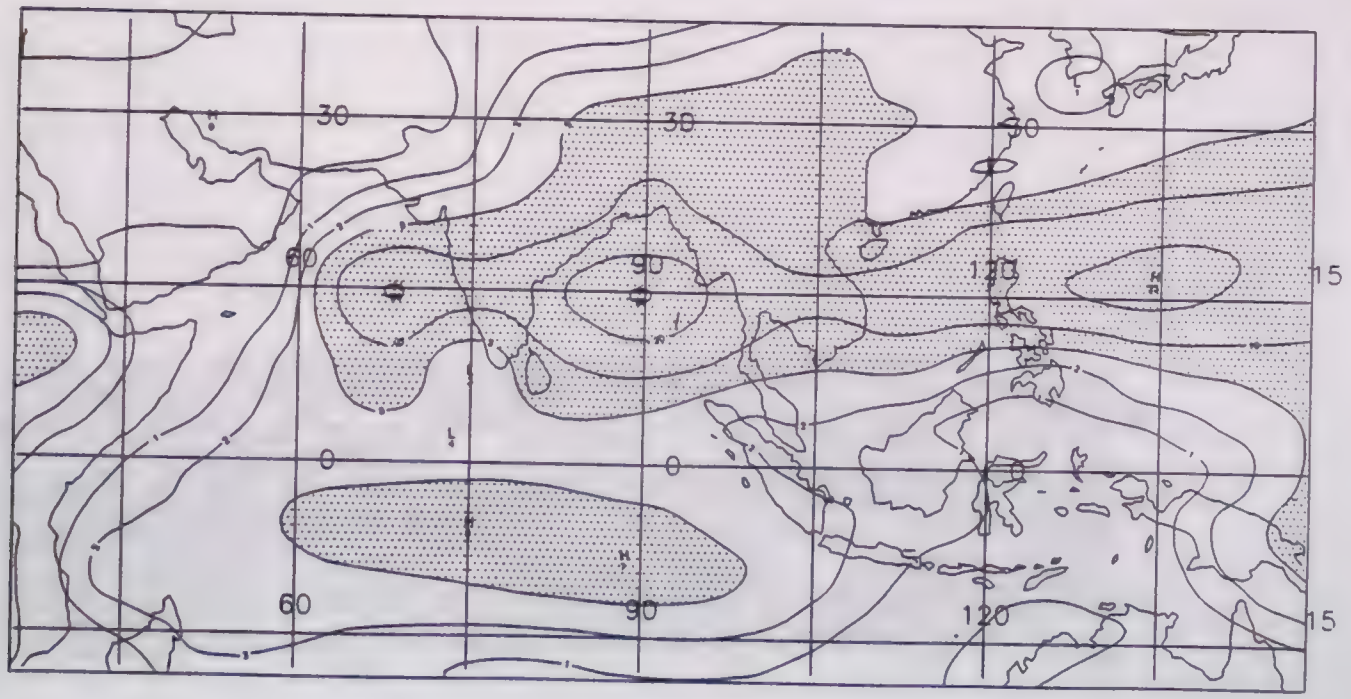
30
30
30
60
90
120
15
0
0
0
60
90
120
15

Figure 17

(a)

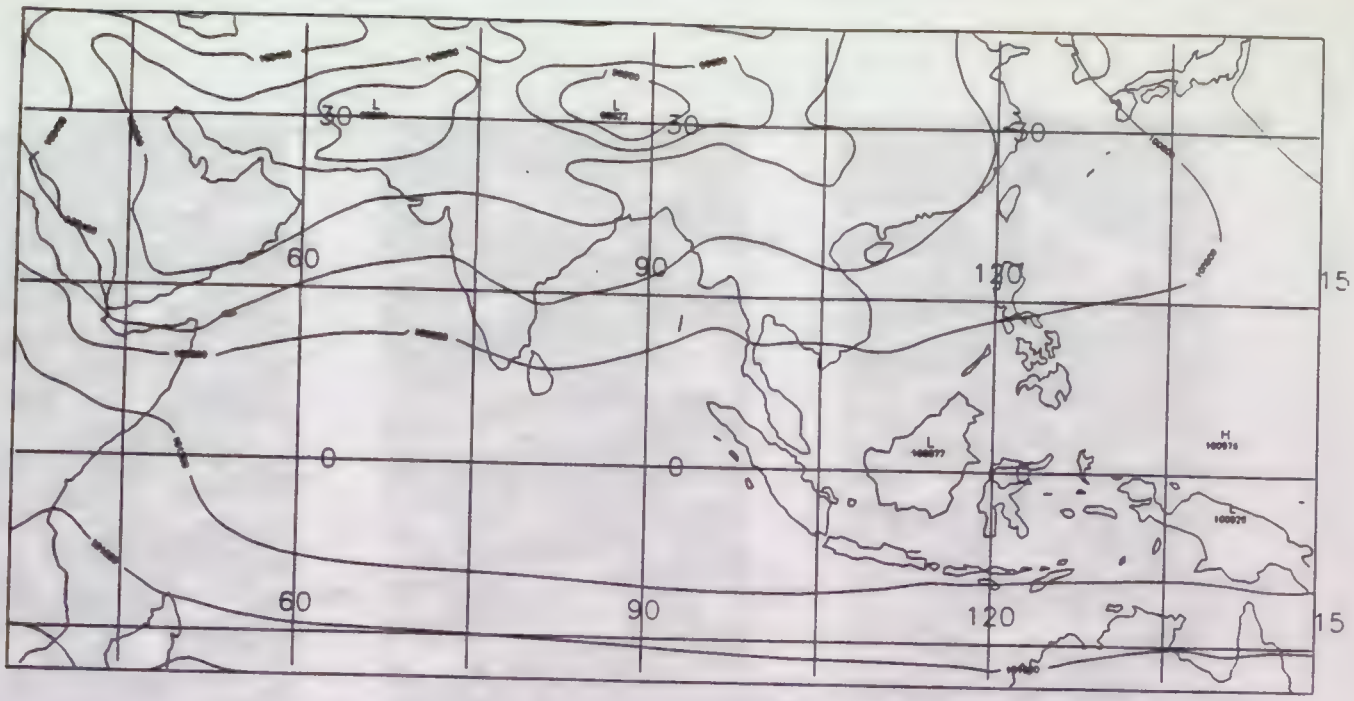
30
30
30
60
90
120
15
0
0
60
90
120
15

(b)

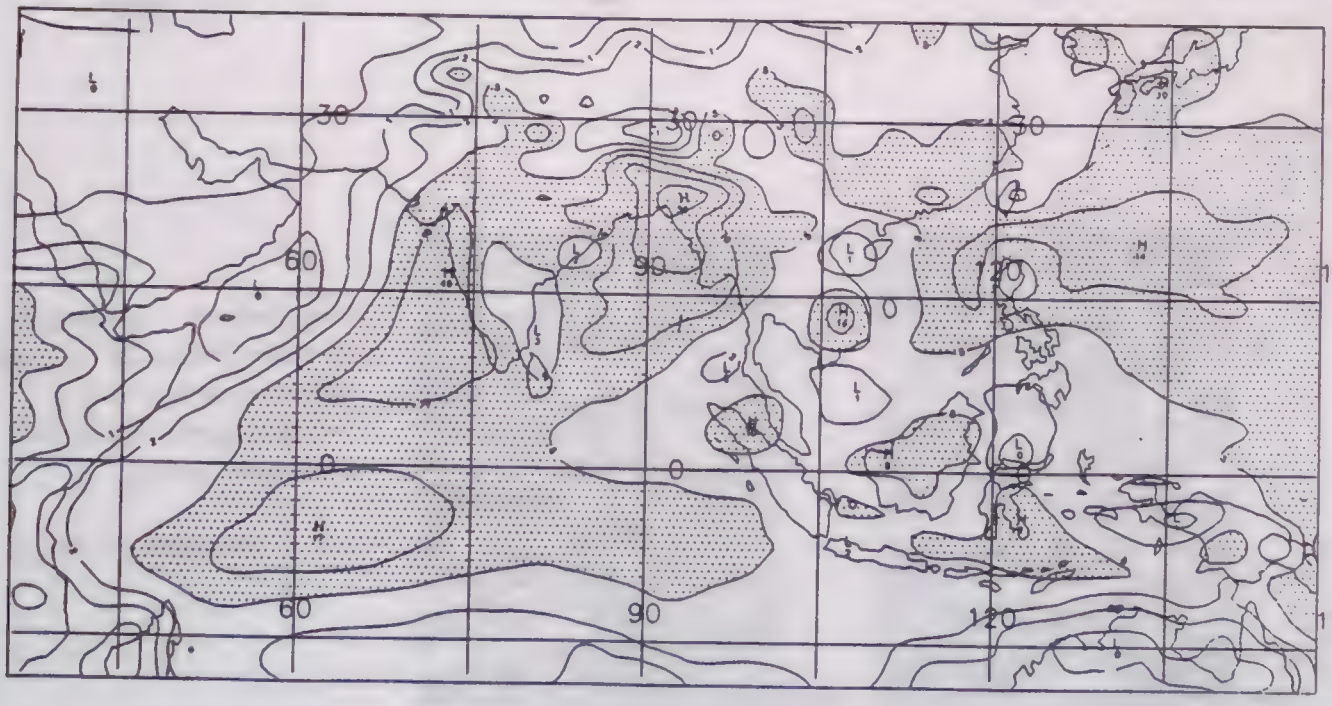
30
30
30
60
90
120
15
0
0
60
90
120
15

Figure 18

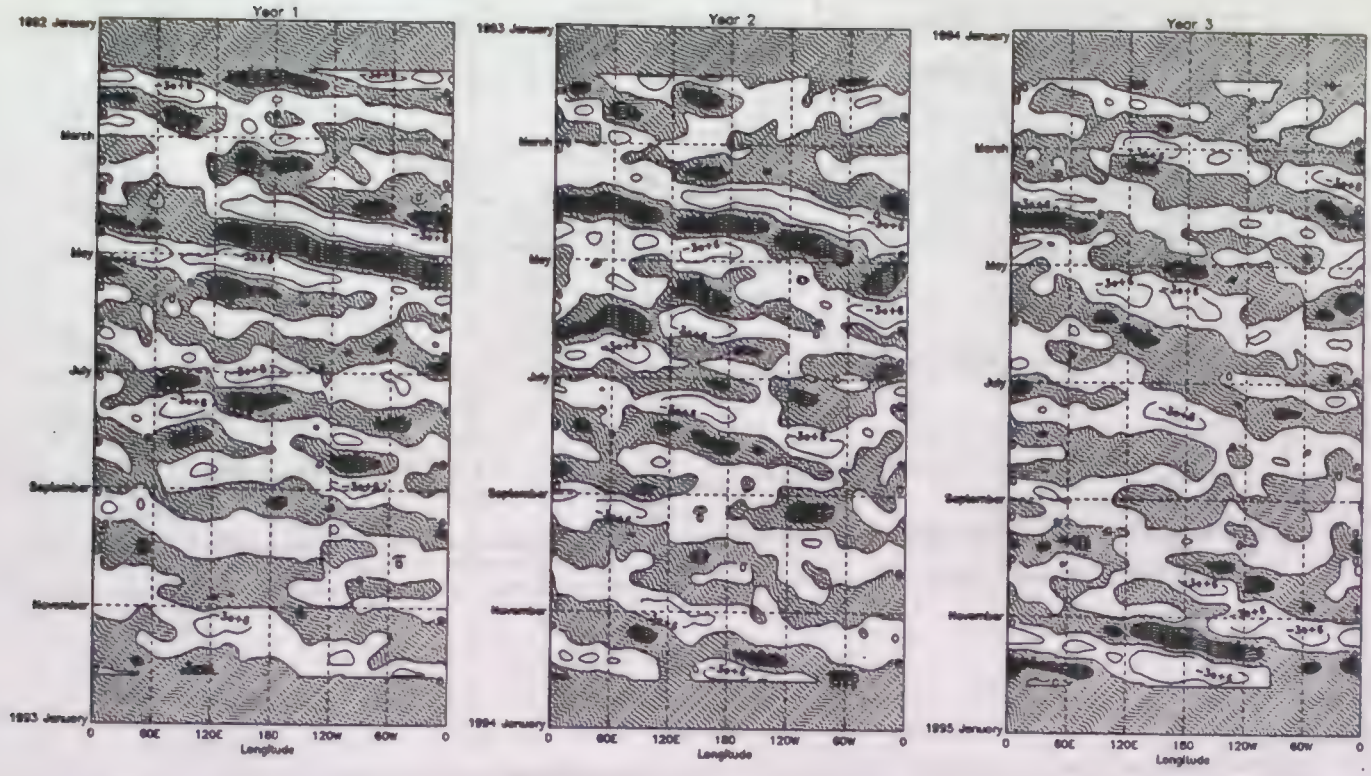

Time/longitude cross_sections of bandpass filtered (20 to 70 day) 250hPa velocity potential, averaged between 5N and 5S. EXPERIMENT CA1SEA.

contour interval=3 x 10^6 m^2s^{-2}

Figure 19(a)

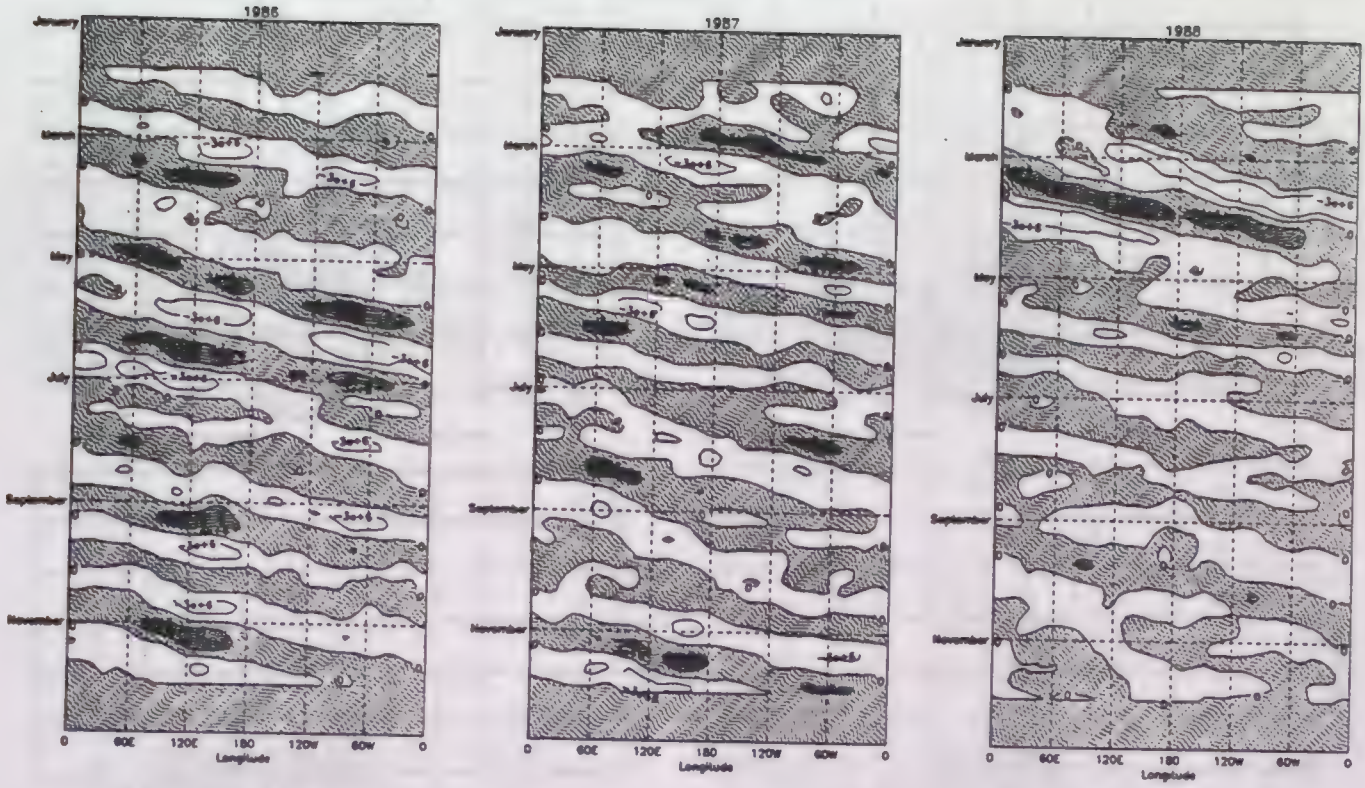

Time/longitude cross_sections of bandpass filtered (20 to 70 day) 250hPa velocity potential, averaged between 5N and 5S.
UKMO ANALYSIS DATA.

contour interval=3 x 10^6 m^2s^{-2}

Figure 19(b)

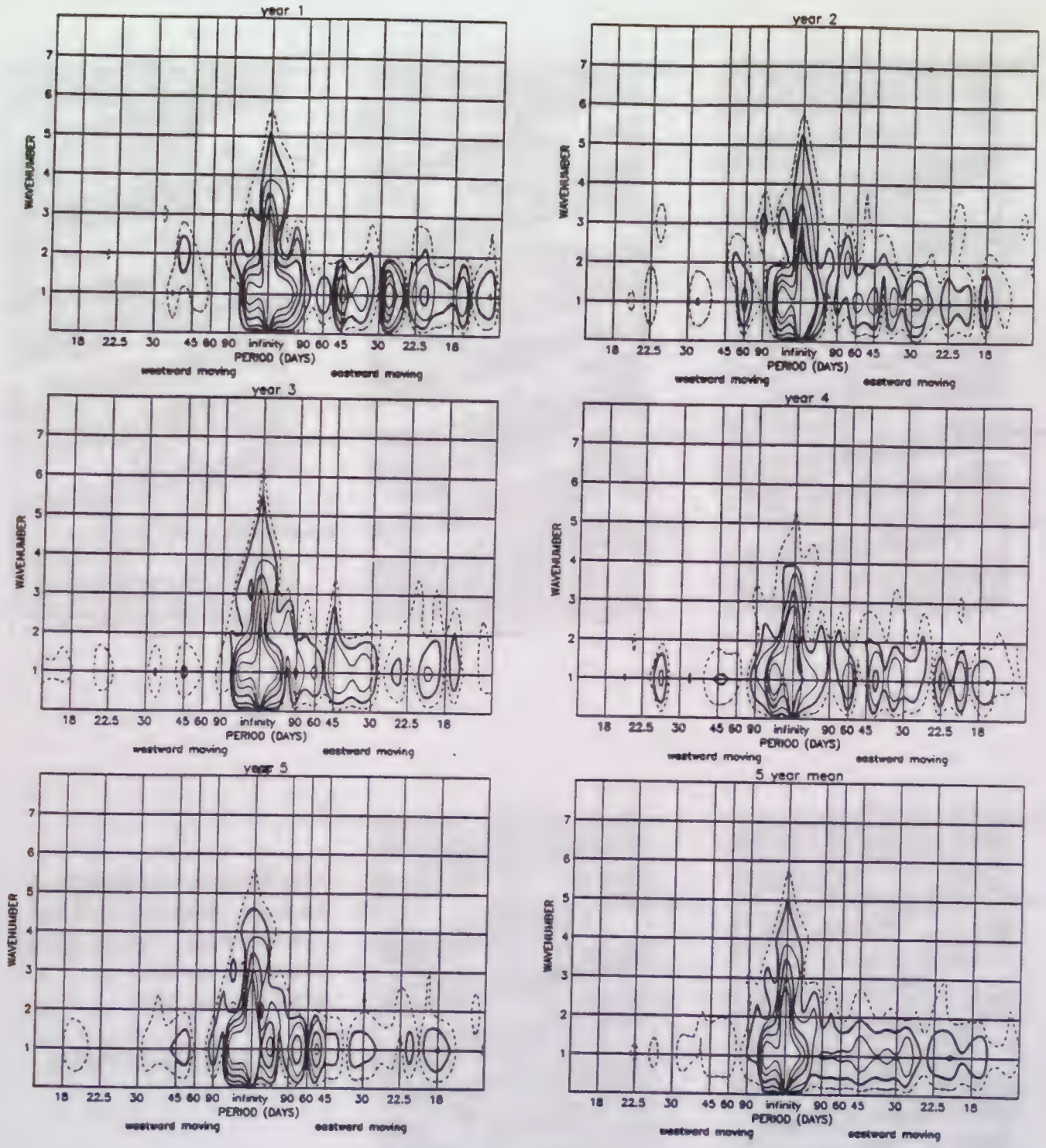
year 1
year 2
year 3
year 4
year 5
5 year mean
WAVENUMBER
1
2
3
4
5
6
7
18 22.5 30 45 60 90 infinity 90 60 45 30 22.5 18
PERIOD (DAYS)
westward moving
eastward moving

Figure 20

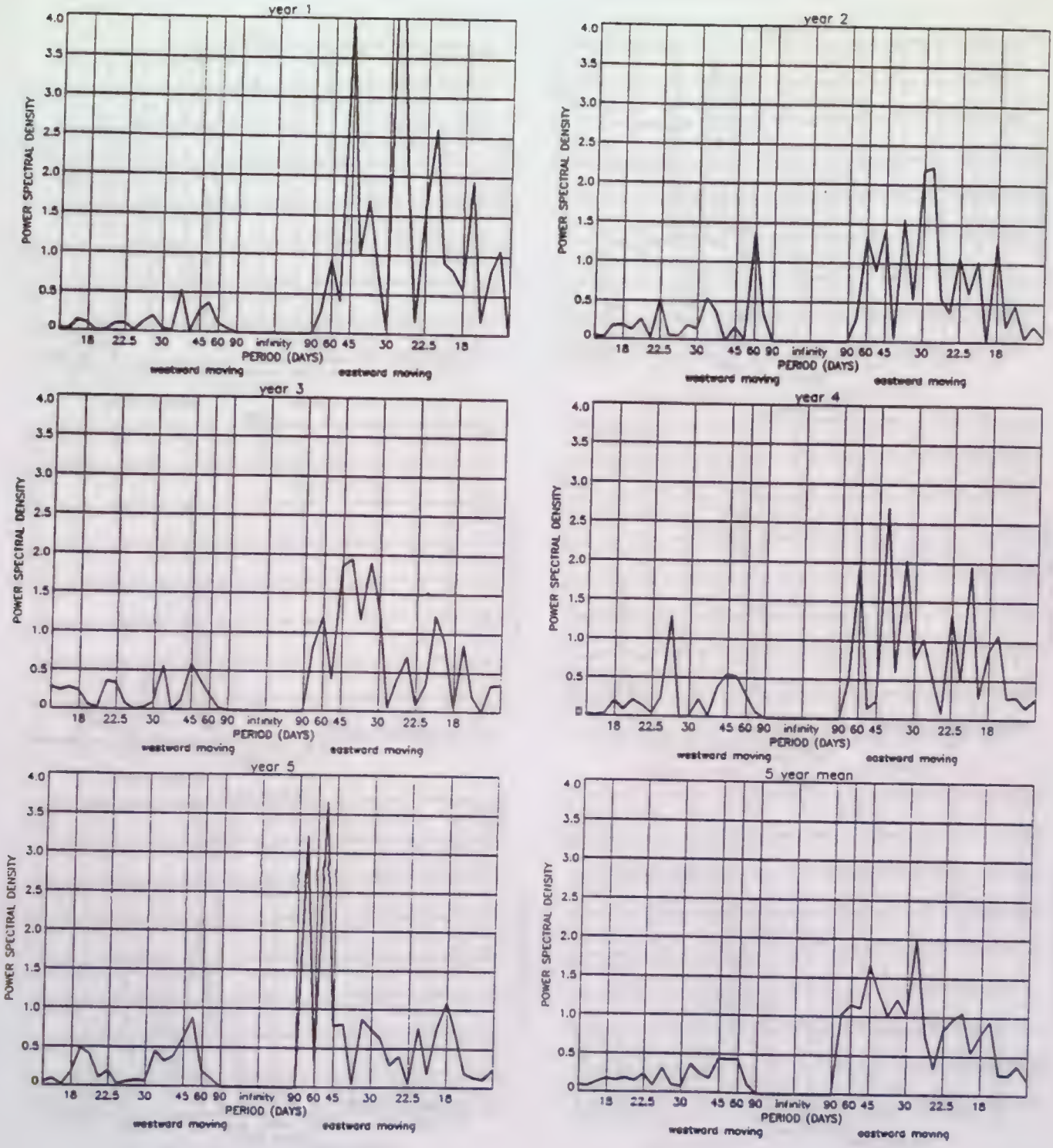
year 1
year 2
year 3
year 4
year 5
5 year mean
POWER SPECTRAL DENSITY
4.0
3.5
3.0
2.5
2.0
1.5
1.0
0.5
0
18 22.5 30 45 60 90 infinity 90 60 45 30 22.5 18
PERIOD (DAYS)
westward moving
eastward moving

Figure 21(a)

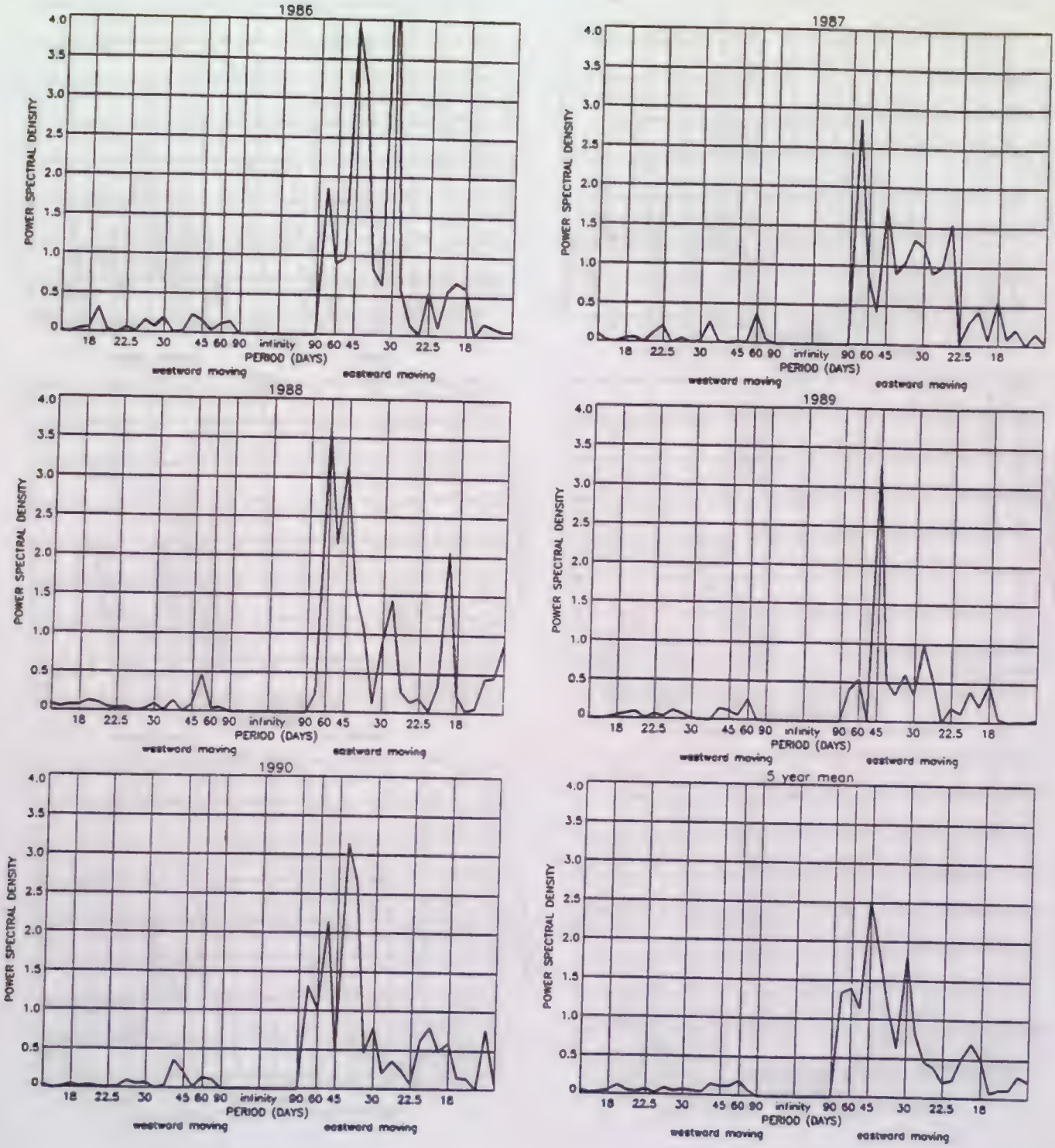
1986
1987
1988
1989
1990
5 year mean
POWER SPECTRAL DENSITY
4.0
3.5
3.0
2.5
2.0
1.5
1.0
0.5
0
18 22.5 30 45 60 90 infinity 90 60 45 30 22.5 18
PERIOD (DAYS)
westward moving
eastward moving

Figure 21(b)

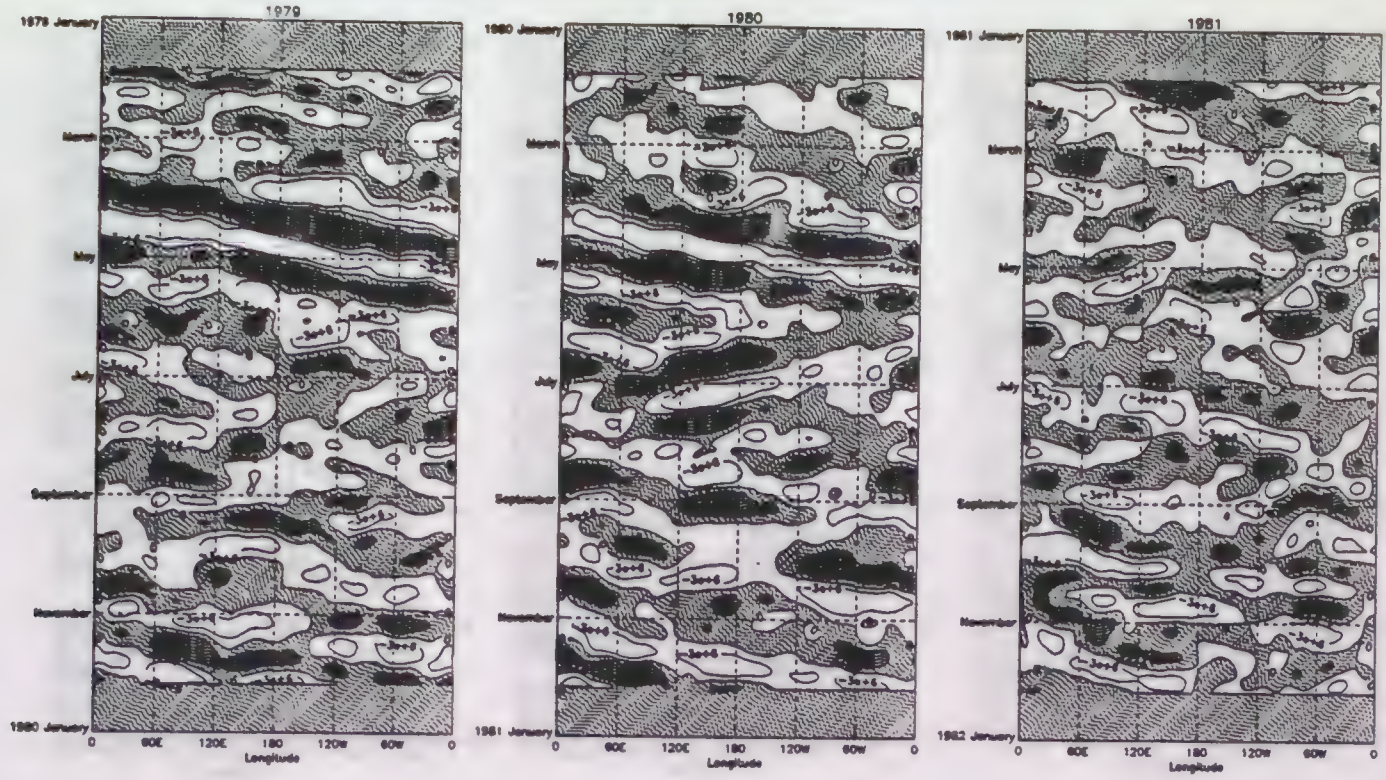

Time/longitude cross_sections of bandpass filtered (20 to 70 day) 200hPa velocity potential, averaged between 5N and 5S. AMIP INTEGRATION.

contour interval=3 x $10^6 \cdot m^2 s^{-2}$

Figure 22(a)

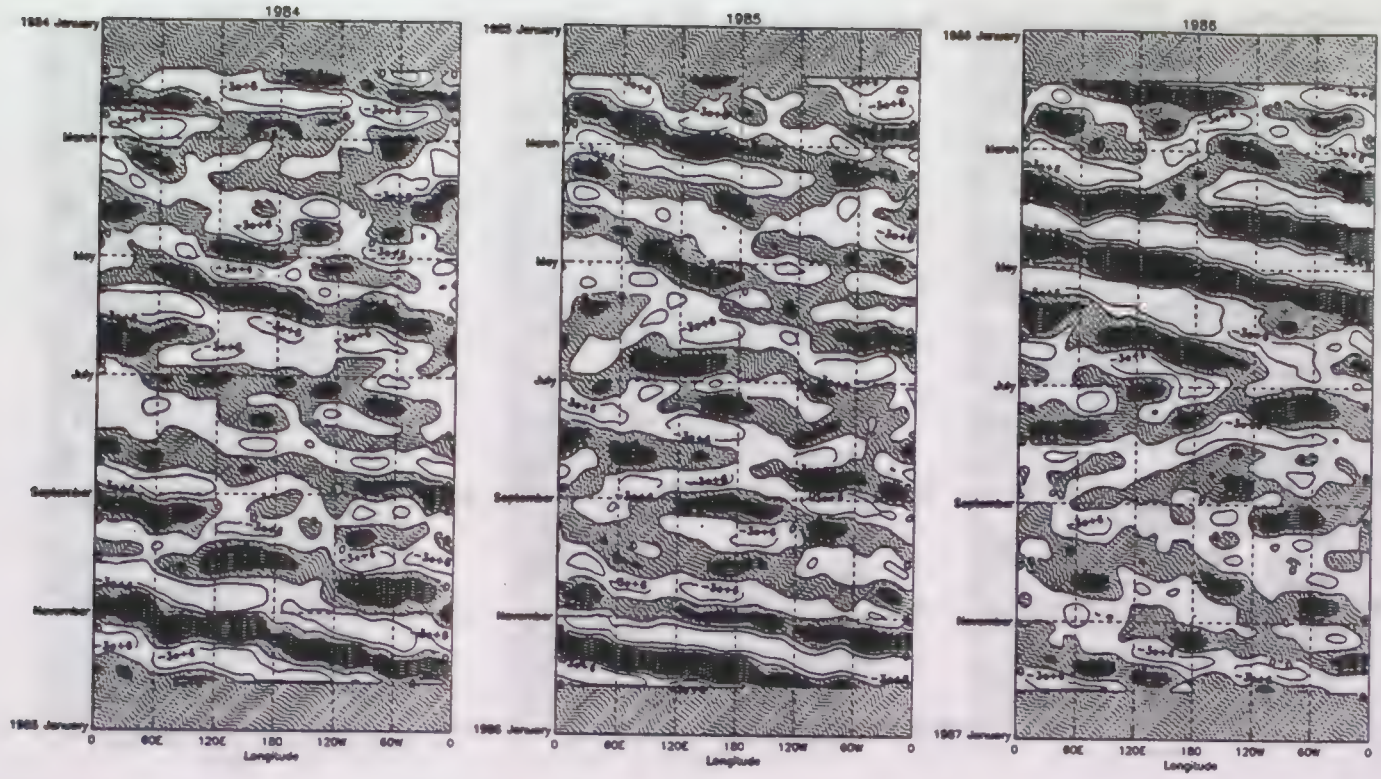

Time/longitude cross_sections of bandpass filtered (20 to 70 day) 200hPa velocity potential, averaged between 5N and 5S. AMIP INTEGRATION.

contour interval=3 x 10^6 m^2s^{-2}

Figure 22(a) continued

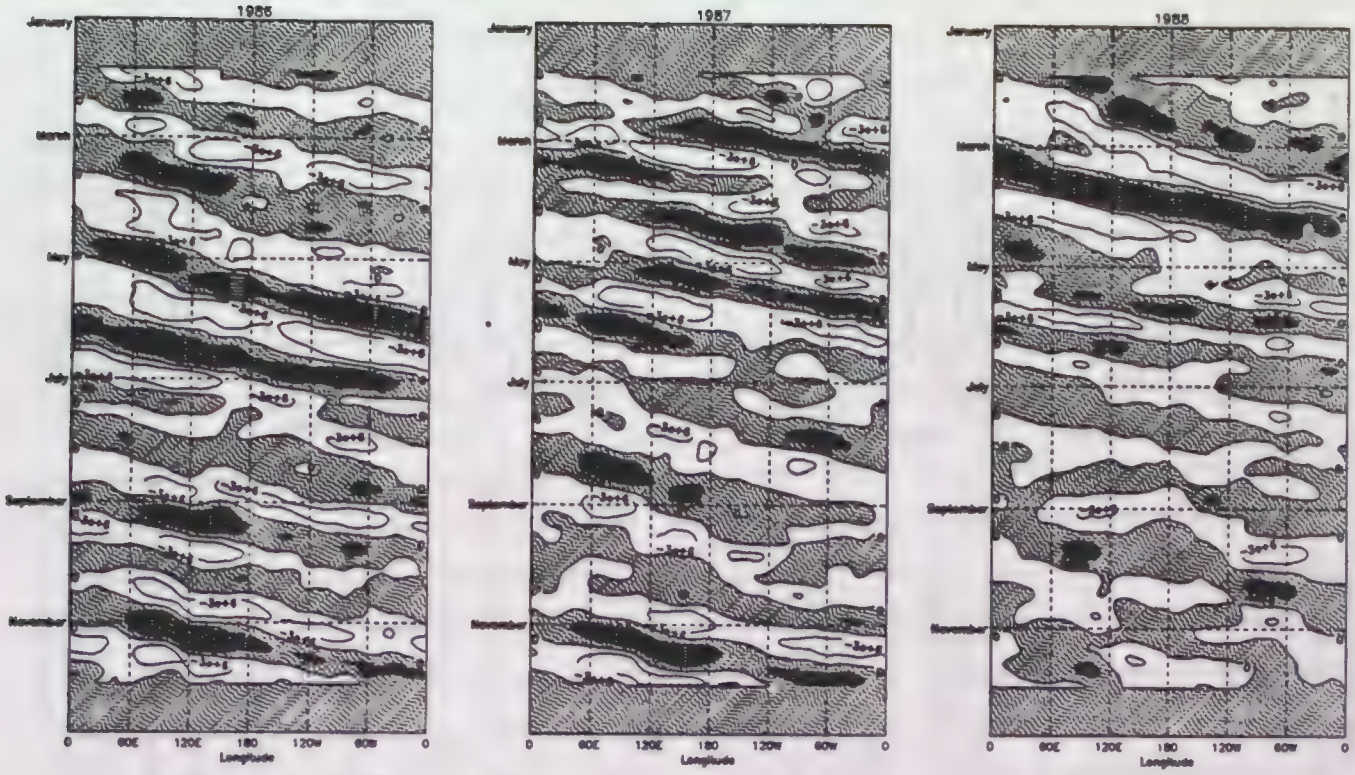

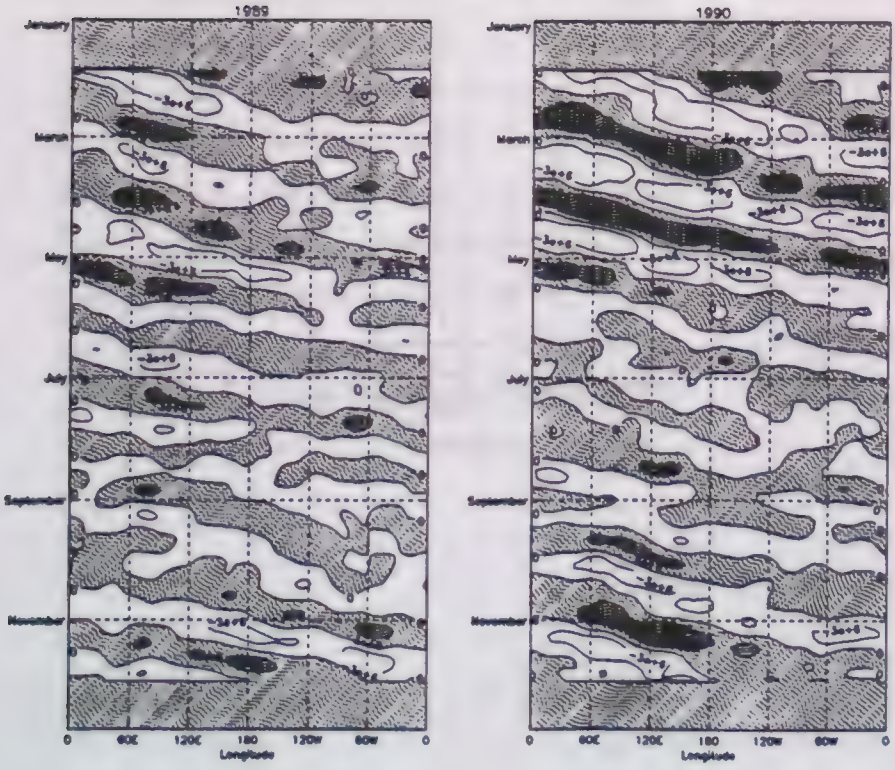

Time/longitude cross_sections of bandpass filtered (20 to 70 day) 200hPa velocity potential, averaged between 5N and 5S. UKMO ANALYSIS DATA.

contour interval=3 x 10^6 m^2s^{-2}

Figure 22(b)

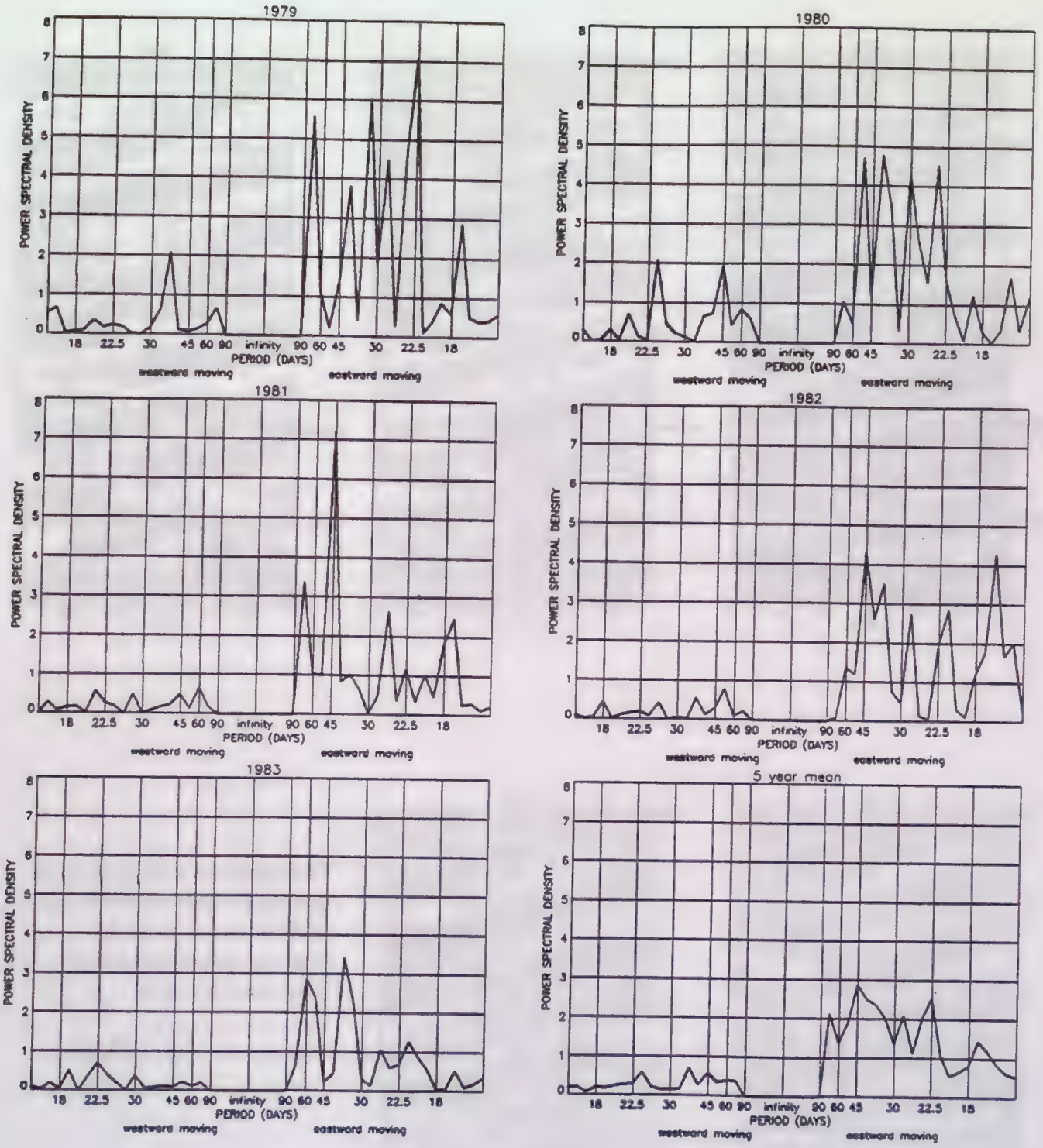
1979
1980
1981
1982
1983
5 year mean
POWER SPECTRAL DENSITY
0 1 2 3 4 5 6 7 8
18 22.5 30 45 60 90 infinity 90 60 45 30 22.5 18
PERIOD (DAYS)
westward moving
eastward moving

Figure 23(a)

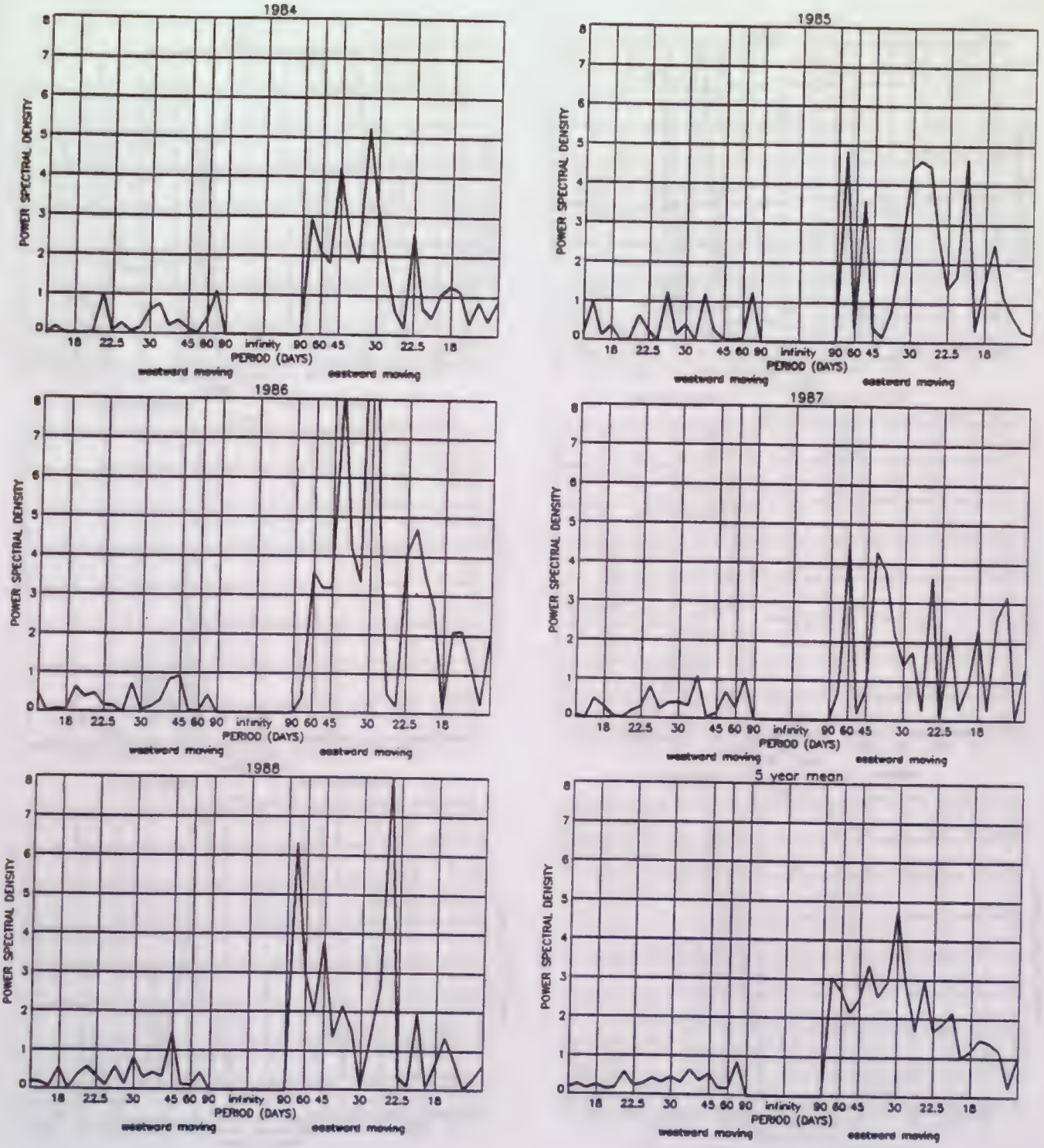

Figure 23(a) continued

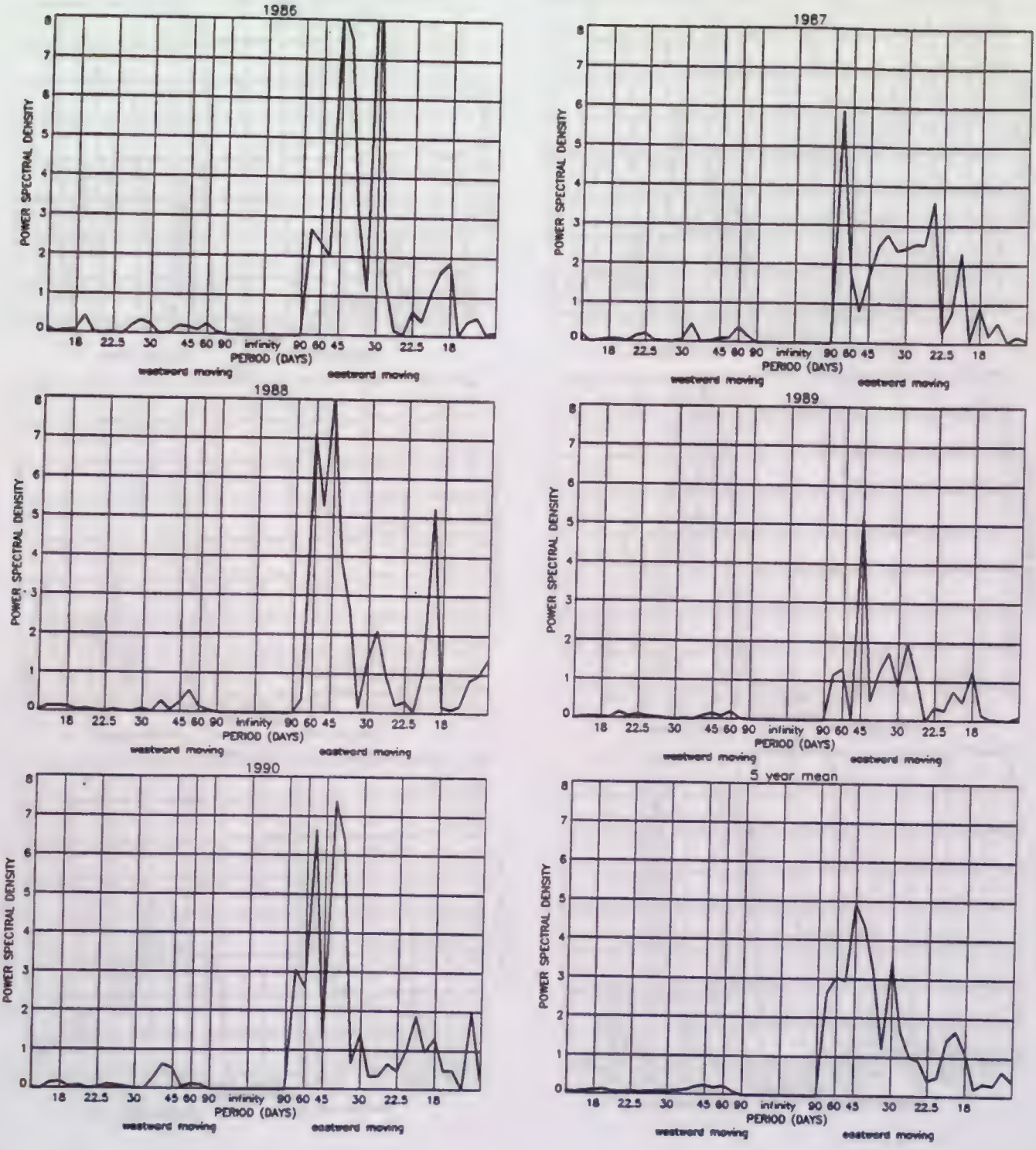
1986
1987
1988
1989
1990
5 year mean
POWER SPECTRAL DENSITY
0 1 2 3 4 5 6 7 8
18 22.5 30 45 60 90 infinity 90 60 45 30 22.5 18
PERIOD (DAYS)
westward moving
eastward moving

Figure 23(b)

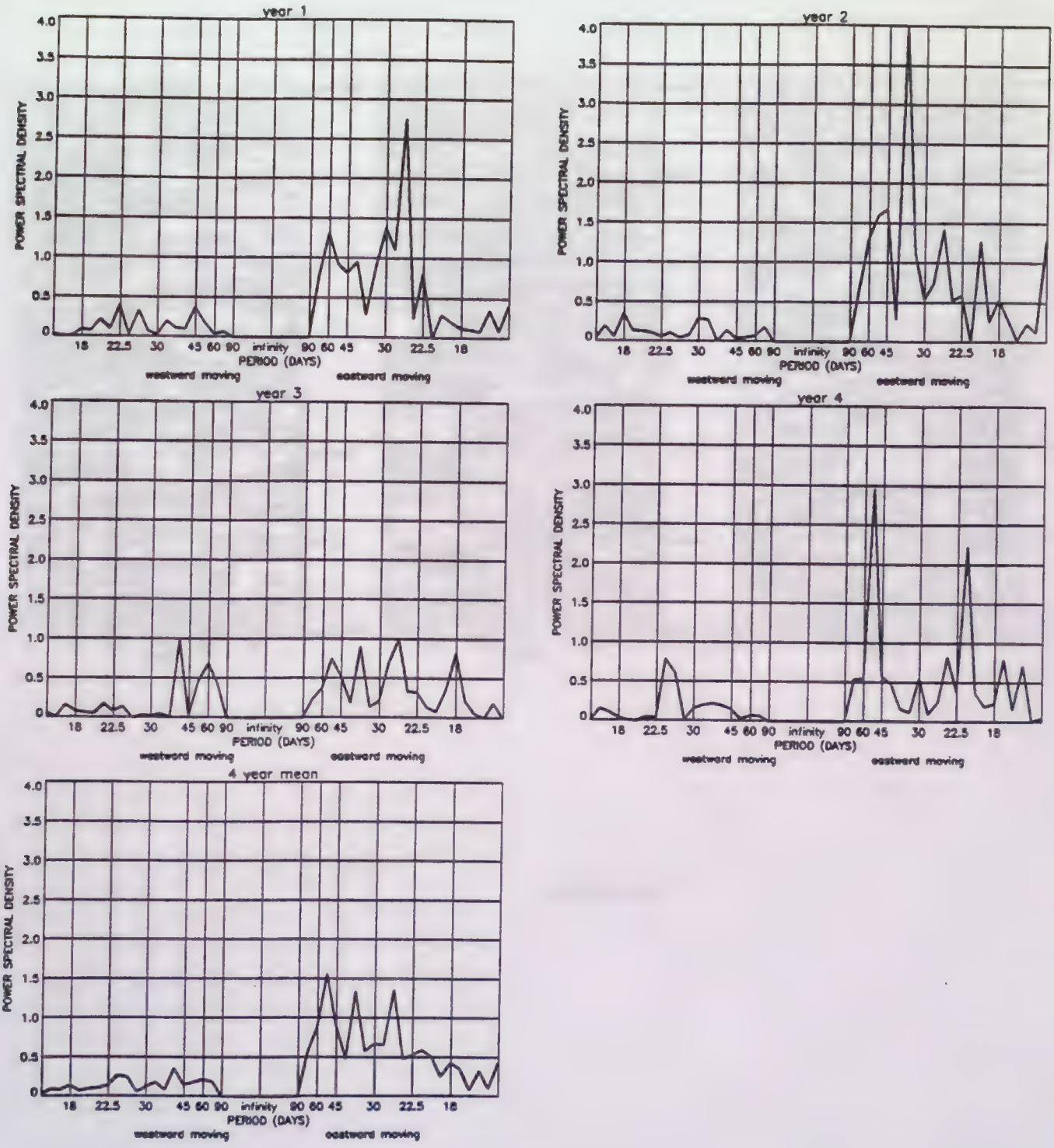
year 1
year 2
year 3
year 4
4 year mean
POWER SPECTRAL DENSITY
4.0
3.5
3.0
2.5
2.0
1.5
1.0
0.5
0
18 22.5 30 45 60 90 infinity 90 60 45 30 22.5 18
PERIOD (DAYS)
westward moving
eastward moving

Figure 24

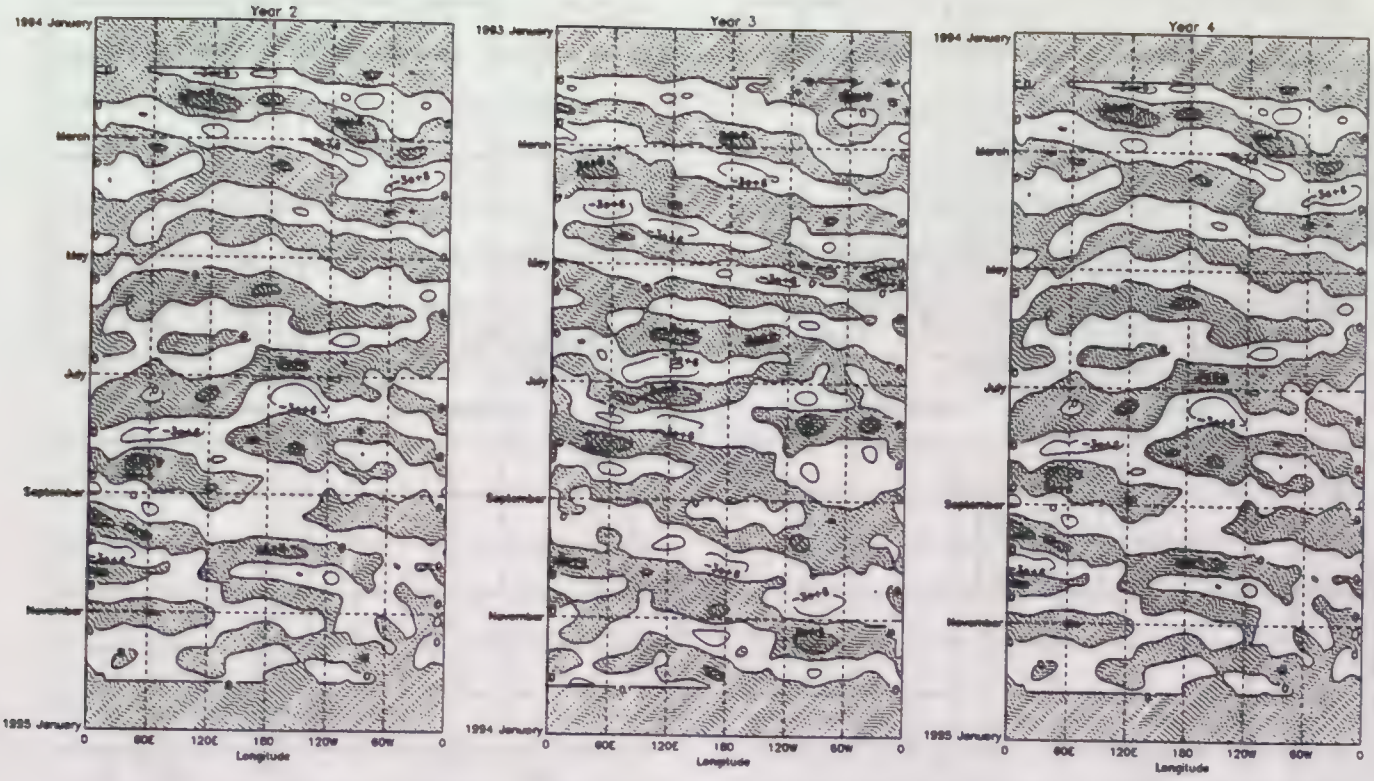
Year 2
Year 3
Year 4
1994 January
March
May
July
September
November
1995 January
1993 January
1994 January
0
60E
120E
180
120W
60W
Longitude

Figure 25(a)

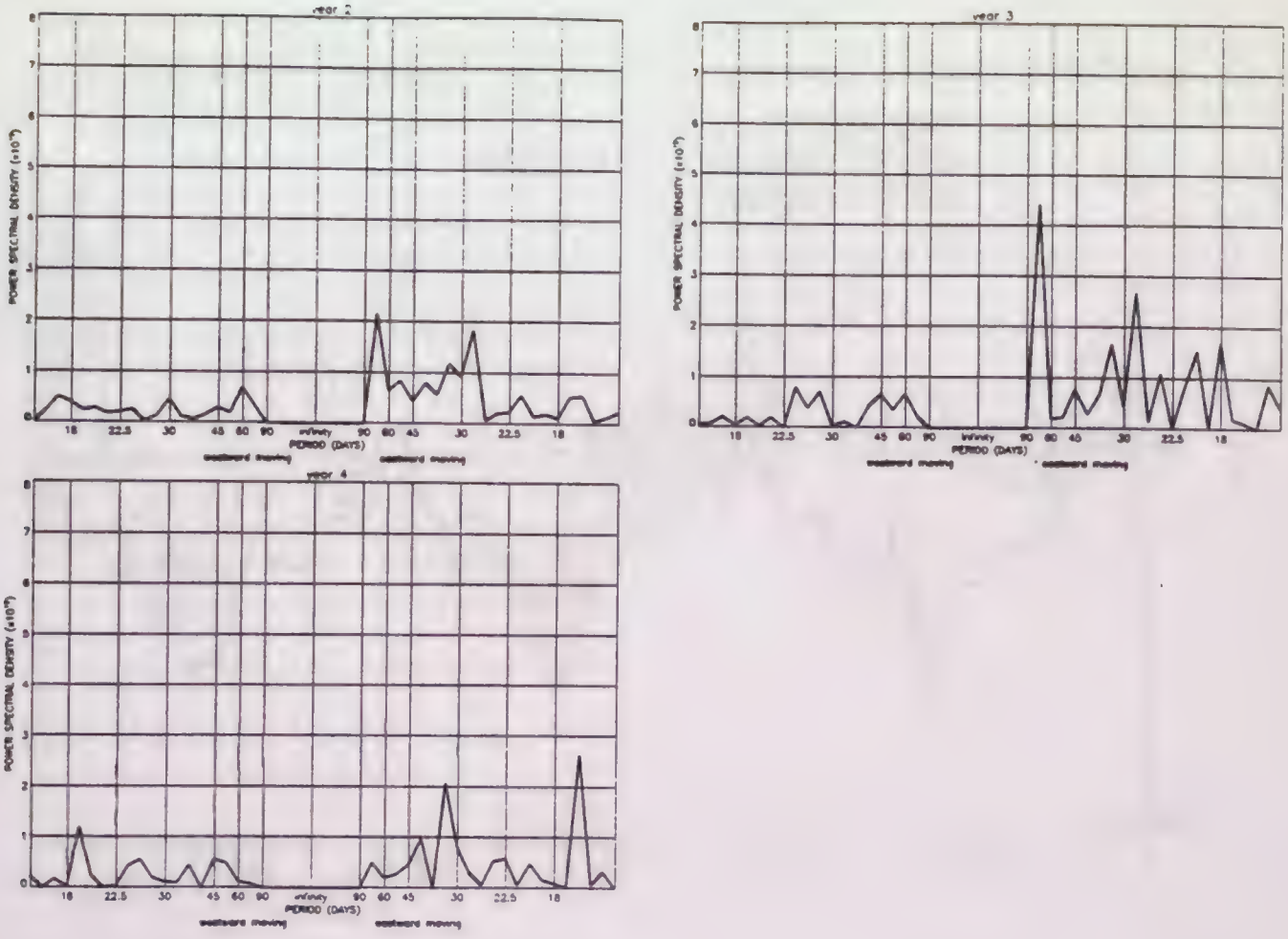
year 2
year 3
year 4
POWER SPECTRAL DENSITY (x10⁴)
PERIOD (DAYS)
18
22.5
30
45
60
90
infinity
westward moving
eastward moving

Figure 25(b)

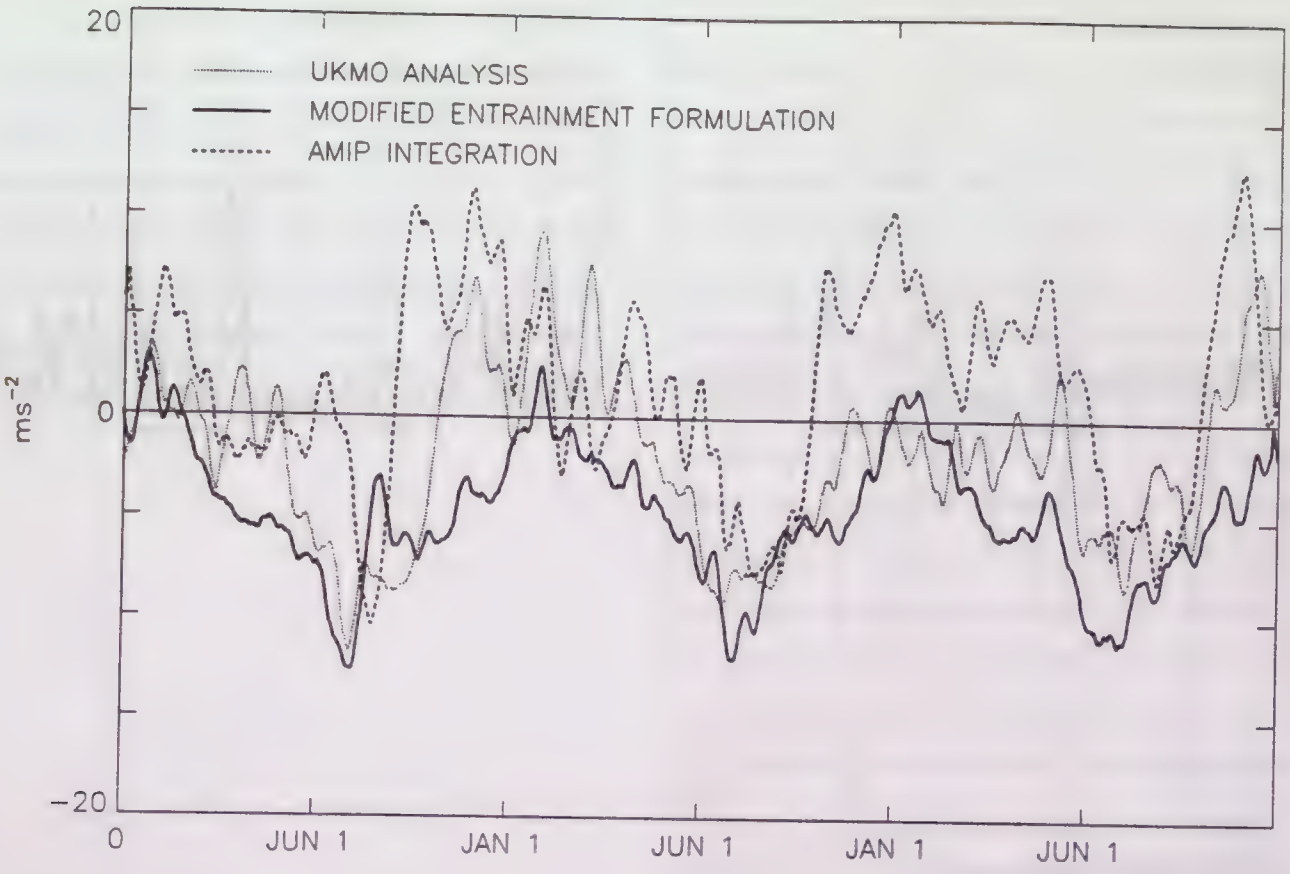
20
0
−20
ms⁻²
UKMO ANALYSIS
MODIFIED ENTRAINMENT FORMULATION
AMIP INTEGRATION
0
JUN 1
JAN 1
JUN 1
JAN 1
JUN 1

Figure 26

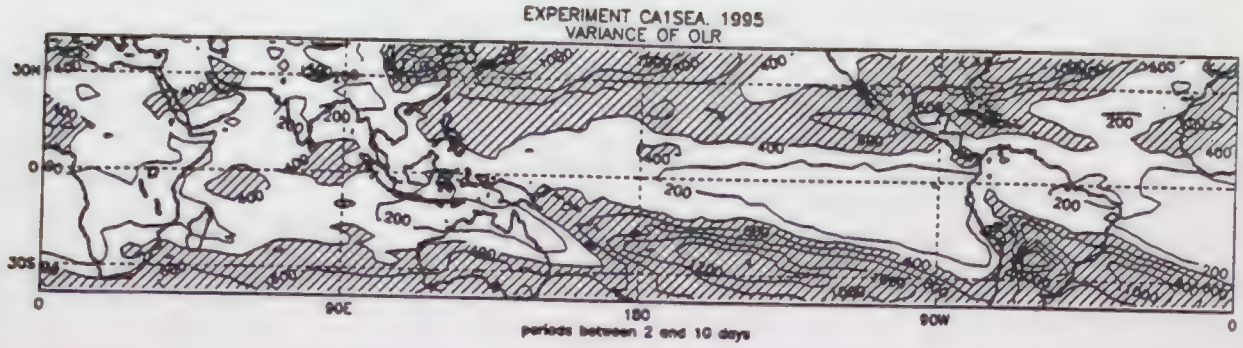
EXPERIMENT CA1SEA. 1995
VARIANCE OF OLR
30N
0
30S
0
90E
180
90W
0
periods between 2 and 10 days

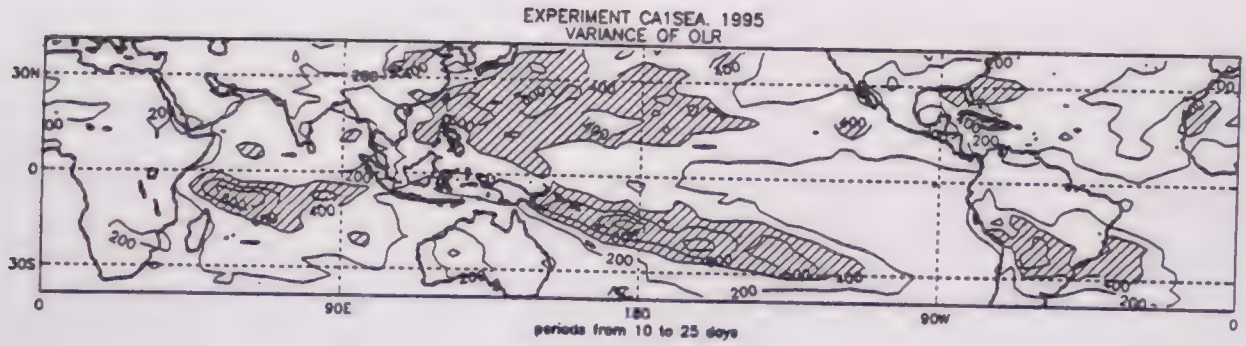
EXPERIMENT CA1SEA. 1995
VARIANCE OF OLR
30N
0
30S
0
90E
180
90W
0
periods from 10 to 25 days

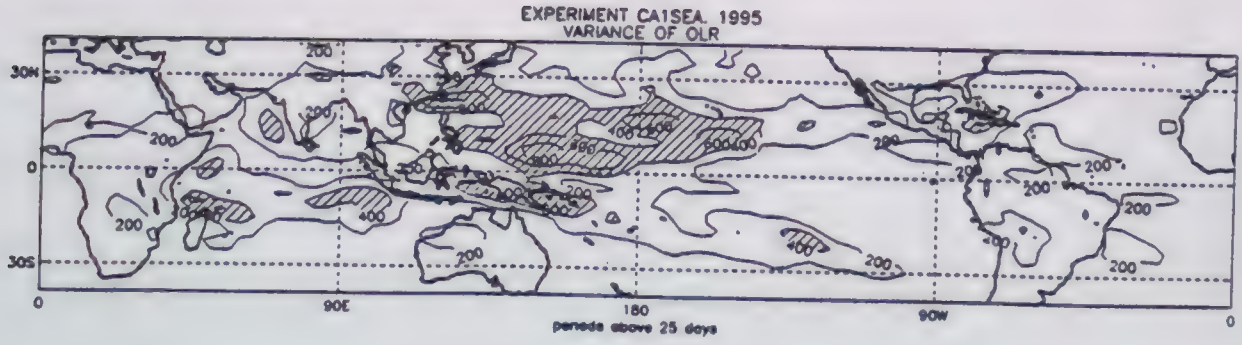
EXPERIMENT CA1SEA. 1995
VARIANCE OF OLR
30N
0
30S
0
90E
180
90W
0
periods above 25 days

Figure 27

CLIMATE RESEARCH TECHNICAL NOTES

CRTN 1	Oct 1990	Estimates of the sensitivity of climate to vegetation changes using the Penman-Monteith equation. P R Rowntree
CRTN 2	Oct 1990	An ocean general circulation model of the Indian Ocean for hindcasting studies. D J Carrington
CRTN 3	Oct 1990	Simulation of the tropical diurnal cycle in a climate model. D P Rowell
CRTN 4	Oct 1990	Low frequency variability of the oceans. C K Folland, A Colman, D E Parker and A Bevan
CRTN 5	Dec 1990	A comparison of 11-level General Circulation Model Simulations with observations in the East Sahel. K Maskell
CRTN 6	Dec 1990	Climate Change Prediction. J F B Mitchell and Qing-cun Zeng
CRTN 7	Jan 1991	Deforestation of Amazonia - modelling the effects of albedo change. M F Mylne and P R Rowntree
CRTN 8	Jan 1991	The role of observations in climate prediction and research. D J Carson
CRTN 9	Mar 1991	The greenhouse effect and its likely consequences for climate change. D J Carson
CRTN 10	Apr 1991	Use of wind stresses from operational N.W.P. models to force an O.G.C.M. of the Indian Ocean. D J Carrington
CRTN 11	Jun 1991	A new daily Central England Temperature series, 1772-1991. D E Parker, T P Legg and C K Folland
CRTN 12	Jul 1991	Causes and predictability of Sahel rainfall variability. D P Rowell, C K Folland, K Maskell, J A Owen, M N Ward

CLIMATE RESEARCH TECHNICAL NOTES

CRTN 13	Jul 1991	Modelling changes in climate due to enhanced CO2, the role of atmospheric dynamics, cloud and moisture. C A Senior, J F B Mitchell, H Le Treut and Z-X Li
CRTN 14	Sep 1991	Sea temperature bucket models used to correct historical SST data in the Meteorological Office. C K Folland
CRTN 15	Aug 1991	Modelling climate change, and some potential effects on agriculture in the U.K. P R Rowntree, B A Callander and J Cochrane
CRTN 16	Aug 1991	The Boreal Forests and Climate G Thomas and P R Rowntree
CRTN 17	Aug 1991	Development of a Stratosphere-Troposphere Data Assimilation System. R Swinbank.
CRTN 18	Sep 1991	A study of asynchronous coupling using a simple climate model. M K Davey.
CRTN 19	Sep 1991	The Oceanic Carbon Cycle. N K Taylor
CRTN 20	Nov 1991	Worldwide ocean-atmosphere surface fields in Sahel wet and dry years using provisionally corrected surface wind data. M N Ward
CRTN 21	Dec 1991	Coupled tropical ocean global atmosphere models at the UKMO. M K Davey, C Gordon, S Ineson and S Lawrence
CRTN 22	Dec 1991	Empirical parameterisation of tropical ocean-atmosphere coupling. M Allen, M K Davey, D L T Anderson and P D Killworth
CRTN 23	Feb 1992	The temporal evolution of Equatorial Currents in the Indian Ocean D L T Anderson, D J Carrington, R A Corry and C Gordon
CRTN 24	Feb 1992	Stratospheric analyses provided by the U.K. Meteorological Office M J Bailey, A O'Neill and V D Pope

CLIMATE RESEARCH TECHNICAL NOTES

CRTN 25	Feb 1992	Modelling interannual variability in the Indian Ocean using momentum fluxes from the UKMO and ECMWF operational weather analyses. D L T Anderson and D J Carrington
CRTN 26	Mar 1992	A GCM simulation of the impact of Amazonian deforestation on climate using an improved canopy representation J Lean and P R Rowntree
CRTN 27	Mar 1992	The parameterization of rainfall interception in GCMs A J Dolman and D Gregory
CRTN 28	Jun 1992	Development of worldwide marine data eigenvectors since 1985 A W Colman
CRTN 29	Jun 1992	A tropical ocean model with reduced physics M K Davey
CRTN 30	Jun 1992	International Temperature Workshop, Boulder, Colorado, USA, 16 January 1992 Edited by D E Parker
CRTN 31	Jul 1992	Simulation of clear-sky outgoing longwave radiation over the oceans using operational analyses A Slingo and M J Webb
CRTN 32	Sep 1992	A prediction of the transient response of climate J M Murphy
CRTN 33	Nov 1992	LEPS scores for assessing climate model simulations and long-range forecasts. C K Folland
CRTN 34	Jan 1993	Stratospheric Data Assimilation System Guide Editer: R Swinbank
CRTN 35	Mar 1993	A Stratosphere-Troposphere Data Assimilation System R Swinbank and A O'Neill
CRTN 36	Mar 1993	Validation of hydrological schemes for climate models against catchment data. P R Rowntree and J Lean

CLIMATE RESEARCH TECHNICAL NOTES

CRTN 37	Apr 1993	Modelling of palaeoclimates: Examples from the recent past J F B Mitchell
CRTN 38	May 1993	A simulation of seasonality in ENSO forecast skill M K Davey, D L T Anderson and S Lawrence
CRTN 39	Jul 1993	ENSO Prediction experiments using a simple ocean-atmosphere model D-H Wu, D L T Anderson and M K Davey
CRTN 40	Sep 1993	Diagnosis of dynamic sea-surface and sea-level changes from the Cox ocean model J M Gregory
CRTN 41	Sep 1993	Seasonal variations of the clear-sky greenhouse effect: the role of changes in atmospheric temperatures and humidities M J Webb, A Slingo and G L Stephens
CRTN 42	Nov 1993	Sea-level changes under increasing atmospheric CO_2 in a transient coupled ocean-atmosphere GCM experiment. J M Gregory
CRTN 43	Dec 1993	Global and regional patterns of climate change: recent predictions for the Arctic P R Rowntree
CRTN 44	Feb 1994	The effect of changing horizontal diffusion in the atmospheric version of the unified climate model C D Hall and R A Stratton
CRTN 45	Mar 1994	Simulation of El-Niño/Southern Oscillation like variability in a global AOGCM and its response to CO_2 increase. S F B Tett
CRTN 46	Apr 1994	Global data required for monitoring climate change. D E Parker and C K Folland
CRTN 47	May 1994	Seasonal uptake of anthropogenic CO_2 in an ocean general circulation model. N K Taylor

CLIMATE RESEARCH TECHNICAL NOTES

CRTN 48	Jun 1994	A tropic-wide oscillation of boreal summer rainfall and patterns of sea-surface temperature. M N Ward, K Maskell, C K Folland, D P Rowell and R Washington
CRTN 49	Jun 1994	Simulation of the tropical Pacific using a simplified ocean model M A Balmaseda, D L T Anderson and M K Davey
CRTN 50	Sep 1994	Simulation of global mean temperature using a box-diffusion climate model P R Rowntree
CRTN 51	Sep 1994	Seasonal dependence of ENSO prediction skill M A Balmaseda, M K Davey and D L T Anderson
CRTN 52	Nov 1994	Simulation of the Indian Monsoon and Tropical Intraseasonal Variability by a General Circulation Model P M Inness and D Gregory